Technische Universität München

New Geodetic Monitoring Approaches using Image Assisted Total Stations

Dissertation
von

Andreas Wagner

Lehrstuhl für Geodäsie
Ingenieurfakultät Bau Geo Umwelt

Ingenieurfakultät Bau Geo Umwelt

Lehrstuhl für Geodäsie

New Geodetic Monitoring Approaches using Image Assisted Total Stations

Andreas A. Wagner

Vollständiger Abdruck der von der Ingenieurfakultät Bau Geo Umwelt der Technischen Universität München zur Erlangung des akademischen Grades eines

Doktor – Ingenieurs

genehmigten Dissertation.

Vorsitzender:		Univ.-Prof. Dr.-Ing. U. Stilla
Prüfer der Dissertation:	1.	Univ.-Prof. Dr.-Ing. habil. Th. Wunderlich
	2.	Univ.-Prof. Dr. techn. habil. A. Reiterer Albert-Ludwigs-Universität Freiburg
	3.	Univ.-Prof. Dr. techn. W. Lienhart Technische Universität Graz, Österreich

Die Dissertation wurde am 17. November 2016 bei der Technischen Universität München eingereicht und durch die Ingenieurfakultät Bau Geo Umwelt am 16. März 2017 angenommen.

Kurzfassung

Image Assisted Total Stations (IATS) vereinen die geodätische Präzision von Totalstationen mit der flächenhaften Erfassung mittels Bilddaten. Ein kalibriertes Instrument erlaubt die Umrechnung einer auf dem Bildsensor gemessenen Pixelkoordinate in eine räumliche Richtung. Jedes aufgenommene Bild ist direkt absolut orientiert und kann sofort für Richtungsmessungen verwendet werden. Verknüpfungspunkte auf dem Objekt oder andere Orientierungsmessungen werden nicht benötigt. Photogrammetrische Auswerte- und Analysemethoden zur Detektion von signalisierten, als auch nicht signalisierten Messpunkten können mit Funktionen der Totalstation (z.B. präzise Winkel- und Distanzmessungen) kombiniert werden.

Neben Prototypen aus dem Forschungsbereich ist eine zunehmende Anzahl kommerziell erhältlicher Lösungen verfügbar. Die zusätzlichen Möglichkeiten dieser IATS werden derzeit allerdings nur genutzt, um bestehende Standardmessmethoden ergonomischer zu gestalten oder die Ergebnisse zu dokumentieren. Das volle Potential von IATS wird noch nicht ausgeschöpft, insbesondere der Einsatz der Geräte für Überwachungsmessungen im automatischen und autonomen Betrieb.

In dieser Dissertation werden vier neue Lösungsansätze und Fallstudien aus dem Bereich Monitoring vorgestellt, die dieses Potential von IATS nutzen. Zwei der dargestellten Methoden beziehen sich auf die Bauwerksüberwachung, die weiteren beiden auf den Bereich des Geo-Monitoring.

Der erste Ansatz zeigt ein Beispiel der Eigenfrequenzbestimmung zur Bauwerksüberwachung (Structural Health Monitoring) einer Hängebrücke mit IATS. Aktive LED-Zielzeichen werden mittels Bildanalyse detektiert und anhand deren Bewegungen Schwingungsfrequenzen des Bauwerks abgeleitet. Die präsentierte Methode ist sowohl in der Lage, mehrere Ziele gleichzeitig zu erfassen, als auch für hochfrequente Anwendungen geeignet. Die Stabilität des Standpunktes kann jederzeit mit den Funktionen der Totalstation (Inklinometer, Richtungsmessungen zu umliegenden Festpunkten, o.ä.) kontrolliert werden. Das System kann sowohl im permanenten Betrieb, als für individuelle Einzelmessungen benutzt werden.

Eine Geo-Monitoring Methode für große Reichweiten wird im zweiten Ansatz präsentiert, die auf der Verwendung von zwei IATS in einer Stereokonfiguration beruht, ähnlich wie sie vom Vorwärtsschnitt oder der Stereophotogrammetrie bekannt ist. Das eingeschränkte Gesichtsfeld der IATS Teleskopkamera wird durch die Aufnahme von mehreren Bildern erweitert, die zu einem sphärischen Panorama zusammengesetzt werden. Mithilfe flächenhafter Matchingverfahren und räumlicher Vorwärtsschnitte werden 3D-Punktwolken erzeugt. Werden Korrespondenzen nicht nur

in einem Stereo-Paar (zweier Panoramen), sondern auch in darauffolgenden Messepochen gefunden, können 3D-Verschiebungsvektoren direkt abgeleitet werden. Eine klassische Deformationsanalyse kann mithilfe zusätzlicher Messungen zu stabilen Festpunkten berechnet und die Ergebnisse somit auf Signifikanz getestet werden.

Ein dritter Lösungsansatz ist die Implementierung von Auswerteverfahren zur Analyse digitaler Nivellierlattencodes in IATS. Im Gegensatz zu klassischen Nivelliergeräten, werden damit nicht horizontale Visuren ermöglicht. Die Methode kann für die direkte Übertragung der Kippachshöhe einer Totalstation von einer Höhenmarke oder in einem automatischen Überwachungssystem, das Nivellierlatten oder kurze Barcodestreifen verwendet, genutzt werden. Insbesondere der letztgenannte Punkt ermöglicht eine höhere Flexibilität im Bereich der Bauwerksüberwachung. Der Ansatz ist des Weiteren ein Beispiel für die Verwendung passiver Zielzeichen, da der Nivellierlattencode durch jedes beliebige Muster ersetzt werden kann.

Die Scanfunktionalität moderner IATS für eine kombinierte Auswertung von Punktwolken und Bildinformation wird im vierten Ansatz vorgestellt. Sphärische Farbbilder/-panoramen (RGB) werden mit einem Distanzkanal „D“ zu RGB + D Bildern erweitert, in denen 3D Koordinaten direkt abgegriffen werden können. Wie im Stereo-Ansatz können direkt 3D-Verschiebungsvektoren erzeugt werden, falls Korrespondenzen in aufeinanderfolgenden Messepochen detektiert werden. Die Vorteile der verschiedenen einzelnen Sensorinformationen werden vereint und deren Nachteile reduziert. Wie in o.g. Methode präsentiert, erlauben zusätzliche Messungen zu stabilen Festpunkten die Berechnung geodätischer Deformationsanalysen.

Diese verschiedenen Lösungsansätze werden in der Dissertation detailliert beschrieben, sowie deren individuellen Stärken, Chancen, aber auch Schwächen dargestellt. Es wird gezeigt, dass IATS insbesondere in der Bauwerksüberwachung und dem Geo-Monitoring weit mehr Potential bieten als derzeit genutzt wird. Die Instrumente sind ideal für den automatischen und autonomen Betrieb in geodätischen Überwachungssystemen geeignet.

Abstract

Image Assisted Total Stations (IATS) unify the geodetic precision of total stations (TS) with the areal coverage of images. A calibrated system allows the expression of measured pixel positions on the image sensor as field angles in the object space. Captured images are directly geo-referenced and can be used for direction measurements with no need for object control points or further orientation processes. Photogrammetric image measurement methods in order to detect signalized as well as non-signalized targets can be combined with functions of the base total station, such as precise angle and distance measurements.

Meanwhile, next to research prototypes, an increasing number of commercial solutions are becoming available. However, the additional functionalities of these IATS are only used to support classical standard TS procedures or for documentation purposes. The full potential of IATS, in particular for automatic and autonomous operation in monitoring systems, is not yet exploited.

This thesis presents four new monitoring approaches and use cases for IATS in order to fill this gap. Two methods relate to structural monitoring and two are suited for geo-monitoring applications.

The first approach demonstrates structural health monitoring with an IATS of a suspended bridge. Active LED targets are tracked over time by image analysis techniques and oscillation frequencies of the construction are derived. The presented monitoring solution is able to detect multiple targets simultaneously and is suited for high-frequent applications. The stability of the instrument station can be verified by TS functionalities including inclinometer, orientation measurements to surrounding control points, etc. at any time. Further, it is possible to use the system in a permanent or periodical operation mode.

A long range geo-monitoring method is presented in the second approach, based on two IATS in a stereo configuration, as used for TPS intersection or stereo-photogrammetry. The limited field of view (FOV) of the instruments' telescope cameras are extended by taking multiple images which are composed to a spherical panorama. 3D point clouds are generated using a dense matching algorithm and spatial intersections. 3D displacement vectors can be directly derived if correspondences are found not only in a stereo (panorama) pair, but also in subsequent measuring epochs. A classical geodetic deformation analysis can be calculated using additional measurements to stable control points, allowing the results to be tested for significance.

The third approach is an implementation of analyzing strategies to read the code pattern of digital leveling staffs with IATS. In contrast to classical leveling instruments, non-horizontal lines of sight

are also possible. The method may be used for a height transfer of the total station's transit axis from a benchmark or in an automated monitoring system to measure on leveling staffs or short barcode stripes. In particular, the last mentioned point provides more flexibility to the field of structural monitoring. The approach is also an example for passive target signalization, as the code pattern of the leveling staff could be replaced by any arbitrary template.

The scanning capabilities of modern IATS are used for a combined analysis of point cloud and image data, based on RGB + D images. Here, spherical color (RGB) images/panoramas are extended by a distance channel "D", enabling a direct pickup of 3D coordinates. If correspondences are found in subsequent measurement epochs, 3D displacement vectors can be extracted, similar to the stereo approach. The advantages of the different (single) sensor information types are merged and their disadvantages are reduced. As mentioned above, additional measurements to stable control points enable geodetic deformation analyses.

These different approaches are described in detail in this thesis along with their individual strengths, opportunities, but also weaknesses. It is shown that IATS offer much greater potential as currently used, particularly in the fields of structural and geo-monitoring. These instruments are ideally suited for automatic and autonomous operation in geodetic motioning systems.

Contents

Preface

This cumulative dissertation is primarily based on the following four first-author publications:

P-I Wagner, A., Wasmeier, P., Reith, C., Wunderlich, T., 2013. Bridge Monitoring by Means of Video-Tacheometer - A Case Study. avn - Allgemeine Vermessungs-Nachrichten 120 (8-9), pp. 283–292.
Peer-Reviewed Journal Paper.

P-II Wagner, A., Huber, B., Wiedemann, W., Paar, G., 2014. Long-Range Geo-Monitoring using Image Assisted Total Stations. Journal of Applied Geodesy 8 (3), pp. 223–234.
Peer-Reviewed Journal Paper.

P-III Wagner, A., Wiedemann, W., Wunderlich, T., 2016. Using IATS to Read and Analyze Digital Leveling Staffs. In: Paar, R., Marendić, A., Zrinjski, M. (Eds.), Proceedings of the International Symposium on Engineering Geodesy - SIG 2016. Croatian Geodetic Society, pp. 515–526.
Peer-Reviewed Conference Paper.

P-IV Wagner, A., 2016. A new approach for geo-monitoring using modern total stations and RGB + D images. Measurement 82, pp. 64–74.
Peer-Reviewed Journal Paper.

Within this thesis, the papers are cited using the abbreviation "P" for "publication" and a Roman number for the number of the paper.

The publications P-I, P-II and P-IV are peer-reviewed journal articles, P-III is a peer-reviewed conference paper. All manuscripts are included in this thesis in Section 4 as full-text. The included versions are the final ones sent to the respective journals/conference. Only minor formatting changes were made to include the papers in this thesis. Please note that some of the articles are using British and some American English in accordance with the regulations of the respective journal/editor.

In addition to the included publications mentioned above, the following eight first- or co-author publications are related to this thesis and supplement its findings:

- Reiterer, A., Wagner, A., 2012. System Considerations of an Image Assisted Total Station – Evaluation and Assessment. avn - Allgemeine Vermessungs-Nachrichten 119 (3), pp. 83–94.

- Wagner, A., Stylianidis, E., Smagas, K., Trdlicka, J., Paar, G., Huber, B., Reith, C., Reiterer, A., 2013. Geo-Monitoring By High-Resolution Optical Sensors. In: Luhmann, T., Müller, C. (Eds.), Photogrammetrie - Laserscanning - Optische 3D-Messtechnik. Beiträge der Oldenburger 3D-Tage 2013. Wichmann, H, pp. 166–177.
- Wagner, A., Wasmeier, P., 2014. Flächen- und Feature-basiertes Monitoring mit Videotachymetern. In: Sternberg, H. (Ed.), Multi-Sensor-Systeme – Bewegte Zukunftsfelder. Vol. 75 of Schriftenreihe des DVW. Wißner, pp. 75–88.
- Wunderlich, T., Wasmeier, P., Wagner, A., 2014. Auf dem Weg zum geodätischen Universalinstrument – wie nahe am Ziel sind IATS und MS50? In: Terrestrisches Laserscanning 2014 (TLS 2014). Vol. 78. Wißner, pp. 177–192.
- Wagner, A., Wasmeier, P., Wunderlich, T., Ingensand, H., 2014. Vom selbstzielenden Theodolit zur Image Assisted Total Station. avn - Allgemeine Vermessungs-Nachrichten 121 (5), pp. 171–180.
- Wagner, A., Wiedemann, W., Wasmeier, P., Wunderlich, T., 2016. Improved concepts of using natural targets for geo-monitoring. In: 3rd Joint International Symposium on Deformation Monitoring (JISDM). pp. CD–ROM.
- Wagner, A., Wiedemann, W., Wasmeier, P., Wunderlich, T., 2016. Monitoring Concepts Using Image Assisted Total Stations. In: Paar, R., Marendić, A., Zrinjski, M. (Eds.), Proceedings of the International Symposium on Engineering Geodesy - SIG 2016. Croatian Geodetic Society, pp. 137–148.
- Zhou, Y., Wagner, A., Wunderlich, T., Wasmeier, P., 2016. Calibration Method for IATS and Application in Multi-Target Monitoring using Coded Targets. Journal of Applied Geodesy (ahead of print).

1 Introduction

1.1 Motivation

This thesis presents new monitoring approaches using Image Assisted Total Stations (IATS). These types of instruments unify the geodetic precision of total stations (TS) with the areal coverage of images. One or more cameras are integrated into or at the telescope of standard TS, forming this new class of instruments. Two different types of cameras are used: (1) wide-angle overview cameras with fixed focus, which are mounted at and rotate with the telescope, and (2) telescope cameras, which are installed coaxial[1] to the collimation axis and are subjected to the optical magnification and the variable focus.

Each image taken by an IATS camera – including the live video stream – is absolutely orientated by using the instrument's station, orientation, mounting offsets, and additional calibration parameters for high precision results. This means that the exterior orientation is directly known in the world or object coordinate system. In combination with image processing and recognition techniques, as well as the polar methods of the base instrument, new measurement approaches can be developed. By using image sequences of subsequent measurement epochs, objects or features are detected and tracked in fully automated operation.

Currently, the camera images are only used to ergonomically optimize the standard TS measurement procedure. For instance, the view through the telescope is replaced by transferring the image to a remote control. This feature is especially beneficial if the instrument is being used in one-man station mode. The image and video functionality is currently also used to support standard field survey tasks. Such functions include, for example, documentation, aiming support, or an overlay of the live video stream with measurements, planning data, or sketches.

Nevertheless, the full potential of a combined photogrammetric evaluation and analysis is not yet exploited in commercial systems. Based on the automatic detection and location of (interest) points, shapes, or textures in the camera image, almost any kind of signalized or non-signalized structure can be used as a target. Each extracted two-dimensional image coordinate can be expressed as a field angle in the object space by appropriate calibration parameters. Additional (reflectorless) distance information or alternatively, the spatial intersection of two directions, are able to deliver full 3D coordinates. These broad possibilities are useful for the development of automatic and autonomous monitoring systems based on IATS.

[1] In this thesis, coaxial camera and telescope camera are used equivalent.

The following sections of this thesis will present prerequisites and implementations of different monitoring approaches using IATS. These methods and case studies fully exploit the potential of integrated cameras in TS and are going beyond the present manufacturers' solutions.

1.2 Structure of the work

The work is divided into three main parts:

1. A detailed introduction to IATS is presented in Section 2, covering the historical development, current commercially available instruments, and research prototypes. An overview of the state of the art is given by indicating relevant research done with IATS. In Section 3, a definition of structural and geo-monitoring, as it is used in this thesis, is presented.
2. The main part, Section 4, contains a summary of the four publications of this cumulative dissertation. The most important results are summarized in short, and the individual contributions of the co-authors are declared. In the following, the full-text of each paper gives examples and case studies of new geodetic monitoring approaches.
3. A detailed discussion is given in the third part. The individual methods are compared based on selected features and the scientific contributions of the publications are described (Section 5). Possible future developments (Section 6) close this part and the thesis.

2 Image Assisted Total Stations

Many different sensors and measurement methods are combined in a total station (TS): highly accurate angle reading, electronic distance measurements (EDM) to prisms and (less precisely) to nearly any other surface, 2-axis inclinometer, Automatic Target Recognition (ATR), Global Navigation Satellite System (GNSS) positioning and others. TS with (additional) integrated cameras into or at the telescope are commonly denoted as Image Assisted Total Station (IATS). In literature, a number of alternative terms exist for this class of instruments: Photo-Theodolite, Video-Theodolite/-Tacheometer, Image Assisted Photogrammetric Scanning Station, and others. In particular, a differentiation was often made between video and image/photo. This fact was valid in the past, considering analog imaging devices and video cameras. Today however, no significant difference can be made when using a CCD or CMOS sensor. One could argue that there is a difference if the information is extracted from a single image (point of time) or a sequence; in other words, if it is a static or kinematic process[1]. With modern digital imaging sensors both measuring tasks are possible and no differentiation of the instrument is necessary. In the author's view, all instruments – either equipped with camera(s) and/or scanning functions – can be collectively referred to the term modern total station, or Image Assisted Total Station if special mention should be made to the imaging capability.

In the following section, the early development on IATS at the end of the 19th century (Section 2.1) will be presented as well as its disappearance from the market until its revival about ten years ago (Section 2.2). In between, most research was done based on prototypes (Section 2.3). A summary of the conducted research and its results based on commercial IATS and prototypes is given in Section 2.4.

2.1 Historical development

Looking back at the history of IATS, the development can be separated into two different lines, resp. areas of application: (1) A static, photogrammetric usage with the main intention to take images by a photogrammetric camera from a leveled, rotatable platform. These instruments were called Photo-Theodolites in case elements of the exterior orientation, partly or in its entirety, were determined by means of the instrument itself (Figure 2.1a). Named should be C. Koppe (Koppe,

[1] This is one reason that the term Video-Tacheometer is used in P-I. Another one is that it should be highlighted that the high frequencies were only possible using an IATS prototype instead of one of the commercially available instruments at that time.

1889) or S. Finsterwalder (Ott, 1895) representative of many others. In this development line, the theodolite served as supporting tool for photogrammetric surveys.

A further development (2) started shortly after World War II at the Institute of Applied Geodesy in Frankfurt (Germany), with first tests for automated aiming with theodolites based on differences of two currents in a photoelectric cell. Named as *Electronic Eye* (Figure 2.1b), this method was developed further to enable bearing accuracies of 1″ as mean of 6 sets of directions in the late 1950s (Gigas and Ebeling, 1957). Finally, this concept was commercialized with the introduction of the One-Man-System from Geodimeter in 1987, cf. Wagner et al. (2014b). Automated target aiming and tracking have hence become standard functions in all state-of-the-art TS. In this development line, photogrammetric methods are the supporting tool for the base instrument theodolite.

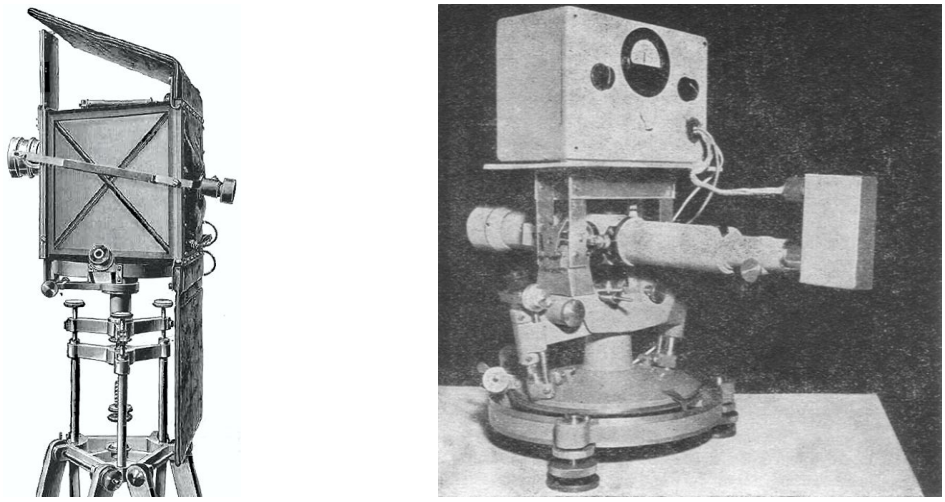

(a) (b)

Figure 2.1 – (a) Phototheodolite designed by S. Finsterwalter and reconstructed from Ott (1895)
(b) *Electronic Eye* of the Frankfurt Institute of Applied Geodesy (Gigas and Ebeling, 1957)

Instruments with ATR functions are, in the strict sense also IATS, since camera chips or segmented photodiodes are used for the detection. However, these sensors do not provide a useful image of the (measuring) scene and are not treated as cameras in the sense of an IATS. The reasons is that in most cases (1) the operator has generally no access to the image data, and (2) that only light in the spectrum of the measurement signal is detected by those cameras/photodiodes (Grimm et al., 2015).

When talking about the historical development, special mention should be made of Theodolite Measurement Systems (TMS) in the 1980s. Electronic theodolites equipped with imaging sensors were used to measure spatial forward intersections using two or more instruments. The automatic aiming to fixed target points or projected laser spots was realized by image analysis techniques. Most of these devices were used for industrial application. In particular notable is the Kern *E2-SE* (Gottwald, 1987) and the Wild *TM-3000V* (Katowski, 1989). With the marked launch of laser

trackers systems in 1991, TMS – and therefore theodolites with built-in cameras – were replaced within a few years.

It took until the year 2005, when Topcon released the *GPT-7000i* system and brought cameras back into theodolites, resp. total stations, for a new generation of IATS to be spawned. More details on this era is given in the next section.

A more extensive overview to the historical development can be found in Wunderlich (2005) or Wagner et al. (2014b).

2.2 Current commercial systems

The current generation of most commercial IATS was – as mentioned previously – introduced by Topcon in 2005 with the instrument *GPT-7000i* after the long gap following the retracted image assisted TMS. The instrument was distributed under the slogan „Capture Reality“ and was already equipped with two different VGA cameras: (1) a wide-angle camera with a fixed focus mounted next to the telescope so that it could rotate with it, and (2) an additional coaxial camera which records the operator's view through the telescope including the variable focus. The images of these cameras differ widely. The first camera has a large field of view (FOV) covering 28° x 22° and gives an overview of the surveying area. The second camera benefits from the magnification of the telescope, resulting in a very small FOV, but providing a more detailed view (Topcon, 2004). The successive model *GPT-9000Ai* (released in 2007) was equipped with an automated focus and remotely controllable actors. It could therefore be used as one-man station, without any need for the operator to stand behind the instrument. It was also the first device which combined imaging and scanning via an additional simple scanning function (up to 20 points per second) into IATS (Topcon, 2007). Meanwhile, these kinds of instruments are distributed by Topcon under the term *Imaging Station*, currently in the 3rd generation, Figure 2.2a. Both cameras working with a resolution of 1280 x 1024 pixels. A 10 Hz live video can be streamed to the instrument or to a remote control display (Topcon, 2012).

Trimble released its first IATS under the name *VX Spatial Station* in 2007. The device came with a fixed focus 3 megapixel (MP) color camera and a FOV of 16.5° x 12.3° (Trimble, 2010). The same overview camera is also integrated into the following high-end total stations series, including the current Trimble *S9* (Trimble, 2015), Figure 2.2b. The photogrammetric analysis of the calibrated camera images (post processing), the live 5 Hz video stream, panorama stitching, and measurement data overlay are called "Trimble Vision" which are similar to the Topcon concept. A simple scanning function with up to 15 points per second is also available, including the possibility to colorize the scan points based on the captured image data.

The integrated overview cameras of the Pentax *Visio* instruments (introduced 2009, Figure 2.2c) provide the smallest FOV of all currently available IATS, with 7.0° x 5.3°. The resolution of 3 MP is comparable to the Trimble devices. The video stream rate is specified at 10 Hz (Pentax, 2013).

(a) (b) (c) (d)

Figure 2.2 – Current available IATS: (a) Topcon *IS-3* (b) Trimble *S9* (c) Pentax *Visio* (d) Leica *Nova* (source: respective manufacturer)

Interesting is also the modular construction. The camera and the control screen are a compact unit above the telescope which can be exchanged with the corresponding component at a non “vision” instrument. Thus it can be transformed into an IATS.

Leica Geosystems followed 2010 as the last major manufacturer implementing a built-in overview camera in the *Viva* instrument series. The 5 MP camera has a FOV of 15.5° x 11.7° (Leica Geosystems, 2012) and is used for similar supporting functions as the above mentioned devices. Instruments of the succeeding *Nova* series, released in 2013, (Figure 2.2d) provide an additional focusable ocular camera, similar to the Topcon *Imaging Station*. The camera FOV is reduced to 1.4° x 1.1° as the images are taken through the telescope and therefore magnified 30 times (Leica Geosystems, 2015). A special feature of this instrument is the advanced scanning function with up to 1000 points per second, which is comparable to (“real”) laser scanners of the first generation. Based on this accelerated scanning performance and the imaging component of the device, the combined scan and image analysis approach of P-IV was developed.

A new generation of IATS was presented in October 2016 by Trimble with the instrument *SX10*, Figure 2.3. It is the first total station – distributed commercially – that completely omits an ocular. Previously only a TS prototype *SET3110MV* from Sokkia was presented without ocular in 2002, however, it was never launched as a product (Wasmeier, 2009a). The new Trimble instrument is sold as "Scanning Total Station" which combines surveying, imaging, and 3D scanning in one solution. Three different 5 MP cameras (overview, primary, and telescope) with varying FOV support the user in controlling the device. The maximum scan rate is stated at 26,600 points per second, at a range of up to 600 m (Trimble, 2016). The instrument is therefore ideally suited for a combined analysis of scan and image data as described in P-IV.

There is some controversy as to whether the Trimble *SX10* can still denoted as an IATS. One could argue that the imaging component is no longer only a supplementary supporting feature. Instead, the camera(s) is now mandatory due to the absence of the ocular. A camera is needed for the

Figure 2.3 – Trimble SX10 (Image: Trimble Inc.)

operator to control the device, in particular aiming towards a specific direction. However, it is still (correctly) classified as a total station from the manufacturer. There are TS characteristics, like a rotatable telescope, single point determination, the output of angle and distance values, and the possibility to stake out points. IATS is therefore also a valid definition of the instrument, as this term has been generally accepted for total stations with integrated cameras.

Common in all above mentioned commercial instruments is that the images and video streams are used to only support the conventional surveying workflow. The standard measurement procedure is optimized, e.g. by replacing the view through the telescope and transferring it to the range pole via remote control. It is possible to aim with the instrument to a direction selected by a pixel in the (live) image (sometimes denoted as "tap and turn" function). An image can be taken automatically of each measured or set-out point for documentation purposes. It is possible to visualize these points, planning or sketch data as an overlay to the live camera stream. Additional software enables photogrammetric measurements in post-processing, e.g. the generation of points by intersection. If a scanning function is available at the instrument, additional image based support functions like a scan area selection are offered. Further information can be found, e.g. in Lienhart (2011), Müller (2009) or at the manufacturers' websites.

Nevertheless, the full potential of IATS is not yet used by the commercially available devices and their functions.

2.3 Research prototypes

A number of instrument prototypes have been used for research purposes next to commercially available IATS. In particular, the developments over the last 15 years significantly influenced current instruments, as well as the work at hand.

Easy access to the measurement and image data is important for the research and development of new survey and analysis methods for IATS. To guarantee this, two different approaches were used in the scientific community: (1) standard total stations which are permanently modified as research prototypes, and (2) modular systems in which a clip-on camera exchanges the eyepiece of a total station temporarily.

The main advantage of the first approach is the fixed connection between camera and base instrument, ensuring the constancy of calibration parameters. Wasmeier (2003), for instance, used a modified Leica *TCA2003*, where the ATR chip could be read out by an additional video output. At the University of Bochum, a Leica *TCRM1102* was extended by three different cameras. The instrument – designated as system *TOTAL* – consisted of an ocular, a telephoto, and a wide-angle camera (Scherer, 2002). Another Leica TPS1100 series instrument was used by Walser (2004), named *IATS* (Figure 2.4a). The succeeding prototype *IATS2* (Figure 2.4b) built in a (very) small-series production in 2008, is i.e. used in this thesis (P-I & P-II) and there described in more detail. A base instrument from the company Zeiss (now Trimble) was used by Vogel (2006) to develop a new calibration model.

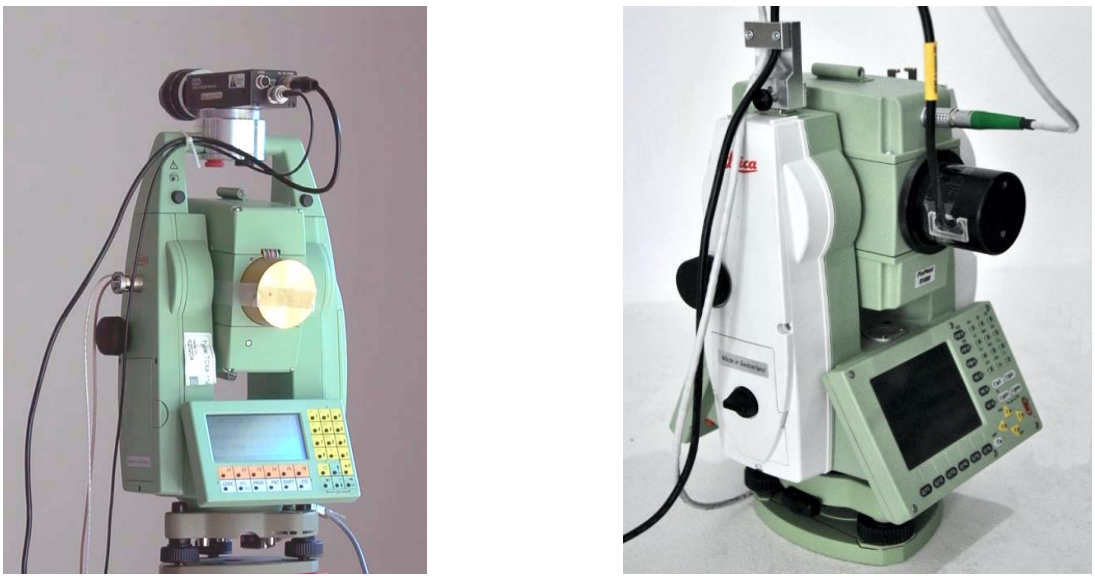

(a) (b)

Figure 2.4 – Examples of permanently modified instruments (a) *IATS* (Walser, 2004) (b) *IATS2*

In the second modular approach, cameras are attached to, resp. exchanged with the eyepiece of a base theodolite. The main advantage is that a standard surveying instrument may be used as an

IATS only for a specific task and, if desired, disassembled back to its original state. Examples of such systems are described by Machotka et al. (2008) (Figure 2.5a) and Bürki et al. (2010), the latter is denoted *DAEDALUS*. Both cameras are primarily designed for astro-geodetic measurements. A system for exclusively terrestrial usage, named *MoDiTa*, is developed and used by the i3mainz (Hauth and Schlüter, 2009), Figure 2.5b.

(a) (b)

Figure 2.5 – Examples of modular IATS systems from the (a) Brno Univerity of Technology (Machotka et al., 2008) (b) i3Mainz (Hauth and Schlüter, 2009)

All of the above mentioned prototypes – either modifications or modular cameras – utilize a coaxial camera configuration (among others). This means the images of the telescope's visual field are projected onto a camera chip. The main advantage of this approach is, that the optical magnification of the telescope can be exploited, resulting in a high resolution (low ground sampling distance) of the camera image. Another approach is the biaxial alignment of the optics of the theodolite and the CCD-camera. Therefore, it is not necessary to install a complex beam splitter element and the telescope view remains preserved, i.e. it is technically less complicated (Walser, 2004). In the past, a lot of research was done using such instruments, e.g. Wester-Ebbinghaus (1988); Huang (1992); Chapman et al. (1994); Chikatsu and Murai (1994); Hovenbitzer and Schlemmer (1997); Gong et al. (1999); Varshosaz et al. (2000); Zhang et al. (2004); Sakimura and Maruyama (2007); Zhu et al. (2011). All current commercially available IATS use at least one camera in this biaxial configuration to give an overview of the scene (Section 2.2). However, the different lines of sight (of the camera and the telescope) lead to parallactical errors which must be considered. As described in P-IV, the position of the physical crosshair of the theodolite can only be mapped into a non-coaxial camera image if the object distance is known.

As part of a separate group of devices, a pan-tilt-system developed by Uffenkamp (1995) should also be mentioned. The instrument is comparable to an IATS, but here a camera entirely replaces the telescope. The measurement method differs in the data analysis from the work described in this thesis and is more comparable to the former Photo-Theodolites (Section 2.1). The camera is the central element of the instrument and is mounted rotatably. The image processing, in particular the panorama generation, is based on bundle block adjustment instead of theodolite axis readings. A similar concept is presented by Lato et al. (2012).

2.4 Previous research

In this section, a brief summary of previous research using Image Assisted Total Stations is given. However, this list does not claim to be exhaustive.

A lot of research was done at the Vienna University of Technology under the supervision of Prof. Kahmen (Kahmen, 1993). Basis of many publications was, in particular, the instrument *TM-3000V* (Section 2.1). Fabiankowitsch (1990) developed a target detection approach based on difference images. Roic (1996) worked on image pre-processing for (semi-)automatic acquisition and analysis of non-signalized objects. A measurement system using an interest operator for point selection of non-signalized points and two video-theodolites in master and slave mode is described in Mischke (1998). De Seixas (2001) developed a scanning method based on different grid-line methods, which was continued by von Webern (2007). A high frequency and strictly synchronous observation of simultaneous reciprocal zenith angles by two *TM-3000Vs* was realized by Kabashi (2003). Reiterer (2004) used a knowledge-based decision system to choose the best suited pre-processing strategy, image analysis, and target selection for IATS measurements. This was advanced to a deformation measurement system based on stereo IATS (Reiterer et al., 2009). The last mentioned work delivered the basic idea for the long range geo-monitoring system presented in P-II. The image processing algorithms in both projects were implemented by Huber (2014) from the Graz University of Technology (Institute of Remote Sensing and Photogrammetry).

At the Technical University of Munich (TUM), Schirmer (1994) used a CCD camera attached to a KERN *DKM 3-A* theodolite for astro-geodetic measurements as continuation of the work of Schnädelbach (1966). Under supervision of Prof. Wunderlich, research contributions appeared i.e. based on the previous mentioned modified Leica *TCA2003*. Wasmeier (2003) used the ATR camera for automatic targeting based on object recognition. Despite the reduced contrast quality due to the infrared sensitivity of the system, non-signalized targets could be automatically measured with comparable accuracy as from a human operator. The prototype *IATS2* was used for the evaluation and combination of two existing calibration models (Wasmeier, 2009a), for monitoring using natural (Thuro et al., 2010) or artificial targets (Wagner and Wasmeier, 2014), see Figure 2.6. This prototype was utilized in an approach to model atmospheric refraction influences by optical turbulences (Reiterer, 2012). The publications P-I and P-II also belong to the application list of

this instrument. Meanwhile state of the art instruments are used at the TUM, as shown in P-III and P-IV or Wagner et al. (2016a), Wagner et al. (2016b), Zhou et al. (2016a) and Zhou et al. (2016b).

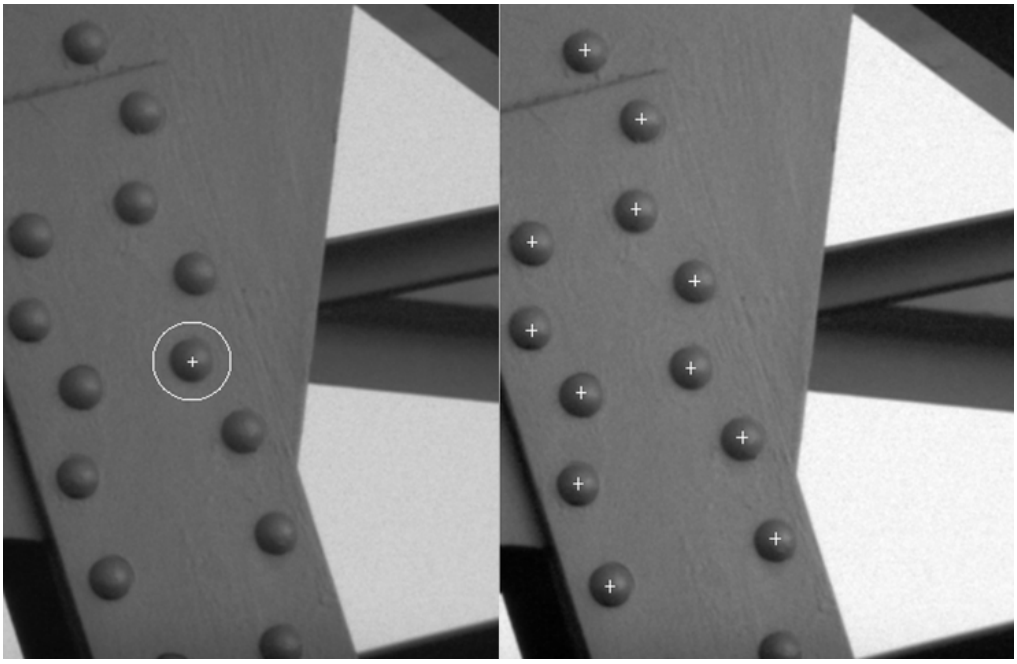

Figure 2.6 – Template matching of non-signalized artificial targets: training pattern (left), highlighted detected objects (right) (Wagner and Wasmeier, 2014)

The IATS prototype *TOTAL* was developed by Scherer (2002) at the Ruhr-Universität Bochum. It is used for architectural surveying, e.g. to generate ortho-images derived from rectification on-site or intelligent scanning (Scherer, 2004). A relationship between image coordinates and geodetic directions based on a gnomonic projection is given in Juretzko (2004).

At the Swiss Federal Institute of Technology (ETH) Zurich used Flach (2000) the *TM-3000V* and the Monin-Obukhov similarity theory to determine the current atmospheric refraction coefficient. Hirt et al. (2010) conducted simultaneous reciprocal vertical angle measurements and the modular IATS *DAEDALUS* (cf. Section 2.3) for the identical task. This system was designed and developed at the ETH, primarily for automated on-line astro-geodetic measurements (Bürki et al., 2010), but it is also used for many other applications, like vibration measurements or micro-triangulation (Guillaume et al., 2012, 2016).

Knoblach (2009) developed a suspended IATS (i.e. an instrument in hanging position) at the TU Dresden under supervision of Prof. Möser. The system can be used in shaft plumbing or industrial metrology. Ullrich et al. (2012) implemented an automated geometrical alignment using the ocular camera of an IATS. Both methods are based on the modular IATS *DAEDALUS*. The commercially available Trimble *VX Spatial Station* is used for clearance gauge measurement in railway applications, as described in Möser and Müller (2010).

At the University of Applied Sciences Mainz and its institute i3Mainz, the aforementioned modular system *MoDiTa* (Section 2.3) was developed and used for academic research. Application examples include the calibration of inclination sensors and the control of the long-term stability of lasers and tripods (Hauth et al., 2012). High-speed image analysis and monitoring tasks in the kilohertz area have also been tested (Hauth et al., 2013).

Next to the above mentioned work of Huber (2014), IATS research is being conducted at the Institute of Engineering Geodesy and Measurement Systems at the TU Graz. The focus of the research group, under the supervision of Prof. Lienhart, is on applications using state of the art IATS. Examples include accuracy assessments and strategies for high accurate measurements (Ehrhart and Lienhart, 2017) and vibration monitoring (Ehrhart and Lienhart, 2015b). The last cited work is especially worth mentioning, as it is the continuation of the approach presented in P-I. The concept, on the one hand, is transferred to a commercially available instrument. On the other hand, additional image analysis concepts are presented, which are generally based on non-signalized structures.

Currently, very few articles exist, using state of the art IATS for monitoring applications beside these publications. Mentioned should be Huep (2010), which describes a crack detection method based on a Trimble *VX Spatial Station* and the already stated work of Möser and Müller (2010).

Further literature on previous research can be found i.e. within the conference proceedings "Optical 3-D Measurement Techniques" (1989 - 2009) organized by Prof. Kahmen (TU Vienna) and Prof. Gruen (ETH Zurich).

2.5 Calibration

The use of an appropriately calibrated system is an essential basis for the above mentioned research. This allows any two-dimensional image coordinate to be expressed as a field angle in the object space. All intrinsic and extrinsic parameters are known for each captured image, which means that the images are directly geo-referenced. They can be used for direction measurements with no need for object control points or further photogrammetric orientation processes.

Instrument manufacturers have generally supported academic research projects covering different calibration methods of integrated cameras. For example, Walser (2004) used the previous mentioned prototype *IATS* in cooperation with the company Leica Geosystems. He described the camera with an affine chip model and developed a combined approach for camera and instrument calibration. Vogel (2006), in contrast, was supported by Trimble and extended the collinearity equations by additional camera parameters to describe the pixel to angle relationship in IATS. Both mentioned methods are compared and combined by Wasmeier (2009a). Other publications dealing with IATS calibration worth mentioning here are Bürki et al. (2010); Juretzko (2004); Schlüter et al. (2009); Ehrhart and Lienhart (2017) and Zhou et al. (2016a).

All of these methods are based on an array of virtual control points for data acquisition during calibration process. In reality, this array consists of only one single "real" point, measured multiple times by rotating the telescope (incl. camera). The approach is based on the work of Huang and Harley (1989) and suited for all cameras mounted rigidly on the telescope of a theodolite, especially for IATS.

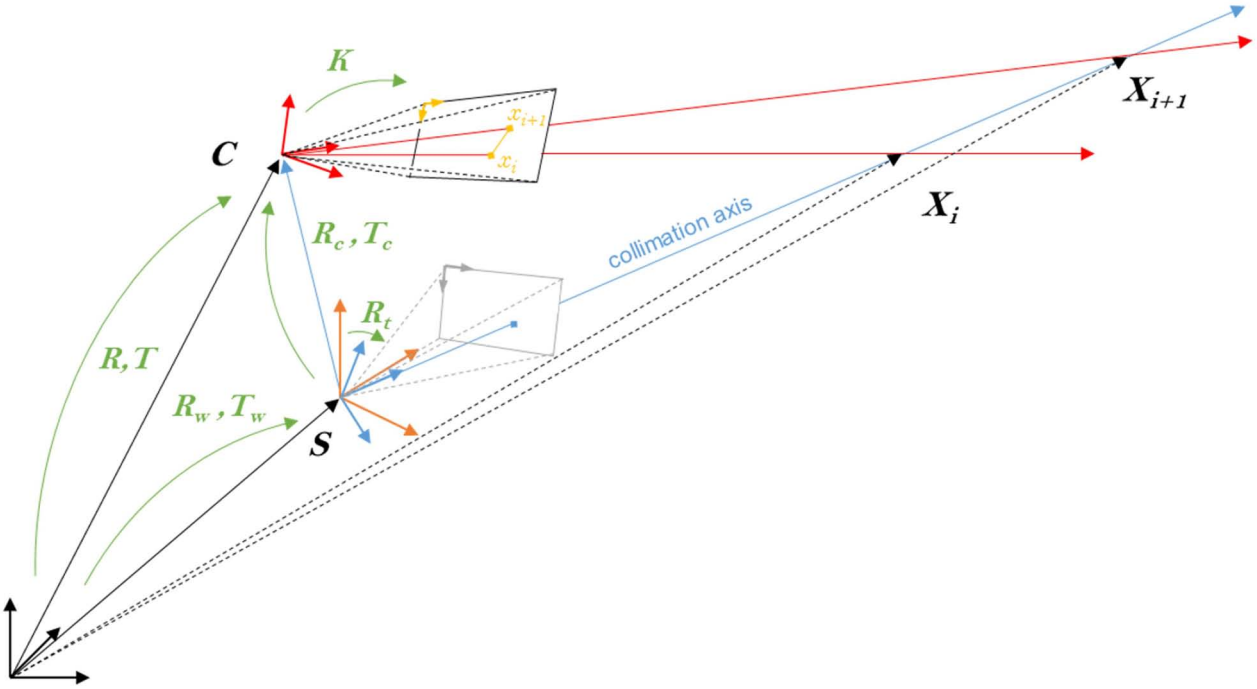

Figure 2.7 – Transformations needed to convert image coordinate as theodolite angles and vice versa (modified from P-IV)

P-IV provides more details regarding the individual calibration methods and also includes a description of the different transformations, which are necessary to convert 3D world coordinates into theodolite angles and vice versa. As shown in Figure 2.7, the conversion consists of a combination of three different Euclidean transformations:

1. Transformation from the world or object coordinate system into the theodolite coordinate system ($\boldsymbol{R}_w, \boldsymbol{T}_w$).

2. Transformation (pure rotation) into the telescope coordinate system ($\boldsymbol{R}_t$).

3. Transformation into the camera coordinate system ($\boldsymbol{R}_c, \boldsymbol{T}_c$).

In the case of overview cameras, for which the projection center must be different to the total station center, the collimation axis is projected as a line into the image, cf. Figure 2.7. This means the point to which the instrument is aiming can only be displayed precisely within the image if the object distance is known.

In order to achieve the highest possible accuracy, it is more advantageous to use a coaxial camera which benefits from the high magnification of the telescope. Therefore, the further parts of this thesis are based on this type of camera only.

As shown in Wagner and Wasmeier (2014), resp. Briechle (2014), an appropriate calibration model must be chosen for the individual application task. Figure 2.8 and 2.9 depict the residuals of two different exemplary models: a gnomonic projection as described in Juretzko (2004) and the combined approach of Wasmeier (2009a), based on work done by Walser (2004) and Vogel (2006).

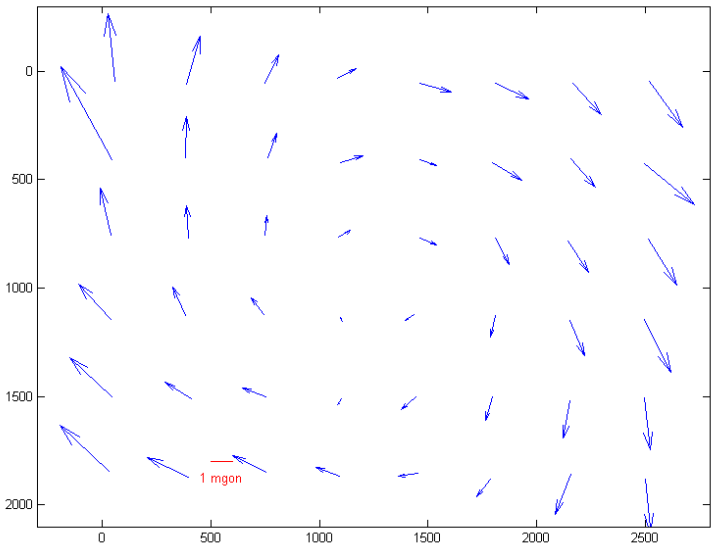

Figure 2.8 – Residuals using a gnomonic projection as calibration model

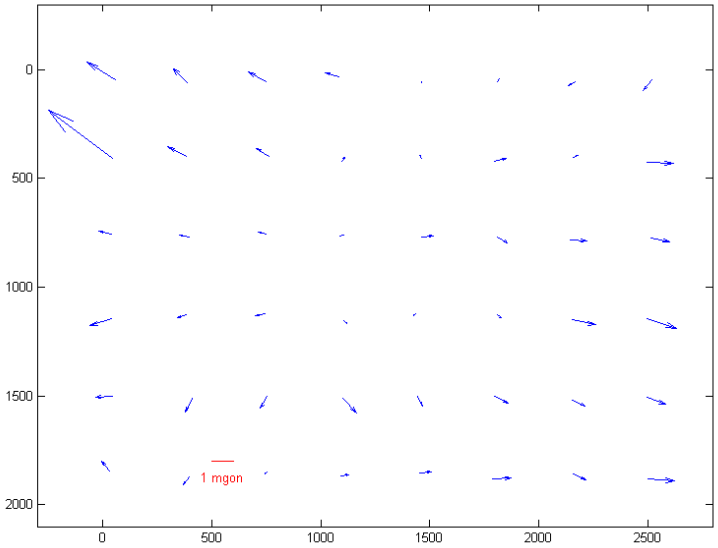

Figure 2.9 – Residuals using the combined approach as calibration model

In this exemplary calibration of a Leica *MS50* instrument, the first method delivers a mean residual of 1.7 mgon and clearly visible systematic errors (Figure 2.8). The existing camera chip rotation

cannot be directly considered in the mathematical model and influences the results, in particularly at the image borders.

In contrast, the result of the combined calibration approach has a mean residual of 0.5 mgon, not considering the clear visible outlier (Figure 2.9). In this mathematical model, a camera rotation around the line of sight is considered, as well as different distortion parameters.

This example shows the importance of the calibration model used. For some applications, like a coarse target selection (tap and turn) or for overlay functions, the first method will be sufficient. However, more precise and accurate monitoring tasks mandate the use of advanced methods. It should be noted that the first approach can be extended by rotation and distortion parameters. For demonstration purposes the simplest form was used.

Ehrhart and Lienhart (2017) present similar experiments, further prerequisites, and additional strategies to archive the highest possible accuracy for measurements done with the telescope camera of IATS.

3 Monitoring

3.1 Definitions

Monitoring is one of the fundamental tasks in engineering geodesy, next to site surveying and setting out[1], cf. DIN 18710-1 (2010). It is the process of repetitive or continuous check and control of artificial or natural structures. Key aspect is to (periodically) gather information about the current state of the observed object (Settles et al., 2008). In the case of geodetic monitoring, the main objective is the determination of changes in the geometry, position, or orientation. The measurements and results must be reliable and tested for significance.

This thesis deals foremost with two subtypes of geodetic monitoring: structural monitoring and geo-monitoring. These two terms are described in the following as used in this work. However, these definitions do not claim general validity.

- **Structural monitoring** refers to the measurement and evaluation of civil engineering structures such as: bridges, dams, railways, or tunnels, i.e. in general of man-made objects.
- **Geo-monitoring**, in contrast, is used as a term for the determination of changes, movements, or deformation of natural structures, such as mountain slopes.

3.2 General development

In recent years, a general trend towards automated and autonomous monitoring has been observed. One of the main reasons for this trend is economics. Rising personnel costs lead to a continuous reduction of manpower in survey groups, resulting in a fully autonomous data acquisition. In particular, monitoring applications are predestined for automation due to (pre-)defined observation points and repeating measuring epochs. Next to personnel costs, the general price pressure on construction projects is pushing the autonomous trend. Additionally, the budgets of the public sector (municipalities, cities, etc.) in their role as contractee are permanently low.

Another reason for the increased presence of automated and autonomous measuring is the increased demand for 24/7 monitoring. Dense building development and riskier construction projects require a continuous control of predefined thresholds. This also includes construction in hazardous

[1] Wunderlich (2013) goes a step further and extents this list by a fourth task: navigation.

locations, which have not been used in the past, e.g. buildings or infrastructure in avalanche prone regions. Climate change and, in particular, the degradation of permafrost are also influences. Previously stable areas are changing into risk regions.

Today, geodetic monitoring systems can be used much more frequent and for other applications as in the past. On the one hand the instrumental conditions have become more favorable; hi-tech hardware components and software programs specially designed for monitoring applications are becoming increasingly available on the market at a lower price as compared to the past. Monitoring systems, on the other hand, are meanwhile also being used in advance of building activities to study normal construction behavior, e.g. to detect daily and yearly deformation cycles (Wasmeier and Reith, 2009). Other new use cases are the monitoring of damaged infrastructure which will not be repaired or replaced for reasons of economy, e.g. Schäfer et al. (2006). Considering the aging infrastructure, especially the high number of bridges in need of rehabilitation in Germany, a huge opportunity for geodetic monitoring systems and IATS is emerging.

IATS can be applied in stationary monitoring systems in the same way as periodically or temporarily installed systems. The benefit of the additional camera(s) starts with the possibility of a visual site check via remote, i.e. there is no need to go there physically. It enables to gather additional supporting information for the standard TS measuring task, such as the automated extraction of prism constants from coded targets attached to corresponding reflectors (Zhou et al., 2016b), ending with the fully automated extraction of measurement elements/information of captured images, as will be shown in the further parts of this thesis.

3.3 Research question

A Terrestrial Positioning System (TPS) is the conventional geodetic method for monitoring, if not even the standard method. High accurate 3D polar vectors can be measured sequentially from a station point to co-operative prisms automatically, in some cases and with restrictions also to any kind of surface. Due to the ability for automated operation, low data volumes (to process or to transfer), and high flexibility, automatic monitoring systems based on total stations are widely spread. The data analysis strategies range from the simple comparison of measurement values to highly sophisticated network adjustment and deformation analysis methods. To summarize, TPS monitoring systems and their evaluation methods are well studied and successfully established in practice.

As presented in Section 2, IATS are an extension of the TPS hardware by one or more additional cameras and thus ideally suited for monitoring tasks. However, so far missing is the integration of these additional sensor(s) into the evaluation methods and analyzing software. The aim of this integration is to make use of the full potential of the IATS hardware. As shown in the previous section, the monitoring developments point an increased demand and thus a chance for an increased use of IATS. The high potential for automatic and autonomous operation must be exploited, par-

ticularly in the fields of structural monitoring and geo-monitoring. The current implementations of the instrument manufacturers (Section 2) do not give sufficient solutions for the possible applications.

Terrestrial Laser Scanners (TLS) are other widely spread geodetic instruments used in monitoring applications. The contactless, rapid acquisition of dense point clouds over large areas are the main advantage of this kind of sensor and the reason for its abundant usage. TLS measurements do not, however, provide identical points between repeated scans, and a direct comparison of discrete points is not possible. In most cases, statistical tests of significance are missing if deformations of two TLS measurement epochs are compared. This is often done based on visual representations (e.g. heat maps) and straightforward comparison of deformations with fixed thresholds. In some cases, even by simple line of sight differences only (Wunderlich et al., 2016).

A system is missing (hardware, software, strategies) which unifies the advantages of the existing geodetic monitoring systems: TPS delivers deformation vectors including statistical tests of significance, but only for single polar vectors. TLS instead enables areal monitoring, but without any attested significant results.

The publications presented in Section 4 will give examples of such kind of sensor fusion using IATS, in particular in structural monitoring and geo-monitoring applications.

4 Publications

This section summarizes the four publications that form part of this cumulative dissertation. The most important results are described and the individual contributions of the co-authors declared. In the following, the respective articles are included in full-text.

P-I: Bridge Monitoring by Means of Video-Tacheometer - A Case Study

In this paper, a method for structural monitoring using IATS is presented. The movement of one of the world's longest suspension bridge is examined by active LED targets attached to the construction. Image analysis algorithms are used to evaluate the position of the target in the orientated images and to derive oscillation frequencies in real time. Additional tests show applications with multiple targets and the ability of a high frequency analysis.

For this work, an IATS prototype with a direct wire connection to the telescope camera was used. This direct bus enables high data transfer rates to an external PC. At the time of the measurements, no suitable comparable commercial instrument was available on the market, resp. only instruments with overview cameras. Meanwhile, the approach is transferred to a state of the art (commercial) product by Ehrhart and Lienhart (2015a).

Using video-theodolites or IATS for this use case brings several advantages. It is possible to inherit all possible photogrammetric techniques (even stereo photogrammetry, see P-II) and to combine them with classical methods of total stations. The exterior orientation can be determined by (optical) tie points or terrestrial control points equipped with reflectors. Even the additional use of GNSS antennas is possible. The stability of the station can be controlled by the internal inclinometer as well as any kind of above mentioned orientation measurement. The system is mobile, quick to deploy, and can be used permanently and/or discontinuously for only a couple of hours or days.

Declaration of the individual contributions

The content of the paper has been elaborated by the author of this thesis and a number of co-authors. The idea to use a video-tacheometer for bridge monitoring originated from Prof. Dr. Wunderlich and Dr. Wasmeier during the proposal of the Alexander von Humboldt-Foundation (AvH) research project. The actual measuring concept incl. software development, design of the LED-targets, measurement, and analysis were done by the main author. Ch. Reith supported the time series analyses. The conception of the paper, creation of figures, and writing of the first manuscript

version were done by A. Wagner. The co-authors helped to improve the manuscript through discussion and comments on the content.

P-II: Long-Range Geo-Monitoring using Image Assisted Total Stations

This paper presents a method for high-resolution, long-range survey of geo-risk areas using two IATS devices in stereo configuration. Five different terrestrial geodetic geo-monitoring methods are described and their main features are compared in a compact form. It is shown that the use of two IATS is particularly suited for the acquisition of areal and highly accurate information without any need for site access. The practicability of the approach is demonstrated and the achievable 3D point accuracy is derived theoretically and proven practically by ground truth data.

The limited field of view of the instrument's telescope camera is extended by taking multiple images. These image bundles are acquired on each of the two instrument stations and composed to two separate spherical panoramas. Corresponding points in both panoramas are searched by computer vision tools, in this case, using the dense matching algorithm HFVM. Direction values are calculated from the found pixel positions and used for spatial intersections to generate a 3D point cloud.

A use case in a clay-pit, where a temporary local control network was installed is presented. In this experiment, the usability and accuracy of the method are demonstrated by comparing the results with TPS and TLS ground truth data. It is shown that dense point clouds with high single point accuracy, including information about their precision, are generated.

The main advantage of such a system is the detection of distinctive points in contrast to an unstructured point cloud. If point correspondences are found in subsequent measurement epochs, it is possible to derive 3D displacement vectors directly. This may be used to determine rigid body motions of objects and surface patches directly.

Declaration of the individual contributions

The content of the paper has been elaborated by the author of this thesis and a number of co-authors. The basic idea for this monitoring approach is based on a former research project (Reiterer et al., 2009) and has been improved and enhanced to a practically usable product in co-operation with the authors of this paper. The IATS control software was written by A. Wagner, the practical measurements were carried out by the first three authors of the paper. The feature generation and stereo matching were done by B. Huber, the further analysis of the IATS, TPS, and TLS data was performed by A. Wagner, supported by W. Wiedemann. The conception of the paper, creation of figures, and writing of the first manuscript version were done by A. Wagner. The co-authors contributed to the publication through discussions of the results and very constructive iterations of the manuscript.

P-III: Using IATS to Read and Analyze Digital Leveling Staffs

The paper describes the implementation to read and analyze the code pattern of a digital leveling staff using an IATS. With this new approach it is possible to automatically transfer the total station's transit axis height from a benchmark. An automated monitoring system, for example, can use this function to regularly check its station height. Furthermore, leveling staffs or short barcode stripes may be installed at the observation points, as used in automated leveling systems. Height changes can be measured with high precision. In contrast to existing leveling systems, it enables the use of non-horizontal sightings.

In the paper, the staff code pattern of a widely used manufacturer is described and its demodulation explained. A step-by-step program sequence provides a detailed insight at the methodology of the approach. Contrary to the decoding method implemented in leveling instruments, an alternative concept is presented. Different experiments study the precision and accuracy of the method and prove the leveling capabilities of IATS.

Declaration of the individual contributions

The content of the paper has been elaborated by the author of this thesis and a number of co-authors. The idea of using an IATS to read and analyze digital leveling staffs originated from A. Wagner. The methodology, including the alternative decoding method and development of the software code were done by the first two authors. The conception of the paper, the creation of figures, and the writing of the first manuscript version were done by A. Wagner. The co-authors helped to improve the manuscript through discussion and comments on the content.

P-IV: A new approach for geo-monitoring using modern total stations and RGB + D images

In this paper, a new approach for geo-monitoring using scanning IATS is presented. The main feature is the combined analysis of image and scan data to detect object movements. Modern total stations are able to scan objects in the same way as terrestrial laser scanners TLS, albeit with a far lower acquisition rate. This ability may be used in combination with images, taken by the instrument's telescope camera, for a fused data processing using RGB + D (Red Green Blue + Distance) images.

The article describes how an image bundle of the pre-selected region of interest is taken and composed to a spherical panorama. Point cloud data of a subsequent scan using the EDM of the total station is processed to an image channel "D". Therefore, the distance information is converted into a depth image in the same resolution as the RGB (Red Green Blue) image (channels). Each pixel coordinate of the RGB + D image can be expressed as theodolite angle and distance from the station, i.e. a full polar coordinate can be specified. If a correspondence is found in two RGB + D

images, e.g. of two subsequent measurement epochs, a 3D displacement vector can be directly calculated from both pixel coordinates.

Both acquisition types described in the article complement each other. TLS data is well suited to detect changes in line of sight between two data sets. In image sequences, such variations are hard to uncover. By contrast, displacements in transverse direction can be identified easily by image and template matching algorithms, while the evaluation of such displacements in laser scanner data weakens. The method is therefore ideally suited for scanning IATS and uses the full potential of this instrument type.

Declaration of the individual contribution

The content of the paper has been written exclusively by the author of this thesis.

4.1 P-I: Bridge Monitoring By Means Of Video-Tacheometer - A Case Study

Author: Andreas Wagner, Peter Wasmeier, Christoph Reith and Thomas Wunderlich

Publication: avn - Allgemeine Vermessungs-Nachrichten, 8-9/2013, pp. 283-292, 2013

Abstract: Built-in cameras are nowadays standard in modern total stations, but their possible potential of photogrammetric evaluation and analysis is not yet used. This article describes a research project for bridge monitoring using such an instrument at the Fatih Sultan Mehmet Bridge in Istanbul. By image processing algorithms an active LED target is detected and by using the exterior orientation of the total station brought directly into a suitable coordinate system. Thus, additional reference marks in the camera image become obsolete. After the description of the system the practical usability for detecting bridge motions is confirmed by two test measurements and a number of oscillation frequencies derived. So this article shows an example of additional measuring tasks for which video-tacheometer can be employed.

Keywords: Bridge monitoring, Fatih Sultan Mehmet Bridge, Image Assisted Total Station, LED Targets, Structural Monitoring

4.1.1 Introduction

Since bridges are exposed to strong loads, varying load conditions, changing weather conditions as well as associated material stressing, regular control monitoring for the material fatigue as well as of pending damage is essential for early detection of damage. A too late assessment (of damage) does not only increase the general risk, but also raises the costs of structural reinforcement significantly.

Contactless measuring sensors like total stations and photogrammetric cameras are often used for bridge monitoring in which each approach has individual advantages. With photogrammetric measuring techniques it is e.g. possible to simultaneously measure (monitor) an almost infinite number of targets. Thereby signalised and non-signalised targets can be used and high sampling rates are possible. In order to gain 3D information usually two digital cameras are necessary. This can also be obtained by a single total station, however, with non-simultaneous targeting. Observations to stable points enable the relation to a superior coordinate system and the proof of the stability of the station. Recording the inclination values of the total station it is additional possible to detect vibrations of the station (within the sampling rate of the instrument). Through the quick installation and orientation the sensor is applicable in a permanent and discontinuous measurement system.

A video-tacheometer or Image Assisted Total Station (IATS) – an image capturing system in addition to a polar 3D point measurement system as described in Section 4.1.2 – rep-

resents a combination of all advantages mentioned above. Thus, it is obvious to test the use of such a new system for bridge monitoring as described in this article. Bürki et al. (2010) already executed a similar test with a torch light attached to a bridge. Within a project granted by the Alexander von Humboldt Foundation, our realisation goes a step further by using solidly mounted LED (light-emitting diodes) clusters and a permanent station on a pillar with stability proof. A verification by a standard photogrammetric approach was planned as well.

The present paper describes a case study of a bridge monitoring at the Fatih Sultan Mehmet Bridge (Section 4.1.3) in Istanbul, which was performed in cooperation with the Division of Photogrammetry of the Istanbul Technical University (ITU). Our partners were in charge of the simultaneous measurements with classical photogrammetric methods.

As functional specification our system should be able to measure day and night, detect assumed displacements of the bridge deck of $\pm$ 30 cm in vertical and $\pm$ 15 cm in horizontal direction (Apaydin, 2002). To be comparable to the tests of ITU, we planned to record with a similar acquisition rate of 24 fps (frames per second). The main focus is to detect significant frequencies of the bridge movement and compare them with ITU results as well as previous theoretical and practical analyses. According to the approach of structural health monitoring, e.g. Wenzel (2009), changing frequencies give a hint to structural damage of the object.

The following section describes the system components: the prototype of an IATS, the LED targets, the analysis software and strategy used. Section 4.1.3 presents and analyses the measurements in Istanbul including a first test at a pedestrian bridge at the TUM (Technische Universität München) campus area. A summary and outlook (Section 4.1.4) completes the paper.

4.1.2 Sensor system

IATS

The instrument used is a prototype manufactured by Leica Geosystems as a case study series in 2007. It is based on a standard TCRA1201+ with the eyepiece removed and replaced by a 5 Mpixel CMOS coloured camera, see Figure 4.1. The field-of-view of 1.56 x 1.17 gon corresponds to 2.5 x 1.8 m in a distance of 100 m. To allow remote-controlled focussing, the focus drive is also equipped with a step motor (Wasmeier, 2009b). Although there are commercial tacheometers equipped with camera sensors already at the market, at the time of the project none of them was suitable for high-precision image analysis in real time. The respective Leica (Leica Geosystems, 2012), Trimble (Trimble, 2013) and Pentax (Pentax, 2013) instruments only use a wide-angle overview camera which does not allow submgon resolution, while the only instruments being equipped with an ocular camera, the Topcon Imaging Station family (IS, IS-3)(Topcon, 2012), unfortunately do not grant access to uncompressed images (Geiss, 17.04.2013). In addition, none of the instruments available would allow to process a real-time image with external devices (PC).

An essential step for high-quality image analysis (and target mapping to angular readings) is

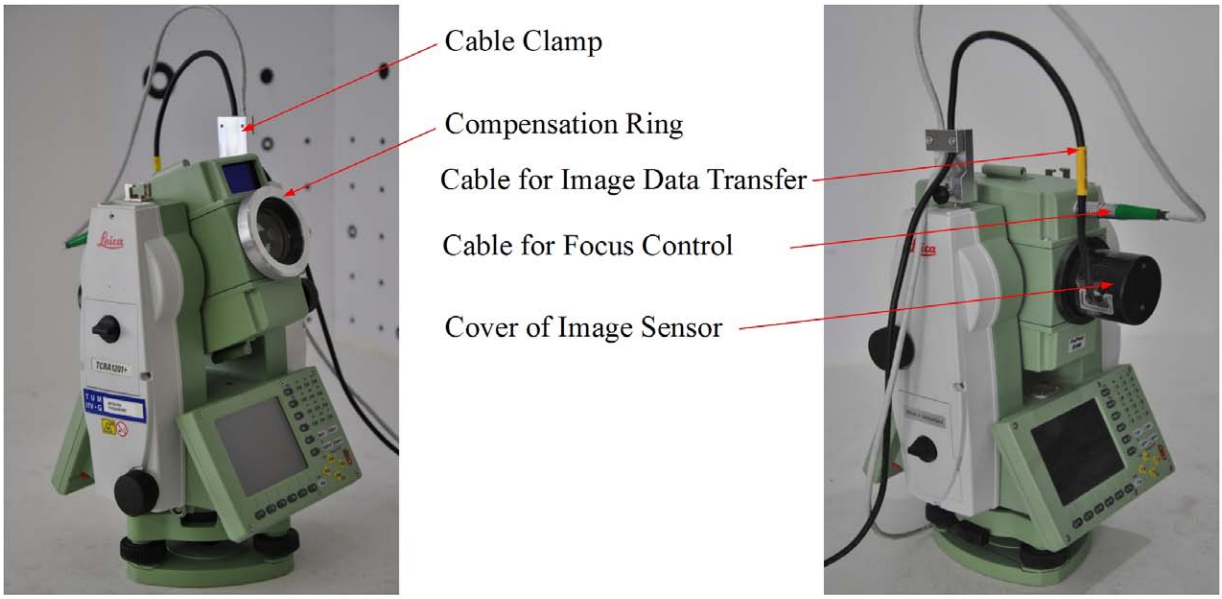

Figure 4.1 – Prototype of an Image Assisted Total Station

the system calibration consisting of a combined camera and tacheometer axis calibration. Due to the fact, that all calibration parameters are functionally linked to a given focus lens position, the calibration has to be done using a laboratory calibration device resulting in a tabulated parameter set. A brief description of the calibration, based on the continuation of work done by Walser (2004) and Vogel (2006), can be found in Wasmeier (2012). As a result oriented angular readings can be calculated for every pixel in an IATS image.

A detailed overview on different image evaluation techniques and accuracy considerations can be found in Reiterer and Wagner (2012). Recently, this also led to thorough examinations of air turbulence effects on the use of IATS. Reiterer (2012) presented studies to turn the problem to an advantage: the IATS prototype shown above was used to derive the actual refraction and temperature gradient from the turbulences within the images acquired.

LED Targets

Illuminated respectively active targets bring several advantages: The receiving sensor (IATS) does not need to focus emitted radiation on a single target and therefore may detect several targets simultaneously (as long as they are contained within the field of view) and the optical detection is even possible at night. For this reason, the choice fell to LEDs, which are low cost, have little power consumption and compact size. Furthermore, these are also available with infrared colour and therefore neither visible nor even disturbing for people. However, the camera system must be sensitive to the corresponding spectral range.

Single LEDs with different wavelengths from blue (~480 nm) up to infrared (~780 nm) were among the first targets tested when the IATS prototype was available. For high quality image analysis without the need of colour interpolation the camera should be used as a monochrome device and it could been shown

that especially infrared diodes brought very good results.

Certainly a major disadvantage of illuminated targets is the need for power supply, even if it is considerable low. In preparation to the test at the Fatih Sultan Mehmet Bridge in Istanbul, see Section 4.1.3, the competent bridge authority, General Directorate of Highways (GDH), has not approved to install cable underneath the bridge. Therefore we had to investigate other ways to power the targets:

The first consideration was to use luminescent targets instead of active LEDs. When the (built-in) laser beam of the total station points to this kind of reflector it will glow autonomously for a certain period of time depending of the material used. This highly promising approach could be realised in practice but has the big disadvantage that a lot of time will be wasted to "recharge" the targets and during this period no measurements can be done. Using a second device doing this work could be helpful but it would increase the effort, complexity and costs inadequately compared to the benefit.

Therefore a second, more favourable way is to use high-performance batteries. We are using a very small power pack with limited weight which is originally designed for RC models. With a capacity of 4200 mAh it is able to energise the LED cluster for at least three days before the battery has to be recharged or replaced. This period of time will be enough for first practical tests. If our measurement approach will be used permanently we have to negotiate a solution with the GDH anyway.

The battery pack and the LED cluster is located in an insulated housing, see Figure 4.2. This protects the electronic system from extreme temperature and is splash-proof. Outside of the box a reflective target mark is attached, which enables a simple reference distance measurement. The additive constant between the reflective surface and the LED cluster must be noted however. Furthermore with this design an easy installing will be guaranteed (it is also not allowed to drill into the bridge) so we have to fix the target by gluing which is more stable using the large surface area of the housing.

Figure 4.2 – LED target in self-made isolated housing. Detail of LED cluster top right

Software and Analysis

The initially round clustering of single LEDs does not necessarily lead to a circle-shaped blob structure. This may be because of divergent radiation performance, assembly and housing of the diode cluster. Of course, this effect intensifies the closer the LED cluster is situated to the observing camera and will lose impact with higher distances; but has to be taken into consideration anyway. Additionally, the outer shape of the blob might change due to meteorological conditions. In a pure geometric way, turbulent air density variations due

to thermal and stochastic convection lead to an aggravation of the image representation of objects as apparent position variations of target points, deformations of target structures and blurring.

With that in mind, there are different possibilities to define the final target centre with respect to the illuminated area which can be extracted by using a simple threshold operator or gradient filter, e.g. Gonzalez and Woods (1992):

- Using the **gravity centre of blob area**: This would be favourable if the blob structure is strongly fragmented and/or divergent from geometrical primitives. Grey value based algorithms are robust with respect to random image deviations and prove to be computed fast and easy.
- Using a **best-fit geometrical primitive**: For initially round spots this, of course, maybe a circle or ellipsis structure incl. possible additional outlier tests. This would be favourable if some parts of the blob temporarily appear occluded or if there were variations in the illumination strength. Geometrical approaches may react sensitive if the spots are too divergent from the primitive structure and are expensive in computation time.

To attain a higher precision in our analysis we choose the second described method. In a first segmentation (threshold) step the image is pre-processed. The resulting regions are tested for their circularity - possible misdetections, e.g. reflections can thus be excluded from further analysis. We also tested to specify the area or radius of the regions but due to the infrared illumination of the target, a low exposure time and the resulting reliable detection there is no need for further restrictions (Wagner et al., 2011). All remaining regions are approximated by ellipses and their centres are stored as (sub-)pixel coordinates. With appropriate calibration these centre points can be converted in angle values of the tacheometer coordinate system.

All image processing steps are implemented in a C# software controlling the IATS device and use the HALCON[1] library. The segmentation of the image and the ellipse fitting following takes 13 ms on average - thus a Maximum Frame Rate (MFR) of 77 Hz is possible. This run-time test was performed using full resolution images (2560 x 1920 pixel) and a common laptop (Intel Core 2Duo 2x2.7 GHz, 4 GB RAM). Using full-size images the MFR of our IATS is limited to 5 Hz due to the USB interface of the camera. By reducing the image size and/or resolution frame rates up to 200 Hz are possible. However, a reduction decreases the evaluation time of the algorithm as well. In contrast, the method mentioned above - using the gravity centre of the blob structure - takes only 8 ms and thus extends the (theoretical) MFR to 125 Hz.

Accuracy consideration

The precision detecting the ellipse centre depends on the size of the target on the camera chip. To determinate the ellipse parameter five unknowns have to be solved. A target size of 100 x 100 pixel leads to a high level of redundancy and therefore to a small standard deviation. Similar subpixel operators are specified with a

[1] MVTec Software GmbH: http://www.mvtec.com/halcon/

precision higher than 1/10 pixel, e.g. Sookman (2006), which corresponds to 0.06 mgon for the IATS system. Due to the fact that the telescope is not moving during LED tracking and the precision of relative angle measurements of the TPS1201+ achieves 0.1 mgon (Wasmeier, 2009a), the precision of the complete system can be specified with 0.12 mgon (according to the Gaussian error propagation law). For a distance of 100 m this is equivalent to a standard deviation of 0.2 mm. For absolute measurements the angle accuracy of the tacheometer will be the limiting factor, cf. (Wasmeier, 2009a). It is specified with 0.3 mgon which corresponds to 0.5 mm at 100 m (Leica Geosystems, 2009).

However, contactless measuring methods are affected by the influence of the atmosphere between the object and the recording device. Under outdoor conditions air turbulences and refraction effects overlay the image acquisition and degrade single measurement accuracy to 1 - 2 mgon (1.6 - 3.1 mm / 100 m).

4.1.3 Experiments and Results

The following section will describe two experiments performed with the system: The first one was taken at a pedestrian bridge at the TUM campus area (Section 4.1.3) to test preparatory the whole system locally. Section 4.1.3 describes the work done at the 2nd Bosporus Bridge (Fatih Sultan Mehmet Bridge) in Istanbul.

Pedestrian bridge

At the TUM campus area two infrared LED targets - as described in Section 4.1.2 - had been attached to a steel construction pedestrian bridge of approx. 25 m span. The IATS instrument was mounted at a pillar at the top of the institute building in an object distance of approx. 80 m, see Figure 4.3. In full resolution (2560 x 1920 pixel) the field of view would be therefore 2.0 x 1.5 m but it was reduced to 1280 x 960 pixel (1.0 x 0.75 m) to achieve a frame rate of 20 Hz. According to Section 4.1.2 this leads to an accuracy of 0.4 mm, disregarding the influence of refraction.

The aim of this measurement was to track multiple targets simultaneously within one image. Therefore two LED targets were mounted on each side of the bridge which allows to detect possible torsions of the bridge deck. Figure 4.3 top right shows a screenshot of the recording software. With low exposure time the IR targets are clearly visible in the camera image and easy to detect.

During the measuring period of several hours the targets could be tracked with only sporadic data gaps when the line of site was temporarily interrupted by people passing by. Before and after the recording time measurements to surrounding control points were used to prove the stability of the station. Through the relative stable construction of the bridge and its sheltered position - the bridge is located in the courtyard and protected from wind - no significant movement or frequencies could be detected during the measurement period and so a comparison of both targets was not meaningful. Therefore we stimulated the construction by a jumping person and imposed an oscillation. Figure 4.4 displays the frequency spectrum - generated by a

Figure 4.3 – Test measurement at TUM campus with screenshot (top right) and used LED target (bottom right)

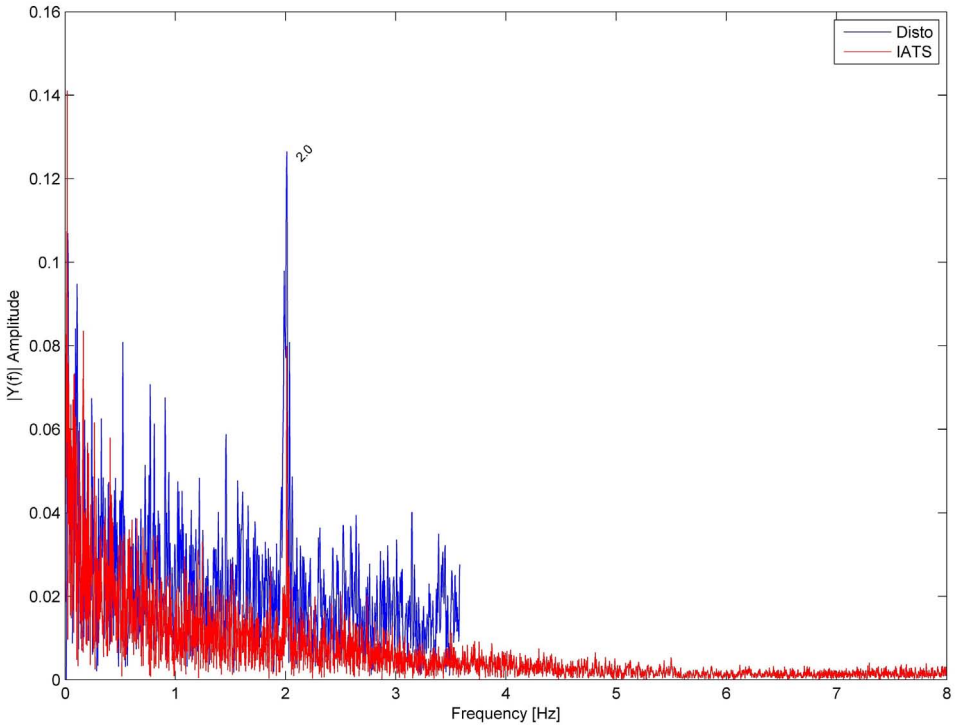

Figure 4.4 – Frequency spectrum of the IATS observations incl. comparative measurement by a distance meter

Fast Fourier Transformation (FFT) - of the observing period. Even though the displacement was still in the range of a few millimetres a dominant frequency of 2.0 Hz, which most probably is the resonance frequency of the bridge is clearly visible.

As reference an additional experiment at the bridge was done using a laser distancemeter (Leica DISTO^{TM} OEM module 3.0 WH15) as independent measuring method. The device has a typical measuring accuracy of +/- 1.5 mm (Leica Geosystems, 2001). A precision of approx. a half a millimetre is possible by averaging the data. The instrument was positioned directly beneath the bridge on a tripod targeting in zenith direction to the underside of the bridge. As in the above described experiment a jumping person stimulated the construction. The determined displacement rates and the detected frequency, cf. Figure 4.4, are both consistent with those of the IATS test.

Fatih Sultan Mehmet Bridge

The Bosporus is considered as one of the most important water ways, because of its role as the connection between the Mediterranean and the Black Sea. The Fatih Sultan Mehmet Bridge is one of two bridges in Istanbul, which span the Bosporus and connect the European and the Asiatic part of the mega city. The bridge had been the 6th longest suspension bridge span in the world when it was completed and released for motor vehicles in 1988. The bridge connects Edirne with Ankara. For this reason an immense importance comes to the bridge, since it is part of the "arteries of the Turkish transportation net" and essential in the transportation of Istanbul. The structure is designed as suspension bridge as shown in Figure 4.5. It spans 1,510 meters from bank to bank and 1,090 meters between the suspension pylons which tower 105 meters above the roadway. The clearance of the bridge from the sea level is 64 meters.

At the lower side of the bridge 16 LED targets, as described in Section 4.1.2, have been installed. The targets were arranged in four rows with four units across the deck. Access to the underside of the bridge was possible using a service crane as shown in Figure 4.6. Most of the targets have been used by our partner ITU which observed them with two wide angle cameras simultaneously.

With the IATS only one of the LED targets in a distance of ca. 128 m from the abutment has been observed (see Figure 4.6). The IATS was positioned on a pillar which is approx. 20 m beside the abutment of the European side and located about 8 m below the deck. The camera field of view corresponds to an area of 3.1 m x 2.4 m in object distance. Around the station several fix points have been monumented to define a local coordinate system. Due to security reasons we could only dispose of two half observation days. On the 12th of December 2012 measurements were taken for one hour and on the following day for five hours. The meteorological data of both measurement periods was similar as shown in Table 4.1. At the first day the measurement was taken between 3 pm and 4 pm. Because of the beginning rush hour period the number of vehicles is higher as during the second measurement which was performed between 10 am and 3 pm.

Figure 4.7 shows a total vertical displacement of 50 cm (blue line) and a lateral one of 3 cm at the first measurement day. These ranges

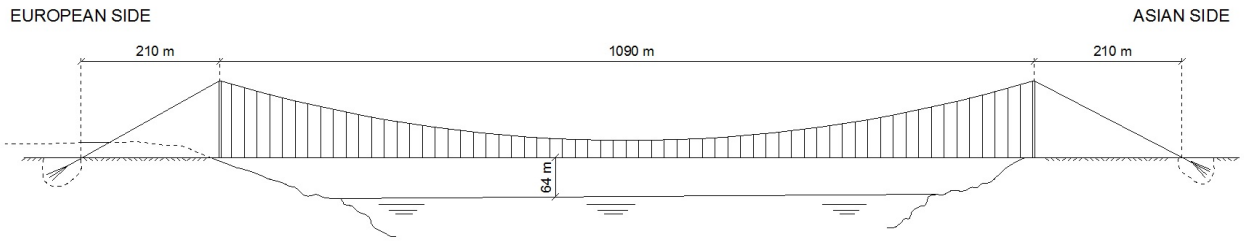

Figure 4.5 – General arrangement of Fatih Sultan Mehmet Bridge, modified from Apaydin (2002)

Figure 4.6 – Fatih Sultan Mehmet Bridge seen from observation pillar with highlighted LED targets. The red circle indicates the IATS observed target

Table 4.1 – Meteorological data of measurement periods

Date	Wind speed	Wind direction	Temperature	Vehicles per hour
12.12.	18 km/h	NW	7 °C	7.400
13.12.	23 - 25 km/h	NW	4 - 5 °C	5.900 - 6.700

are also representative for the measurement at the second day. In both cases the acquisition rate was set to 25 Hz by reducing the field of view to 800 x 900 pixels (1.0 x 1.1 m in object distance). As described in Section 4.1.2 only 5 Hz would be possible in full resolution.

Figure 4.8 displays the frequency spectrum of the two measurement series (vertical displacement) of December 12 and 13. Equal fundamental vibration frequencies can be detected in both days clearly. The amplitudes of day one are larger than those of day two which is probably caused by different traffic loads.

Frequency analyses and finite element models of the Fatih Sultan Mehmet bridge were already presented, e.g. from Apaydin (2002) or Dumanoglu et al. (1992). In contrary to this study accelerometers, seismometers or GPS were used as measurement sensors. For more details about the finite element analysis and theoretical derived quantities it is referred to the specified literature. Table 4.2 compares the results of the previously mentioned studies to our investigation in vertical direction. The detected frequencies correspond to the known determined values in essence. However three frequencies (0.132, 0.176 and 0.272) are slightly higher than the range of the previous tests. Following the approach of structural health monitoring, e.g. Wenzel (2009), this could be a hint to some structural damage and further investigation should be carried out.

It is still pending that these results can be confirmed by the photogrammetric evaluations of our partners from the ITU.

Table 4.2 – Comparison between resonance frequencies of experimental studies (vertical)

Dumanoglu et al. (1992)	**Apaydin (2002)**	**IATS**
Hz	Hz	Hz
0.108	0.102	0.106
0.125	0.118	0.132
0.145	0.154	0.176
0.159	0.205	0.209
0.232	0.255	0.272
0.317	0.374	0.333

4.1.4 Summary and Outlook

The paper at hand presented a case study for bridge monitoring with video-tacheometry in two examples using active LED targets to determine absolute displacements directly - as in contrast to relative measurement methods, like acceleration or inclination sensors. The system is mobile, quick to deploy and can be used permanent and/or discontinuous for only a couple of hours or days. The use of a video-tacheometer allows photogrammetric image measurement methods to detect signalised and non-signalised points in combination with total station methods, such as precise angle and distance measurement (to prisms or reflectorless) to acquire the exterior orientation or to control the stability of the station point incl. inclination values of the instrument. Using non-signalised targets would require neither access to the target area nor energy supply, but measurements at night are no longer possible.

An ocular camera like the one of the used prototype is currently only available in just one commercial device. As long as other manufacturers will not incorporate this additional camera

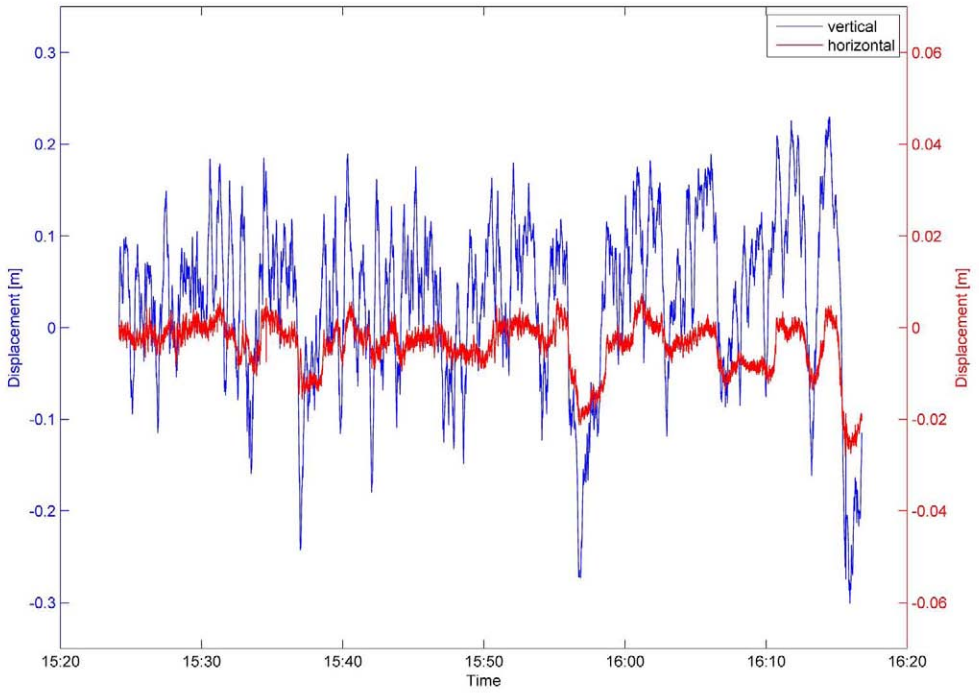

Figure 4.7 – Vertical (blue) and horizontal displacement of the bridge at first observation day (please note different scales on the vertical axes)

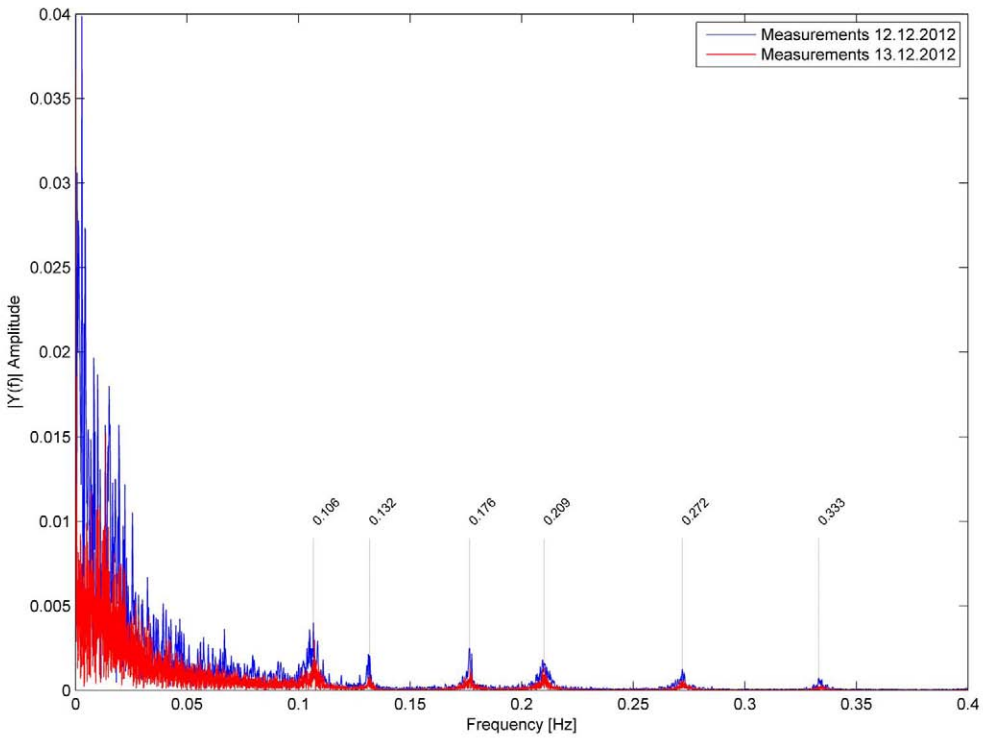

Figure 4.8 – Amplitude spectrum of y-component (vertical) incl. detected frequencies

in their devices, the available overview cameras can be used instead as described above. This would also have the advantage that multiple targets can be detected and tracked simultaneously using the larger field of view. However, since the magnification of the telescope is missing, the achievable resolution is lower which affects the detection accuracy. As example one pixel of a Leica Viva wide-angle camera corresponds to 6.8 mgon, cf. Leica Geosystems (2012) The observed LED target (ø 5.5 cm) at Fatih Sultan Mehmet Bridge would be mapped to 5 x 5 pixels at the camera chip - in contrast to 45 x 45 pixels at the IATS camera chip. A reliable ellipse fit will be therefore problematic and a subpixel accuracy unlikely, which means the angle accuracy of the tacheometer is underachieved.

If a full 3D motion, i.e. also in the viewing direction, is needed, the distance measuring module of the total station or a forward intersection (FI) with two devices could be used. For the first method the available hardware currently allows repetition rates of a few Hertz only. It is therefore necessary to check whether this is sufficient for the measurement task. In addition, with increasing distance, prisms must be used to ensure reliable distance measurements. Using a FI on the other side needs a precise synchronisation of both video-tacheometer which can be done e.g. as described in Bürki et al. (2010): The group made tests for refraction monitoring by simultaneous reciprocal vertical angle measurements using UTC time given by small GPS receivers to synchronise their devices.

Acknowledgement

The research presented in this paper has been supported by the Alexander von Humboldt Foundation.

We are gratefully indebted to Prof. Orhan Altan and Dipl.-Ing. Özgür Avsar from the Istanbul Technical University for complex negotiations with the GDH to enable our campaign and their support at the site.

Remark

During the review process of this article Leica Geosystems released the Leica Nova (series) – a total station with integrated telescope camera. As far as known a direct access to the video stream is not possible but the on-board saved images can be downloaded in full resolution. Thus a trend to the combination of total station and photogrammetric methods is visible and will find its way into surveyors' workaday life.

4.2 P-II: Long-Range Geo-Monitoring using Image Assisted Total Stations

Author: Andreas Wagner, Ben Huber, Wolfgang Wiedemann and Gerhard Paar

Publication: Journal of Applied Geodesy, 8(3), DOI: 10.1515/jag-2014-0014, pp. 223-234, 2014

Abstract: Image Assisted Total Station (IATS) unify geodetic precision of total stations with areal coverage of images. The concept of using two IATS devices for high-resolution, long-range stereo survey of geo-risk areas has been investigated in the EU-FP7 project DE-MONTES (www.de-montes.eu). The paper presents the used methodology and compares the main features with other terrestrial geodetic geo-monitoring methods. The theoretically achievable accuracy of the measurement system is derived and verified by ground truth data of a distant clay pit slope and simulated deformations. It is shown that the stereo IATS concept is able to obtain higher precision in the determination of 3D deformations than other systems of comparable sensor establishment effort.

Keywords: Image Assisted Total Stations, Deformation Monitoring, Geo-risk Monitoring, Long-Range Terrestrial 3D Survey

4.2.1 Introduction

The necessity for monitoring geo-risk areas such as landslides is growing due to the increased probability of such events caused by environmental change. It is known that, in many cases, information about the dynamics of unstable areas (i.e. the determination and measurements of surface deformations in cm-accuracy range) allows the prediction of hazardous events (Poisel and Preh, 2004). Geodetic deformation monitoring therefore turns threat into a calculable risk.

A monitoring concept with modern measurement technologies allows the estimation of the hazard potential and the prediction of life-threatening situations. This implies a need for highly-effective and reliable tools for monitoring potential risk areas at an operational level, in order to obtain better knowledge of the expected dynamics and the spatial distribution of the event. Therefore, geodetic and geotechnical measurements are often combined to multi-sensor systems.

Monitoring data/information gained in such way is extremely important for enhancing the reliability of risk assessment. In consequence, timely and well-targeted measures can be effectively initiated. These reactions may consist of focused, more expensive on-site monitoring, the application of protection installations, closure of infrastructure or, as a last resort, the evacuation of the endangered population. In case of such an event having already occurred, remote monitoring often remains the only way to assess further hazard risks and to determine the

amount of debris movement and damage; thus, saving lives, reducing the risk for field personnel and emergency staff, documenting the expected and post-event economic and environmental damage and efficiently installing protection measures are the immediate benefits of such a system.

The different dynamics of geo-hazard events, and the nature of the site to be monitored, place diverse requirements on such a system in terms of accuracy, measurement speed and measurement frequency:

- Geo-risk areas can stay hazardous for a duration of several years. It is therefore necessary to have either a very low-cost, yet automatic solution that is kept on-site for continuous monitoring, or the system needs to be repeatedly installed in an affordable way, combining multi-temporal measurements in a robust manner and (if necessary) providing high-precision point measurements.
- Other geo-hazard events take place unexpectedly and induce a reaction time for establishment of a monitoring system within hours. This requires the need for a self-calibrating, quickly adaptable solution to the often constrained conditions of application (visibility, accessibility of the site, illumination conditions on the object, etc.). In this case, costs are of minor interest — only the speed of establishment and the quality and reliability of measurement count.

The conclusion is that an effective monitoring system needs to be a highly portable, modular and scalable solution, which can be easily installed, calibrated and adapted to specific applications. The main component of such systems -– besides data analysis and interpretation -– is the data acquisition unit, made up with commonly used geodetic instruments and methods. These are presented in this article. Furthermore, we show why the introduction of a high-precision visual measurement system – based on Image Assisted Total Stations – brings significant benefits. Our monitoring approach is originally based on the i-MeaS (Reiterer et al., 2009) research project and has recently been improved and enhanced to a practically usable product within the FP7 project DE-MONTES, whose main objective was to provide the participating enterprises[1] with a new kind of measurement system (Wagner et al., 2013a). The functionality of this system is described, including the data analysis to derive deformation vector fields from IATS stereo image time series. The theoretical accuracy of our measurement approach is derived and verified by ground truth data.

4.2.2 State-of-the-art geodetic geo-monitoring

At the moment, most movements in geo-hazard areas are monitored by conventional geodetic and/or geotechnical systems. Concentrating on an accuracy class from tenths of a millimetre to some centimetres, there are five different (ground-based) geodetic sensor types and technologies available (Wunderlich et al., 2010):

[1] Cautus Geo (Norway), Dibit Messtechnik (Austria), GeoImaging Ltd (Cyprus) and Neovision (Czech Republic)

Global Navigation Satellite Systems (GNSS)

Using differential GNSS, by measuring the phase of the signal's carrier wave with two or more geodetic receivers, delivers (long) baselines of high accuracy with no need for intervisibility. Such a system is independent of weather conditions and, due to the high number of systems available and being established (GPS, GLONASS, Compass and Galileo), reliability and shadowing are no longer a major limiting factor either. However, site access and energy provision for each receiver is necessary. The high costs for each antenna per observation point may be reduced by using upcoming low-cost systems (Heunecke et al., 2011). Furthermore, GNSS can only be applied point-wise; therefore, the dense mapping of large areas is not possible.

Terrestrial Positioning System (TPS)

Total stations are able to automatically deliver sequential polar 3D vectors to co-operative prisms using automatic target recognition (ATR) or, with some restrictions, prismless to natural targets from one or several stations. Long-range, high-accuracy measurements, including integrated level compensation, are possible. The device may be fully remote-controlled and a combination with GNSS is possible; modern versions also deliver (overview) images for visual control. However, a free line of sight to the object, and in the case of active prisms, a radio link is needed. As with GNSS, the need for target signalisation requires safe access and, as in all methods using dedicated target points, their positions have to be carefully selected to deliver a representative model of the site. With all optical systems, the atmospheric refraction influences the measurements results, in particular the height component.

Terrestrial Laser Scanner (TLS)

Laser scanners generate contactless dense point clouds by distance measurements using the time-of-flight method. Various TLS systems exist on the market for different applications, with an operating distance of between 10 m and 6,000 m. Accuracy decreases with increasing range to the target and with increasing angles of incident. Large laser beam footprints in long-range measurements also have to be considered. The maximum range – besides technical limitation and a restricted pulse energy for safety reasons – also depends on the characteristics and reflectivity of the surface and atmospheric visibility. The main advantage of TLS is its rapid and detailed capture of a wide field-of-view, resulting in a complete point cloud (Bauer et al., 2005). However, it must be taken into account that TLS measurements do not provide identical points between repeated scans. Therefore, a direct comparison of discrete points – as in GNSS or TPS measurements – is not possible. Comparing different epochs, changes can only be detected in sighting direction. This is particularly crucial for the identification of lateral deformation.

Ground-Based Synthetic Aperture Radar (GB-SAR)

A GB-SAR is a portable radar unit which delivers highly accurate displacements of topographic geometry by transmitting microwaves and observing phase differences of the reflected

echoes (Crosetto et al., 2009). As a consequence, changes at the examined area are reported in line-of-sight direction only. The large footprint at the object makes it impossible to detect small structures or their displacement. Out of all the mentioned methods, this system provides the highest possible accuracy for each resolution cell. Atmospheric disturbances and surface material are the main limiting factors (Rödelsperger et al., 2010). GB-SAR is independent of natural light and can cover large area monitoring but, due to the high costs, it is established less frequently.

Stereo Photogrammetry (SP)

The intersection of two homologous rays from two stereoscopic images determines the 3D location of an object point. By using calibrated digital cameras and automated processing (determination of corresponding points, bundle adjustment) in combination with separately measured ground control points, dense digital surface models (DSM) and orthoimages may be produced. Accuracy limitations are the ground sampling distance in the images, the matching algorithm, the determined image poses, movements and changes of the intrinsic camera parameters (e.g. due to thermal influences), change in the refraction indices of the atmosphere between the camera and the landslide and the change in sun illumination (Settles et al., 2008). In order to minimise these artefacts, the images need to contain a stable area that can be used as a reference, preferably equipped with reference targets that can be robustly, accurately and automatically tracked in the images.

As shown in Table 4.3, which compares the main features of the above-mentioned methods, the currently used systems have shortcomings in terms of accuracy, measurement range and the ability to measure lateral motions (motions perpendicular to the viewing direction). In these areas, our stereo IATS approach shows its strengths and gains additional benefits.

4.2.3 Methodology

Stereo IATS

The used IATS (Figure 4.9) are prototypes manufactured by Leica Geosystems as a small batch series in 2007. The instruments are based on a standard TCRA1201+ tacheometer with the eyepiece removed and replaced by a five-megapixel Complementary Metal-Oxide-Semiconductor (CMOS) RGB camera (½ inch, 2560 × 1920 pixel, 2.2 × 2.2 µm pixel size). One pixel on the image sensor corresponds to an angular value of 0.61 mgon at focus position infinity. The field-of-view of 1.56 x 1.17 gon corresponds to 2.5 x 1.8 m at a distance of 100 m. The focus drive is equipped with a step motor, which allows fully remote-controlled operation.

An essential step for high-quality image analysis is the system calibration, consisting of a combined intrinsic camera parameters and tacheometer axis calibration. We used the approach of Wasmeier (2009a) which is based on the continuation of work done by Walser (2004) and Vogel (2006). A calibrated system allows the expression of a measured pixel position on the image sensor as a field angle in the object space. Captured images are therefore directly geo-referenced and can be used for direc-

Table 4.3 – Terrestrial geodetic methods for geo-monitoring

	GNSS	TPS	TLS	GB-SAR	SP	Stereo IATS
Information	Punctual	Punctual	Areal	Areal	Areal + displ. vectors	Areal + displ. vectors
Accuracy[1]	High	High	Medium	High	High	High
Range[2]	High	High	Medium	High	Low	High
Footprint[3]	Small	Small	Medium	High	Small	Small
Line-of-sight	No	Yes	Yes	Yes	Yes	Yes
Site access	Needed	Needed	Utile	Utile	Utile	No
Costs[4]	High	High	High	Very high	Moderate	High

[1] Accuracy low > 5 cm, medium 1 - 5 cm, high < 1 cm

[2] Range low < 100 m, medium 100 - 500 m, high > 500 m

[3] Footprint small < 5 mm, medium 5 mm - 5 cm, high > 5 cm

[4] Costs moderate < 10,000 €, high 10,000 - 50,000 €, very high > 50,000 €

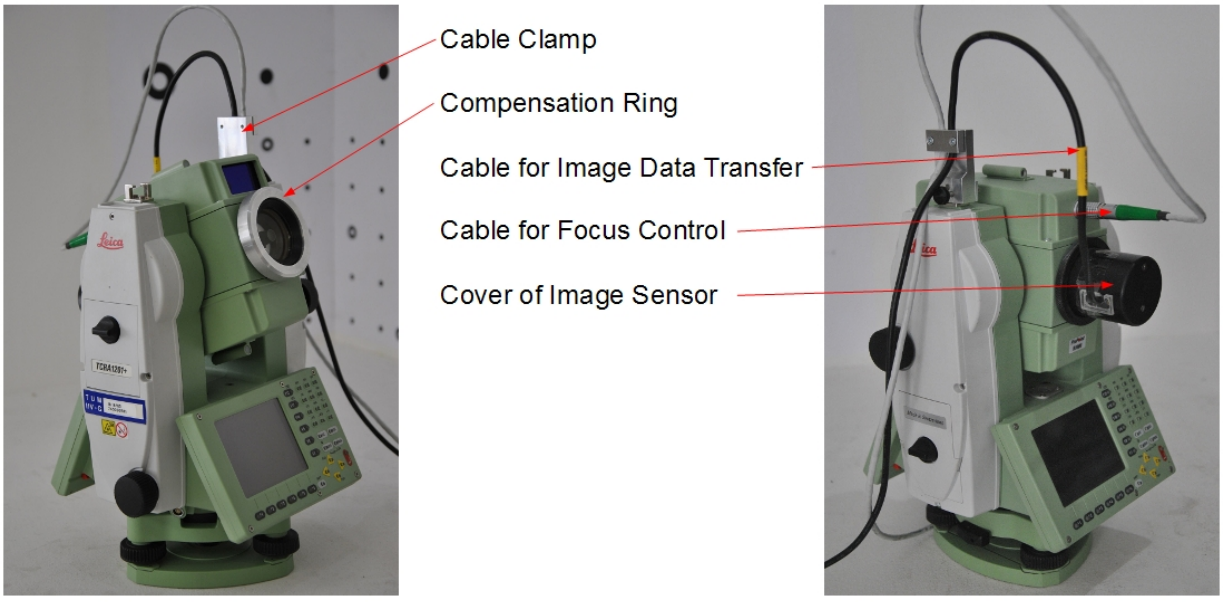

Figure 4.9 – Prototype of an Image Assisted Total Station (Reiterer and Wagner, 2012)

tion measurements with no need for object control points or further photogrammetric orientation processes.

For data acquisition, two IATS are set up in a stereo configuration as used for TPS intersection or stereo-photogrammetry. Considerations of the geometric configuration (like length of the baseline or object distance) are presented in Section 4.2.3. Due to the 30-times magnification of the ocular, it is unlikely that one IATS image will cover the whole observation area. Therefore, each device captures an image bundle of the preselected region of interest (ROI) using the automatic axis drive of the base instrument, which will be composed to a single panorama. Simultaneous data capturing of both devices is not necessary, but does ensure equal illumination conditions and state of the object. All parameters of the exterior orientation – determined by tacheometer angles and calibration parameters – are attached to the image files as meta-data for further processing. It is therefore advantageous if the station coordinates are known in advance, e.g. by a control network, GNSS determination or TPS resection.

Matching

The developed processing and data evaluation chain is shown in Figure 4.10. After recording the data, the main steps are projecting the individual images into unique panoramas, matching these panoramas and reconstructing the object surface via triangulation in the spherical system of the panoramas.

Image bundles are evaluated by loading the respective image pose information from the meta-data. This allows the relation of every image pixel to a real world angle value passing through the defined camera centre. These values are used to project the image texture onto a sphere with an arbitrarily chosen radius. It is possible to define the final resolution of the projected panorama via the angular resolution of each pixel as an input parameter. Using the IATS resolution at infinity (0.61 mgon) per projected pixel results in full resolution panoramas wherein each tile has an image size of roughly 2560 x 1920 pixel; smaller values lead to up-sampled panoramas, larger values result in lower resolution panoramas, which may be matched faster. Areas with overlapping texture towards the image borders are evaluated via an analysis of their distance to the respective image centres. Pixels closer to the centre are favoured in the merging process. To further ensure a smooth transition between the individual tiles, a sub-pixel accurate matching process could be applied at tile borders. However, due to the high registration accuracy of our device (½ pixel) and the applied distortion correction, this was not necessary. It is important to note that each pixel in the generated panoramas is still related to its real world measurement angle.

The generated stereo panoramas from two image bundles are mutually matched via the SURF feature-matching algorithm (Bay et al., 2006) to generate an initial disparity prediction for the dense matching process. Final dense disparity maps are computed via the Hierarchical Feature Vector Matching (HFVM) algorithm (Kolesnik et al., 1998). The method relies on the calculation of feature vectors for each pixel consisting of a wide variety of complementary image features, such as grey levels, edges, corners and other local primitives, thus significantly

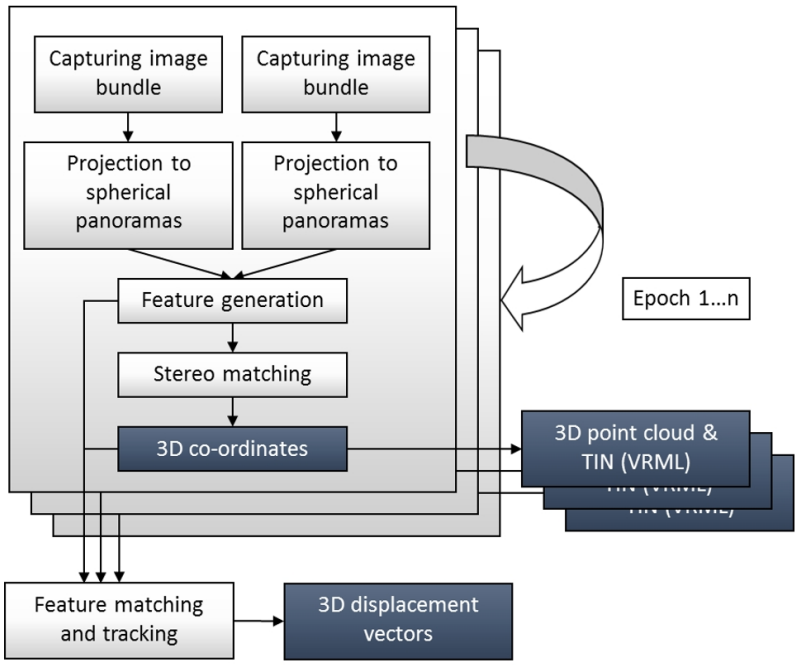

Figure 4.10 – Sequence diagram of data acquisition and analysis

improving the stereo matching set-up in terms of robustness and accuracy. In this context, a feature numerically describes certain properties of the neighbourhood of a pixel. By comparing feature vectors from both the reference and the comparison image, the best correspondences are found, outliers are removed and sub-pixel matching positions are calculated. This process is applied on multiple pyramid levels to improve the robustness and efficiency of the implementation (Figure 4.11). To allow an evaluation and quantification of the matching results, a back-matching process is executed starting at the calculated disparity position in the search image and matching back into the reference image. The resulting sub-pixel offset between the initial starting point and the back-matched position is saved as a consistency value of each evaluated disparity.

Based on the matching results and image pose, the object surface can be calculated via spatial intersection. In deviation from the traditional photogrammetric approach, the disparities are not related to perspective cameras, but to spherical panoramas. Therefore, the triangulation is calculated in the spherical systems, wherein rays in object space are defined by the centre of the spheres the panoramas were projected to and the angle values related to each disparity value position within the panorama. Only pixels with a back-matching distance better than 0.3 pixels are taken into account in the triangulation.

Output

The resulting 3D point cloud is projected into a spherical system centred in between both stations. Pixels of the hereby created spherical Digital Surface Model (DSM) contain the distance values to the sphere centre; the correspondingly-projected orthoimage contains the image texture. In a parallel step, the 3D co-ordinates are used to generate a triangulated

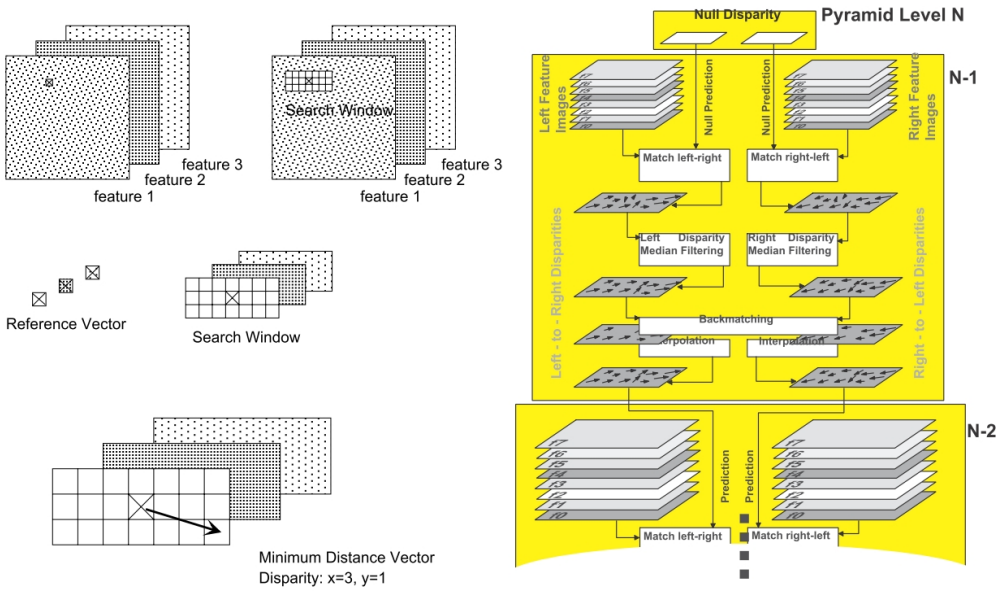

Figure 4.11 – Feature vector matching principle (left), HFVM from pyramid level N to N-1 (right) (Kolesnik et al., 1998)

irregular network (TIN), which is saved as a VRML (Virtual Reality Modelling Language) file format. In a second processing step, datasets from multiple measurement epochs can be compared by a dense matching of the textured orthoimages (cf. Figure 4.10). Each valid position on the orthoimages is related to a 3D coordinate. The matching results directly generate a dense field of 3D displacement vectors which can also be visualised and saved as a VRML file (Figure 4.12). These vectors can be further used e.g. to automatically detect and measure volume differences between the epochs.

Accuracy consideration

Different approaches exist to derive the accuracy of a point determined by spatial intersection: it is possible to use the classical geodetic method of separate position and height calculation (2D + height), or the minimum (spatial) distance of two or more skew lines (3D).

The minimal error of a new point depends on the geometric configuration. If the point is located at the perpendicular bisector of an error-free baseline, the optimum intersection angle (using the 2D+H method) gives different solutions depending on the selected error measure (Grafarend, 1971) which is designated by Friedrich (1927) as geodetic paradox: 121.63 gon for the Helmert, 133.3 gon for the Werkmeister-Wilks and 100 gon for the Helmert-Maxwell-Bolzmann point error. It should be noted that in most geodetic literature, such as Jordan et al. (1963), Möser et al. (2000) or Kahmen (2005), the theoretical accuracy is only derived from measurement uncertainties and does not consider errors of the station co-ordinates. As this does not sufficiently reflect the reality, a calculation taking a baseline uncertainty into account (such as Rinner (1977)) should be used. However, a separate position and height calculation, and its accuracy determination, may only be used in case of near-horizontal sightings, due to the consequent negligible small correlation be-

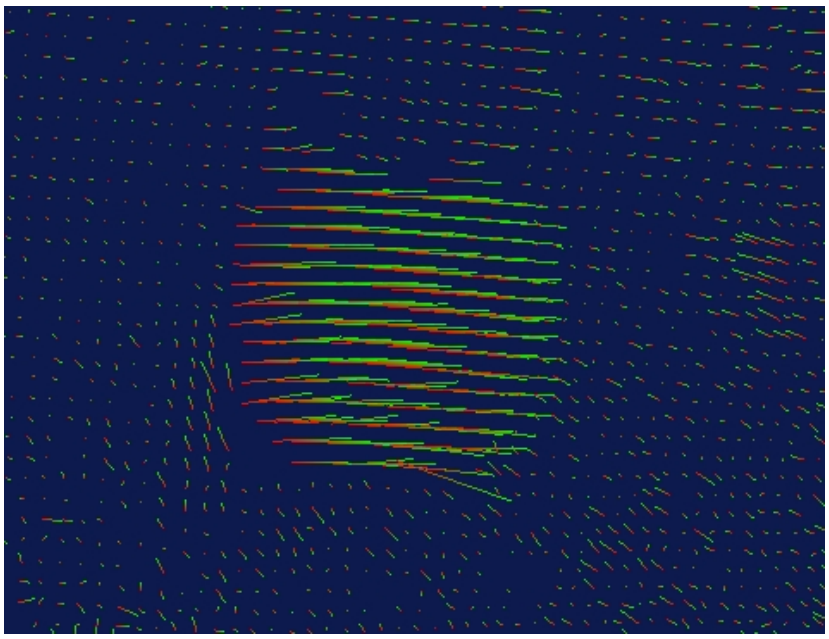

Figure 4.12 – Multi-temporal 3D displacement vectors, exaggerated by factor 10

tween the vertical angle and the resulting position.

A complementary solution is achieved by (spatial) intersection of 3D rays or, in consideration of observations containing small errors, by finding the point with the minimal distance to skew lines. This can be solved as a constrained Gauss-Helmert (Niemeier, 2008) adjustment with unknown intersection co-ordinates derived from the smallest (spatial) distance of two 3D rays starting at the known stations. As a result, error ellipses describing the uncertainty of the computed position of a point (which are a common measure of accuracy) can be calculated by the eigenvalues and eigenvectors of the cofactor matrix of the adjusted parameters. The eigenvalues indicate the square of the semi-major and semi-minor axes of the error ellipse, the eigenvectors give their directions. Rotating the covariance matrix by a principal component transformation into the direction of the baseline, a longitudinal and transverse error can be calculated. According to this approach, the error estimation for a test use case is done in Section 4.2.5.

Figure 4.13 shows a simulation of the resulting position-dependent Helmert point error by an intersection. Ideally, the object point is located on the perpendicular bisector of the baseline. Furthermore, the intersection angle should be between 100 - 133 gon, reliant on baseline and bearing errors as well as the chosen error measure. However, it should be noted that a wider base degrades the matching results, as these are dependent on the viewpoint change between both images. Therefore, a compromise between resulting accuracy and matching requirement must be found for the length of the baseline.

4.2.4 Field Experiment

During the research project, various laboratory and field tests have been conducted. In this paper, we will present an experiment designed to prove the theoretically-derived ac-

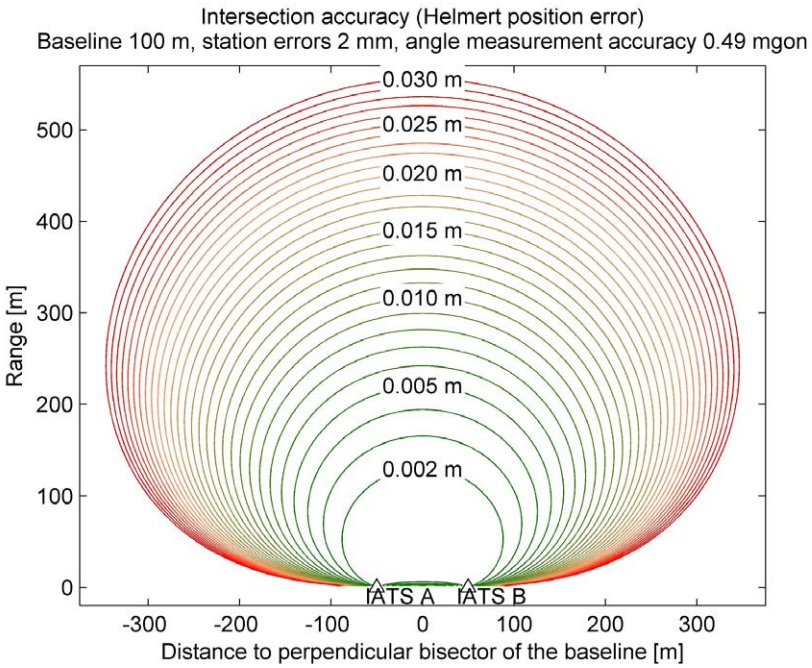

Figure 4.13 – Intersection accuracy (Helmert position error)

curacies of our measurement system by verifying it via ground truth data, validating the data analysis and processing software components.

Test site & experimental set-up

The experiment was carried out in a clay-pit, where a temporary local control network was installed (Figure 4.14). The region of interest – a near-vertical pit slope of the quarry – is shown in Figure 4.15. A couple of different epochs were recorded in order to simulate different scenarios. Due to the fact that a deformation was not expected to occur within the test period, it was simulated by movements of an artificial rock (red rectangle in Figure 4.15). This artificial rock is a 1 m x 1 m structured and textured plate, which was fixed by two ropes and shifted and rotated in varying amounts during the different epochs. Four control points (reflective targets, one in each corner) enable the determination of the exact position and rotation of the plate. Within the ROI, four black and white targets for the TLS data registration were also placed.

Used sensors

During the experiment, five different devices (2 IATS, 2 TPS and 1 TLS) were used for different purposes. These devices, as well as their role within the test, are described in the following:

TPS

For the control and reference points, a Leica TPS1201 and a Leica MS50 total station were used. The accuracy of both instruments is specified for angle measurements with 1” (0.3 mgon), for distances with 1 mm ± 1.5 ppm

Figure 4.14 – Field experiment – overview (aerial photo: Geobasisdaten © Bayerische Vermessungsverwaltung, 2014)

Figure 4.15 – Region of interest (ROI) with highlighted control points and artificial rock

to prisms and 2 mm ± 2 ppm to any surface. Observations from four different stations were carried out, resulting in error ellipses and accuracies after a network adjustment as shown in Figure 4.16, respectively listed in Table 4.4.

Table 4.4 – Result of TPS network adjustment

Point group	Accuracy [m]	
	Position	Height
IATS stations	0.002	0.002
TPS/LS	0.002	0.002
Control points	0.003	0.003
Artificial rock	0.003	0.003

After the network measurements, both TPSs were used to determine the corner points of the artificial target. Since the resulting co-ordinates are over-determined, it is possible to specify accuracies for each point and to compare the simulated displacement with IATS measurements. The results can further be tested for significance.

IATS

Two IATS, as described in Section 4.2.3, were used to determine the object surface within the ROI. The (baseline) distance between both instruments' stations was 84.5 m and the mean range to the ROI 261 m, resp. 292 m, which results in a mean intersection angle of ~18 gon for a point at the ROI.

After the TPS network measurements, both IATS were built up at their stations and an orientation measurement to one control point was done by identifying the centre of this point manually in the IATS image. With a commercial version of an IATS, like a Leica Multistation, it would be possible to use an automated measurement function to prisms (ATR). This function is in principle available in our IATS prototype, however, as shown in Wasmeier (2009a), it is not possible to link the ocular and ATR camera without additional knowledge of the manufacturer.

To verify and optionally refine these (manual) orientation measurements, the images were automatically analysed by a third party software HALCON in post-processing. A template of the used targets (DXF drawing) was searched and matched in the images as shown in Figure 4.17. The resulting pixel values were converted into angles and an intersection for each control point was calculated which can be compared to the nominal co-ordinates of the TPS network. Table 4.5 shows the result of these co-ordinate differences which are below 5 mm.

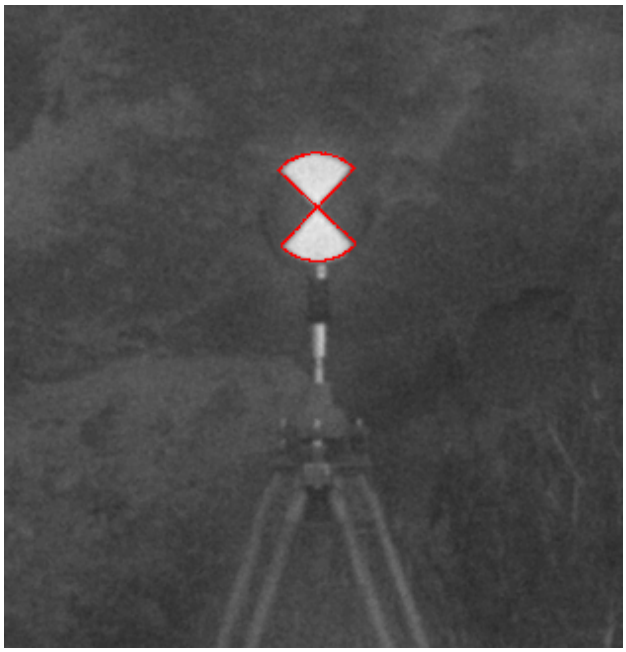

Figure 4.17 – Template matching to verify orientation angle

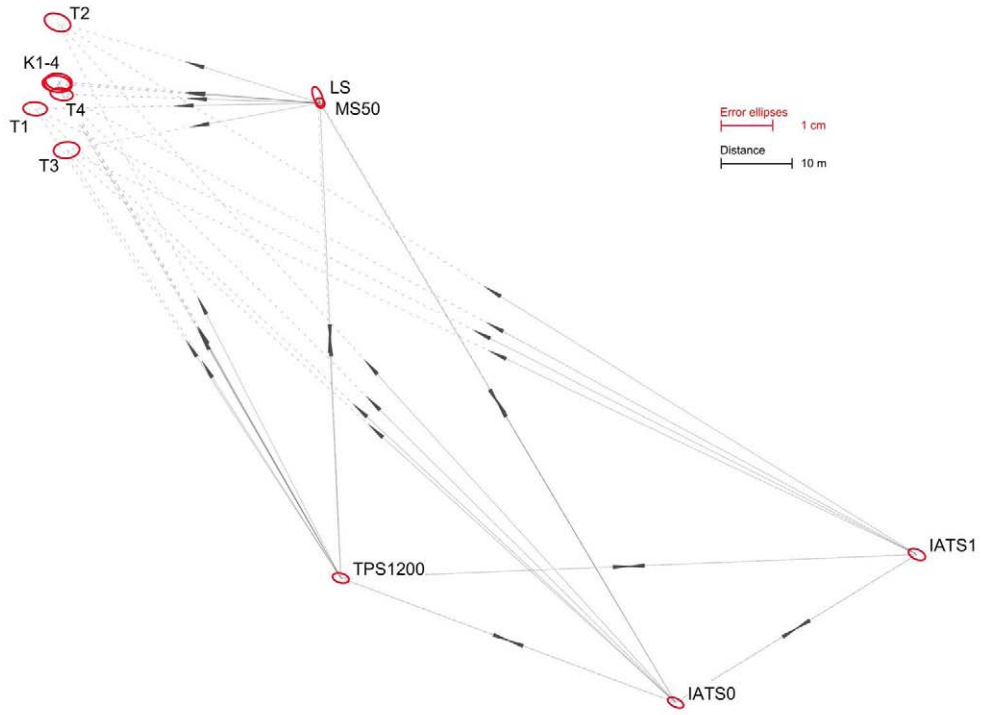

Figure 4.16 – Result of TPS network adjustment

Table 4.5 – IATS residuals to control points (point T3 was not visible in one IATS image bundle)

Target	Δ X [m]	Δ Y [m]	Δ Z [m]
T1	0.005	-0.003	0.001
T2	0.001	0.001	-0.001
T4	0.005	0.004	0.001

Within each epoch, 32 single images (150 MB data within 3 min) from one IATS station and 40 images (187 MB within 4 min) from the other station were taken, covering the ROI. During the analysis, these images are stitched to single spherical panoramas for each station, using the extrinsic parameters of the cameras given by the tacheometer values of the IATS. These panoramas are then matched and reconstructed as described in Section 4.2.3, resulting in a DSM and a 3D mesh (VRML) per epoch. As an example, the first epoch contains 1,073,752 points, which equals a mean point density of ~8,300 points per square metre which is slightly higher than the TLS resolution, but at a three-times-higher object distance from the IATS (see below).

TLS

To validate the IATS measurements, a reference surface was captured using a Leica HDS7000 laser scanner. The TLS was set up at a distance of ~80 m oblique to the artificial rock (Figure 4.14). The scans of the ROI were taken with a resolution of 10 mm point-to-point distance. To fix the unknown orientation and position of the scans, four black and white targets (Figure 4.15) were set up around the ROI. The positions of the targets were determined by TPS network adjustment. To improve the accuracy of target detection and registration, the targets were scanned separately in the highest possible resolution (~4.5 mm point-to-point distance on the

targets). As the HDS7000 does not compensate tilt errors with inclination sensors, an approach with 6 degrees of freedom (3 rotations, 3 translations) was used for registration. The calculated residuals of the target point are below ± 3 mm (Table 4.6).

Table 4.6 – Residuals of TLS registration

Target	Residual of Registration		
	Δ X [m]	Δ Y [m]	Δ Z [m]
T1	-0.003	-0.003	0.001
T2	-0.001	0.001	0.001
T3	0.003	-0.001	-0.001
T4	-0.003	-0.001	0.001

According to the manufacturer's specifications, the HDS7000 is subjected to a linearity error $\leq$ 1 mm and a range noise of 2 mm to 8 mm at 80 m distance, depending on the reflectivity of target surface. The angle accuracy (horizontal/vertical) is 125 µrad. Calculating the accuracy of single laser scan points with these values is not expedient due to the fact that influences, such as errors in absolute distance measurement and meteorology, are eliminated by registration of the point cloud with known target positions. The accuracy of the point cloud is therefore given by the quality of the registration (as shown above) and the specified range noise, which was verified to 2.7 mm by comparing two TLS point clouds.

4.2.5 Results

In addition to the above-mentioned results of the individual sensors, in the following, the accuracy and derived information of the IATS point cloud will be further specified.

Accuracy

To calculate the achievable accuracy according to Section 4.2.3, the following input values are used: the station co-ordinates were determined with an accuracy of σ_x = 2 mm as result of the TPS network adjustment. As direction accuracy, the manufacturer's data (σ_t = 0.3 mgon) and the HFVM matching uncertainty of 0.3 pixel (maximum average back matching distance), which can be expressed as angle error σ_m = 0.18 mgon, is used. The accuracy of a bearing measurement finally results from two direction measurements (orientation measurement and direction to the target) including the matching component. Using the (Gaussian) error propagation law, this gives $\sigma_{t'}$ = 0.49 mgon for the horizontal and $\sigma_{v'}$ = 0.35 mgon for the vertical observation accuracy. Since a zenith angle is defined through the plumb line, for a levelled instrument a single direction measurement accuracy is used. Taking these values as input for the observations' stochastic model in the intersection adjustment, we get an error ellipse with semi-axes of 14.4 mm and 2.1 mm (orientation = 159 gon). The mean Helmert position error follows with 14.6 mm. Applied to the baseline – which roughly corresponds to the orientation of the ROI – this leads to a mean standard deviation of 5.6 mm in transversal, and 13.5 mm in longitudinal direction. The height component of 1.7 mm gives a very optimistic result; however, this disregards the influence of the atmosphere (scintillation, refraction, etc.). Using an IATS, it is possible to minimise these effects by the averaging of multiple images (Thuro et al., 2010) and by derivation of

turbulence parameters as described in Reiterer (2012).

To verify these derived values, the IATS point cloud is compared with the ground truth data of the TLS. This is realised with the 3D point cloud processing and modelling software Geomagic Studio, which provides methods to visualise the differences between a point cloud and a reference surface model. The reference surface model was created by generating a triangulated mesh from the point data. Deviations are reported as the shortest distance from the test point cloud to any point on the reference model.

Figure 4.18 shows the points of the IATS measurement colour-coded by deviation from the TLS reference model (grey background). The colour bar is chosen with respect to a hypothesis test (level of significance 95%). Points within the confidence level are coloured green, which means there is no significant difference between these IATS 3D co-ordinates to the meshed TLS surface. Points with positive derivations (red) are in front of the reference (closer to the observer); points with negative derivation (blue) are behind the reference.

The graphical comparison shows good correspondence of both data sets. Differences are only shown in regions with strong variation in the surface norm, which can be affiliated with the different viewing directions of the two sensor systems. Points in regions which are only represented by one sensor system, are systematically mismatched according to the comparison algorithm. This effect also leads to high deviations at the edges of the modelled area and the boundary of holes in the point cloud.

As already mentioned, the geometric configuration of both IATS stations and the ROI is not ideal for an intersection (cf. Section 4.2.3) but, due to the local conditions, not otherwise possible. The mean intersection angle is ~ 18 gon and the object points do not lie at the perpendicular bisector. A more favourable configuration, e.g. a doubling of the baseline length, would decrease the Helmert position error from 14.6 mm to 5.8 mm.

Artificial deformation

To compare the artificial deformation, simulated by translations and rotations of the artificial rock within the different epochs, the data of the different sensors is analysed based on the resulting parameters of a rigid body transformation:

- **TPS**: Four reflective targets in the corners of the artificial rock are determined in the global co-ordinate system by measurements from both total stations. For each position (epoch), these points are transformed into a local co-ordinate system which is defined as shown in Figure 4.19A. In this local co-ordinate system, the artificial deformation can be expressed as rigid body movement. The displacements (translations and rotations) are estimated as the parameters of an over-determined Helmert-transformation between the epochs.
- **TLS**: In the TLS point clouds, an area around the artificial rock is cut out manually in each epoch. These points are transformed into the same local co-ordinate system as is used in the TPS-approach. After that, the point clouds are transformed into

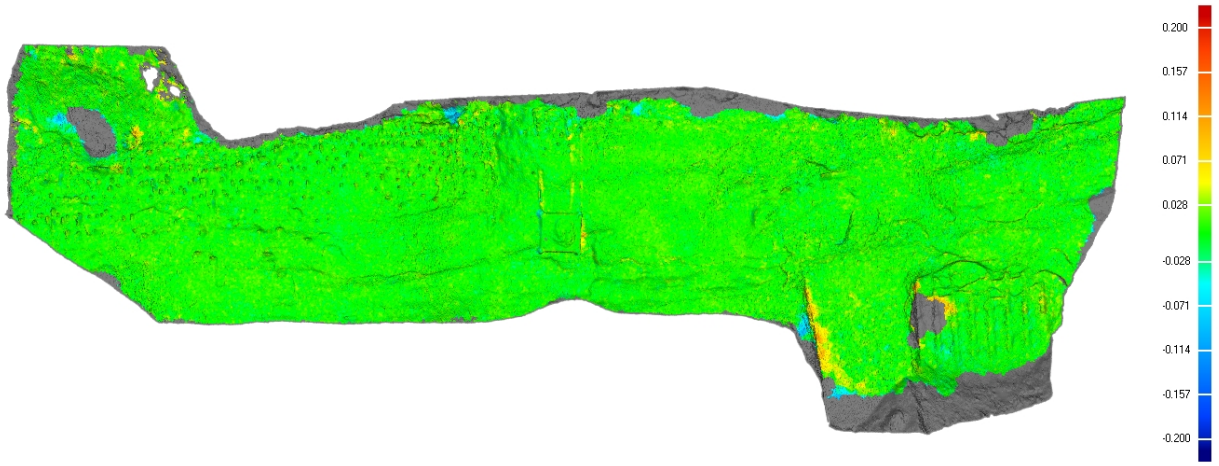

Figure 4.18 – Comparison of IATS and TLS point cloud – differences between DSM [m]

each other using an ICP (Iterative Closest Point) algorithm, see Figure 4.19B. The resulting parameter sets of the ICP algorithm represent the same rigid body motion as in the TPS approach.

- **IATS**: By searching for corresponding points in four images (two stereo images of two different epochs), 3D displacement vectors can be directly derived, as shown in Figure 4.19C. The start and end points of these vectors can be expressed as rigid body motion and therefore represented as translation and rotation.

A comparison of the parameters, calculated from the three different datasets, is shown exemplarily for the artificial deformation between Epoch 0 and Epoch 1 in Table 4.7, which is representative for all conducted tests.

Table 4.7 – Transformation parameters (rigid body motion)

	TPS	TLS	IATS
tx [m]	-0.058	-0.053	-0.055
ty [m]	-0.014	-0.017	-0.007
tz [m]	-0.005	0.000	-0.007
rx [gon]	0.793	0.708	0.966
ry [gon]	0.431	0.343	0.667
rz [gon]	-0.307	-0.375	0.187

For a better understanding of the different parameters, the four corner points of the artificial rock are transformed with the determined values from TLS and IATS. The residuals of the transformed points are calculated to the nominal coordinates given by the TPS network. This results in a mean difference of 6 mm at the corner points for IATS, and 8 mm for TLS, and shows that both systems lead to the same results within their measurement accuracies (the differences are not significant). However, it should be noted that the IATS measurements were determined from a three-times-greater distance. Furthermore, it is possible to calculate

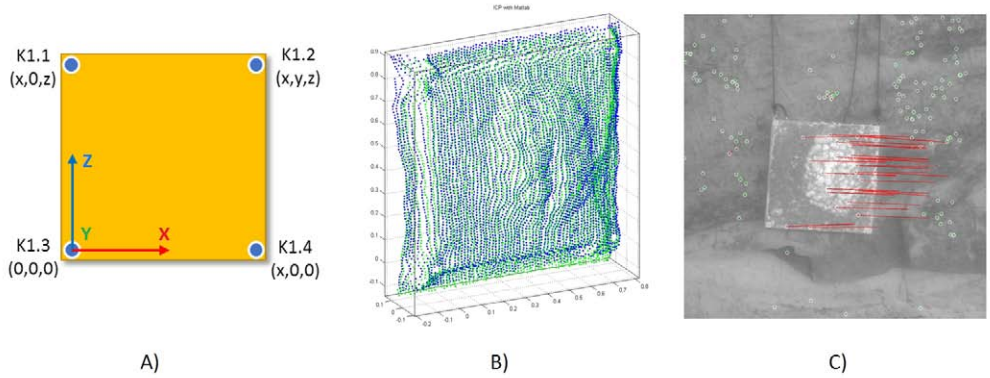

Figure 4.19 – A) Local co-ordinate system of artificial rock; B) TLS data of artificial rock transformed by ICP algorithm; C) Deformation vectors of IATS analysis (subset)

the rigid body motion parameters directly from displacement vectors without manual intervention. Generating the transformation parameters from the TLS point cloud with an ICP is heavily dependent on the chosen algorithm, the selected matching methods and the chosen region.

our prototype – the images are transmitted via a slip ring and not a direct cable connection – and there are less settings for image acquisition (e.g. exposure time). However, the device is equipped with an additional overview camera, a (calibrated) ATR function and there is no need for additional controllers or external cables anymore.

4.2.6 Outlook

The current implementation uses instrument prototypes of IATS which are not available for other users. Currently, a couple of total stations with built-in cameras are available on the market, but most of them are equipped with wide-angle overview cameras only (Wagner et al., 2014b). However, two instrument series – Topcon IS and Leica Multistation – provide additional ocular cameras. With the magnification of the telescope, their images can be used for long-range applications as described. Since our software uses an abstract, hierarchical, multilayer driver model (Wagner et al., 2013a), its simple adaption to a Leica MS50 had already been realised within a master's thesis (Briechle, 2014). First tests showed the usability of this instrument. It achieves slower data transfer rates to PC than

Ongoing work concentrates on the incorporation of TLS data into the system. The proceeding fusion of tacheometer, cameras and laser scanners, and thereby the resulting benefit of simultaneously available sensors, should be taken into account. Area or feature-based matching methods will be used to detect corresponding points and their displacements within the images of different epochs. Intersecting the derived direction vectors with surface models from scan data finally leads to 3D point movements. The position and orientation of the system can be controlled and possibly corrected using GNSS and/or surrounding permanent installed prisms.

4.2.7 Conclusion

With this article, we demonstrate the practicability of the concept using two IATS devices for high-resolution long-range stereo surveys of geo-risk areas. The achievable accuracy of 3D co-ordinates, determined by IATS measurements, has been theoretically derived and practically proven by ground truth from TLS data. Dense point clouds with high single point accuracy, including information about their precision, are generated. 3D displacement vectors can be derived automatically and their significance specified. This may be used to directly determine rigid body motions of objects and surface patches. Compared to TLS measurements, long distances with smaller footprints are possible with our IATS approach and there is no need for reference points within the ROI. The large magnification of the telescope camera, and the ability to capture image bundles, further leads to a higher point density in comparison to simple photogrammetry approaches. The long-range capability of the presented system will be shown in a closing numeric example. Extrapolating the achievable accuracy to greater distances (by using a fixed base-to-distance ratio of 1:3 and the other input parameters of the field experiment), the following Helmert position errors are possible: For 1 km 0.035 m, 2 km 0.069 m, and 3 km 0.103 m.

Acknowledgment

The research leading to these results has received funding from the European Community's Seventh Framework Programme (FP7/2007-2013) under grant agreement n° 285839 DEMONTES. We would also like to thank Hörl & Hartmann Ziegeltechnik GmbH & Co for the use of the clay pit.

4.3 P-III: Using IATS to Read and Analyze Digital Leveling Staffs

Author: Andreas Wagner, Wolfgang Wiedemann, Thomas Wunderlich

Publication: SIG 2016 – International Symposium on Engineering Geodesy. Varaždin, Croatia, 20-22 May 2016, Croatian Geodetic Society , pp. CD-ROM, 2016

.

Abstract: It is possible to use modern total stations for leveling applications. Using digital staffs for relative height transfer gets a higher precision than using automatic target recognition (ATR) for prism detection. The study at hand describes the implementation to automatically read and analyze the code pattern of a digital leveling staff using an Image Assisted Total Station (IATS). The acquired 2-dimensional color image is converted into a binary signal and correlated with the a priori known reference signal. The result is used as initial value for a newly developed, alternative decoding method, in which the height differences of corresponding barcode edges are minimized. In different tests the precision and accuracy of our method is compared with the built-in ATR function of the total station as well as with a digital level. Standard deviations below 10 µm (1σ) prove comparable leveling capabilities of modern total stations – IATS.

Keywords: Automatic Level, Barcode Staff, Digital Leveling, Height Transfer, Image Assisted Total Station (IATS), Leveling, Leveling Staff, Monitoring

4.3.1 Introduction

Almost all manufactures of total stations have instruments with built-in cameras in their product portfolio. These devices are commonly termed as Image Assisted Total Stations (IATS). Today, the images from the instruments' cameras are used to support the field work procedures and for documentation purposes. The onboard processor and the implemented software are able to overlay the images as well as the live video stream with measurement and planning data or sketches. This is possible as the captured images are directly geo-referenced and orientated if the system is properly calibrated. In addition to the manufacturers' usage and applications, the high resolution images taken by an IATS enable the development of new measurement approaches. Examples of such new applications fields are geo-monitoring (Reiterer et al., 2009; Wagner et al., 2014a; Wagner, 2016), Structural Health Monitoring (Wagner et al., 2013b; Ehrhart and Lienhart, 2015b) or industrial metrology (Wasmeier, 2009b; Guillaume et al., 2012; Hauth et al., 2012). We implemented the leveling capability into IATS as a further possible field of use, as described in the following. This is helpful e.g. for the high accurate transfer of the instrument height from a benchmark. It also extends the possibilities for monitoring (Wagner et al., 2016b) and can be seen as the next step towards a geodetic universal instrument (Wunderlich et al., 2014).

4.3.2 Digital Leveling

Leveling is still the most widely used method for relative height transfer of ground points. The measuring equipment comprises of a graduated staff and a level (instrument), which is basically a telescope that enables a horizontal line of sight, e.g. by a mechanical tilt compensator. Digital levels consist of additional electronic image processing components to automatically read and analyze digital (bar coded) leveling staffs, where the graduation is replaced by a manufacturer dependent code pattern. For first-order leveling or other high accurate engineering survey projects precise levels in combination with precise leveling staffs are used, which are stated with a standard error of $\leq \pm 0.5 \frac{mm}{km}$ double-run leveling. Here, the code (modulation) information of the staff is usually engraved at an invar strip which has a low thermal expansion coefficient (<$10^{-6}K^{-1}$). To ensure high accurate results and/or as part of quality management system requirements, such as the ISO 9001, regularly inspections of the devices and the equipment are essential. National and international standards, e.g. DIN 18717 and ISO 12858-1, define parameters to be examined in periodical calibration. For invar leveling staffs these are, for example, the staff scale, the zero-point error, graduation corrections, and the thermal expansion coefficient. There are different calibration facilities, like the Geodetic Laboratory at the Technical University of Munich (TUM), which offer the parameter determination according to the mentioned standards (Wasmeier and Foppe, 2006).

Staff code pattern

Various different code patterns exist for digital leveling staffs, as every manufacturer has developed its own modulation and analyzing method. The main reasons for this are patent rights to the individual solutions (Ingensand, 1999). Common to all versions is that a barcode is longitudinally imprinted on the leveling staff; the bars run transversely to the upright direction. The code pattern is converted into a digital intensity- and position-information via a CCD line sensor. Every implementation uses high contrast transitions (black-white or black-yellow) at the edges of the code-bars. At the moment, we implemented the code pattern used by the company *Leica Geosystems* in our approach, which is described in the following only. Here, an aperiodic pseudo-stochastic (binary) code sequence is used for encoding digital leveling staffs, which seems to be randomly composed. However, the code elements are arranged in such way that already short code sections are unique in the code sequence. The overall code is composed of black or white/yellow integer multiples of a 2.025 mm wide base element. The widest occurring code element has the width of 15 elements, i.e. 30.375 mm. The entire code sequence is unique over a length of 4050 mm, which also defines the maximum extent of this type of leveling staffs (Ingensand, 1999).

Demodulation

To decode the (*Leica*) code pattern into staff/height readings the pseudo-stochastic sequence must be known, resp. must be stored in the instrument. Two signals – the reference signal and the pre-processed image sig-

nal – are shifted stepwise against each other and each time the correlation coefficient is calculated. This value describes the statistical relationship between two random variables or two signals and has its maximum at perfect match. The overall correlation function C_{PQ} of the measurement signal $Q(y)$ and the reference signal $P(d, y - h)$ is (Ingensand, 1990):

$$C_{PQ}(d,h) = \frac{1}{N}\sum_{i=0}^{N} Q_i(y) \cdot P_i(d, y-h) \quad (4.1)$$

From the maximum of this (two dimensional) function the desired distance d resp. scale (ratio pixel/mm) and height h can be derived. The position of the focus lens – determined by a displacement transducer or rotary encoder applied to the focus drive – provides a rough distance information as initial value. To speed up this process, especially for the levels of the first generation, the processing is split into a two-stage correlation, a coarse and a fine correlation.

4.3.3 Method

In engineering survey projects, it is often necessary to accurately determine the total station's transit axis height. If the height is transferred from a benchmark, preferably a manual reading of a leveling staff should be used, instead of the less accurate reflector pole. To increase the reliability and accuracy of such a procedure a fully automatic digital reading and analysis would be desirable. For this reason, we transferred the processing method of a digital level to a modern total station, resp. an IATS. The on-axis camera offers a comparable high magnification of the telescope and the on-board processor is meanwhile capable of simple image processing tasks. The main difference between both instrument types is that the telescope of the total station allows rotations in the vertical plane. In an automatic level, in contrast, a mechanical compensator ensures a horizontal sight for an approximately leveled instrument. The vertical angle of the total station is determined with respect to the plumb line, refined by an electronic inclinometer. This means, if the accuracy of the vertical angle reading is high enough, it is possible to level with a total station in the same way as with a leveling instrument. However, due to practical reasons such as greater weight or much higher price of total stations, it is unlikely that levels will be replaced. But in some special applications it may be useful, e.g. to transfer the station height from benchmarks, as mentioned before. Further, it is possible to do non-horizontal sightings to leveling staffs and thus also cover large height differences with one single observation (with high accuracy). As we also have access to the (image) processing chain, we are able to consider additional special calibration parameters of the leveling staffs. As mentioned before, international and national standards specify periodical calibrations which determine adjustment parameters but these are applied only occasionally. With our proposed decoding method, it is even possible to correct the graduation of each single codebar without difficulties. In the following sections we will first describe the new approach when using a total station instead of a level. In the second part the alternative decoding method will be presented.

Program sequence

The measuring procedure to read coded staffs by an IATS consists of several steps as shown in Figure 4.20 and as described in the following.

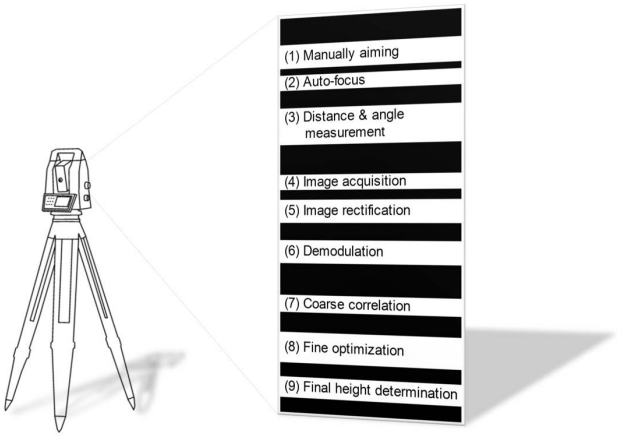

Figure 4.20 – Program sequence to read and analyze a digital leveling staff using IATS

For the data acquisition the leveled IATS must be manually aimed to the vertically aligned leveling staff (1). It is necessary that the vertical crosshair is centered on the leveling staff. During the further processing the image domain will be reduced to a small vertical stripe left and right of the crosshair. The vertical alignment is of minor relevance, as long as a few code-bars are visible in the image (that the code pattern is unambiguous). For the further processing the staff must be (2) focused either manually or by an integrated auto-focus of the total station. An additional reflectorless distance measurement (3) provides more accurate distance information as if it would be derived from the focus lens position (as done in digital levels). The horizontal and vertical angles are read out simultaneously with the image acquisition (4). In connection with the a priori determined camera calibration parameters the image is therefore fully orientated. If the image is taken under a non-horizontal alignment (V $\neq$ 100 gon $\parallel$ V $\neq$ 300 gon) it is subjected to a perspective-based distortion, which has to be corrected by an image rectification (5). The distortion effect is a function of the camera location as well as its orientation in respect to the observed staff. As both parameters are known, the image can be transformed as it would look like as in a horizontal view. The rectification (projective transformation) can be expressed by a planar homography, as the code pattern on the leveling staff is present in a plane. For the further processing, the image is reduced to a small vertical stripe which only contains the staff code pattern. The width of this region is automatically determined depending on the later measured distance to the staff. During the demodulation (6) the RGB information is transformed into an 8-bit grayscale, see Figure 4.21. The pixels of each row are averaged, which effects a smoothing for noise reduction. The 1-dimensional signal is normalized, i.e. the intensities are stretched to the full 8-bit range (0 - 255).

To achieve faster processing the actual data analysis is separated into a coarse and fine correlation. (7) The initial value for the staff reading is calculated using 1-bit signals. Therefore, the normalized mean values are converted into binary values and state the measurement signal $Q(y)$, c.f. Equation 4.1. The correlation of C_{PQ} is calculated by the XNOR-operator (exclusive NOT OR) of $Q(y)$ and the shifted copies of the 1-bit reference signal $P(y-h)$ as a function of the height h. In our case, the distance d is fixed due to the high accurate determination by the electronic distance meter (EDM) of the total station, which gives

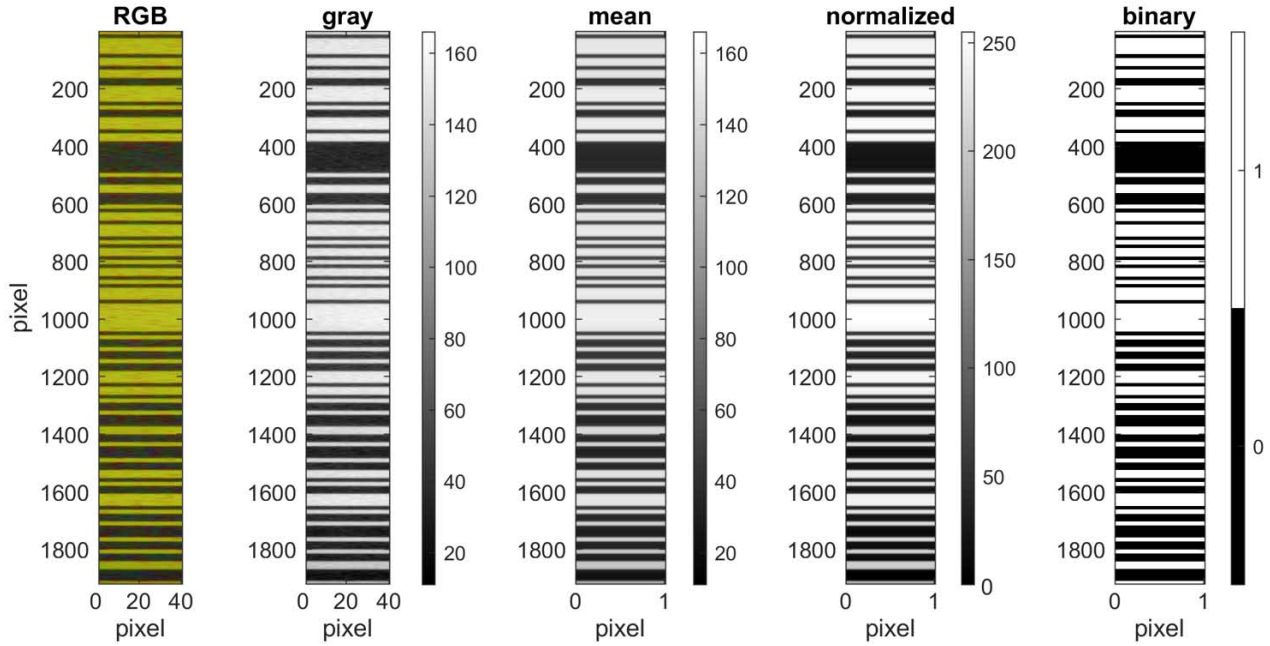

Figure 4.21 – Image pre-processing steps for the demodulation of the digital staff code pattern. The 2-dimensional RGB image section is converted stepwise into a binary signal

$$C_{PQ}(h) = \frac{1}{N} \sum_{i=0}^{N-1} \overline{Q_i(y) \otimes P_i(d, y-h)} \qquad (4.2)$$

In digital levels, in contrast, the correlation is extended to the second dimension, by taking the distance into account. In both cases, the result of the function has a clear visible peak in the correlation coefficients which specifies the offset of both signals and finally the corresponding staff reading. The fine optimization (8), implemented in digital levels, uses the previous results as starting values for a second correlation. This time the full 8-bit intensity information of the input signal is used. Likewise, the step width of the shift in distance d and height h is decreased to refine the results of the correlation procedure. In our case we replaced the fine correlation by a new processing approach, as described in the next section. When using a total station instead of a level a further final height determination step (9) is necessary. The staff reading, i.e. the result of the fine correlation or the alternative approach must be corrected by the influence of the non-horizontal alignment. This trigonometric height difference Δh can be calculated by the vertical angle ζ and the measured horizontal distance d or slope distance s using:

$$\Delta h = d \cot \zeta = s \cos \zeta \qquad (4.3)$$

An additional correction for curvature and refraction may also be applied.

Alternative decoding method

An alternative approach to the fine correlation of both signals is to minimize the height differences of corresponding barcode edges, related to the implementation used in the *Zeiss DiNi* level series. The image of a leveling staff is processed with a subpixel edge detection algorithm to extract linear features at each code el-

ement transition. We implemented an approach based on Burns et al. (1986) but modified it to our needs, in which similar gradient directions are grouped into potential line regions. If certain thresholds – regarding size and shape of the regions – are met, a line is fitted through each group by least squares estimation, weighted by the gradient magnitudes. The result is a vector with measured barcode positions $\boldsymbol{E}_M$ in image coordinates. The visible code sequence of the reference gives a vector $\boldsymbol{E}_R$, in which each element represents the distance of a black and white transition (and vice versa) from the zero point of the staff. Both vectors are connected by a scale factor s and a translation, resp. height difference h:

$$\boldsymbol{E}_R = s \cdot \boldsymbol{E}_M + h \tag{4.4}$$

We solve this equitation system with the least squares method, by minimizing the distance of corresponding edges. The results of the coarse correlation are used as the initial values. The pairwise assignment is determined by a forward and backward search of nearest neighbors in both vectors. A distance filter and an outlier test remove (remaining) lines which may be caused by failed edge detection or partial occlusion of the observed code pattern. The adjustment is performed iteratively to ensure a correct assignment of corresponding edges. The classical fine optimization, which is implemented in digital levels (of the company *Leica*), is a two-dimensional correlation where the two parameters scale (distance) and height have to be solved iteratively. The correlation function, Equation 4.1, has to be calculated in two processing loops step by step with slightly changed parameters to find the maximum correlation coefficient. In our approach the same parameters are solved in a linear equitation system directly which leads to a faster computation. Only a limited set of iterations is used for the correct edge assignment and outlier removal. The additional time for the necessary image processing is negligible.

4.3.4 Experiments

To investigate the performance of our approach we conducted several tests which are described below. All tests were performed indoor in a laboratory under controlled atmospheric conditions. The digital leveling staff used is a 2 m length invar staff from *Leica*, the IATS a *Leica Nova MS60*. The telescope camera has a resolution of 2560 × 1920 pixel with a respective size of 2.2 × 2.2 µm. The image is magnified 30-times by the telescope optics, which gives a field of view of 1.5° (1.67 gon). One pixel on the image sensor corresponds to an angular value of 0.61 mgon. The angular accuracy (horizontal and vertical) is specified with 1″ (0.3 mgon), the accuracy of the reflectorless distance measurement is listed with 2 mm + 2 ppm (Leica Geosystems, 2015).

Precision

In one experiment the repeatability of measurements with our approach is investigated. In a static setup both, the *Leica MS60* and the barcode staff, are installed on pillars in the laboratory with unknown, but constant height offset. The horizontal distance between the instrument and the invar staff is ~15.5 m. Over a time period of 3 hours we take 400 images and process them with the algorithm described in the previous sections. To compare and monitor the instrument's behavior over time, we also

take 400 measurements with the built-in automatic target recognition (ATR) of the instrument to a co-operative prism next to the leveling staff. For both time series the vertical angle is nearly 100 gon (horizontal aiming). All measurements are reduced by the mean value of their time series. The height deviations calculated from the staff readings are shown in Figure 4.22. A standard deviation of 0.008 mm (1σ) is obtained for height observations derived from barcode staff readings with a maximal deviation from the mean value of 0.029 mm. This is slightly better than the ATR measurements with a standard deviation of 0.012 mm (1σ) and a maximum deviation from the mean value of 0.039 mm.

To ensure the repeatability of the height readings in different barcode sections we run additional tests. In a static setup of instrument and digital leveling staff we take 15 images under different vertical angles showing independent barcode segments that should result in the same height offset between the total station and the leveling staff. This test was repeated 6 times (90 independent measurements). Due to the changing vertical angles the results are influenced by the additional trigonometric height differences, i.e. by the uncertainty of the angle and distance measurements. The mean standard deviation within the 6 sets of the height readings is 0.015 mm (1σ) with a maximum absolute deviation from the mean value of 0.038 mm.

Accuracy

To obtain the accuracy of our method, we used a different setup. On the one side we compare the results with a commercial precise digital level, on the other side with a measuring system of higher order. The leveling staff is installed in the vertical comparator of the TUM Geodetic Laboratory, allowing a controlled stepwise vertical movement of the staff. We simulate small displacements of 0.05 mm, the same as it occurs e.g. in subsidence surveys. The single increments are measured by the IATS (*Leica MS60*) and a precise digital level (*Leica DNA03*), both instruments are built up in a distance of ~5.1 m, and are referenced by a high accurate laser interferometer (*Hewlett Packard 5518A*, ~1 µm).

Figure 4.23 shows the heights values of the interferometer plotted against the IATS heights (left) and against the digital level (right). In total 100 increments are measured, for better visibility only a part of the data is displayed. Both data sets show similar behavior. The standard deviation of both residuals is 0.006 mm (1σ), the maximum deviations to the interferometer value are 0.016 mm (IATS) and 0.019 mm (level).

4.3.5 Discussion

The presented experiments are based on distances of 5 m and 15 m - limited by the dimensions of our laboratory. Even though, they can be seen as a proof of concept of the IATS leveling capabilities. The first test scenarios demonstrate that the developed algorithm allows to repeat height readings from a digital leveling staff with high precision. Compared to the ATR function of the total station even slightly better results can be reached. In case of non-horizontal views, the standard deviation increases marginal as the trigonometric part is additionally influenced by the uncertainties of the angle and distance measurement. In the second test sce-

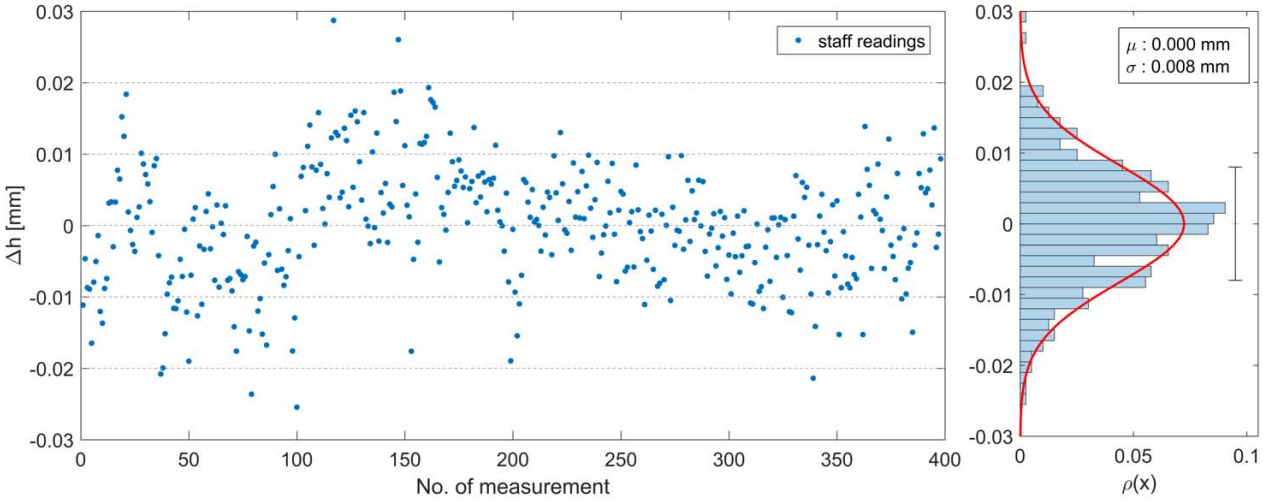

Figure 4.22 – Result of 400 IATS staff readings at a fixed height difference in a distance of ~15.5 m. Residuals to the mean value (left) and probability distribution function fitted through the histogram of the sample data (right).

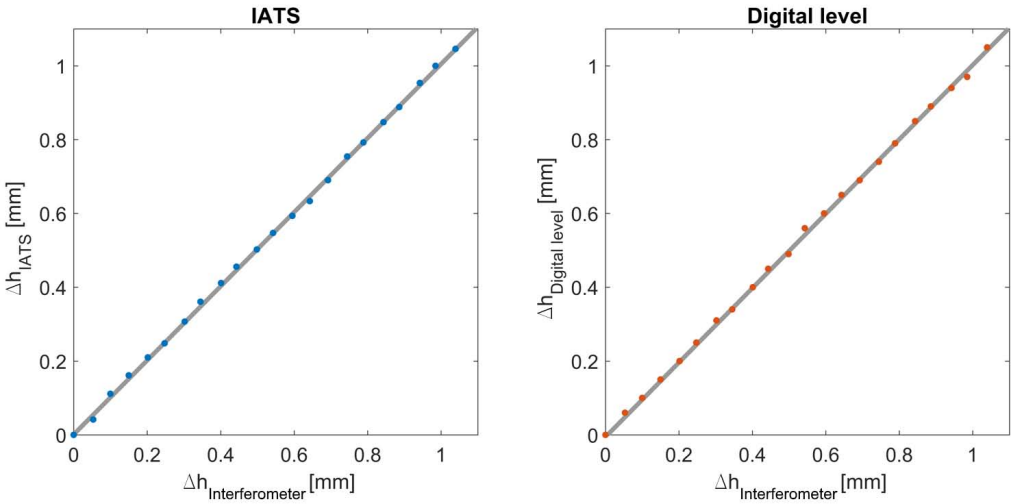

Figure 4.23 – Comparison of IATS (left) and digital level (right) height readings with the interferometer reference. The digital staff is displaced in 0.05 mm steps (for better visibility only a part of the data is displayed)

nario, we compared our method with measurements of a precise level and references of a laser interferometer. The simulated height deviation can be detected with equivalent high accuracy. This means there is no significant difference in the results using either a precise level or an IATS for leveling. In first additional measurements in 20 m, 30 m and 40 m distance we achieve results with no significant differences to those of a digital level (direct comparison of height readings IATS – digital level) (Lichtenberger, 2015). The detailed results will be published in future.

4.3.6 Conclusion

In many use cases it is important to precisely transfer the instrument height of a total station from a reference point. Up to now this has often been done by manual reading from a leveling staff on a benchmark. In this paper we show the capability of modern total stations (with built-in in telescope cameras) to solve this task with high accuracy by automatic readings. With the presented method for decoding digital barcode staffs – based on subpixel edge detection and least square adjustment – an efficient on-board application can be implemented. The results obtained by IATS are competitive with those of modern digital levels. The possibility of a non-horizontal aiming is the biggest advantage of leveling with an IATS. It allows to handle large height differences between the instrument and the staff. However, these measurements are influenced by uncertainties in the vertical angle reading and distance measurement. This is also possible using the built-in ATR function, but as shown, we get a slightly better object/code pattern detection. In combination with the more accurate leveling staff instead of a reflector pole, the final result will be improved. Further, by using a leveling code pattern it is impossible to do (manual) misalignments, as the vertical aiming of the crosshair to the barcode is not necessary. This is e.g. useful in monitoring applications where repetitive measurements to the same target(s) need to be done. In contrast to level instruments also multiple targets in different heights can be surveyed. The presented analysis method to read digital leveling staffs with total stations is highly versatile. Next to the already mentioned monitoring tasks, like bridge load tests or subsidence measurements, methodology applications, such as the examination of linearity or machine alignments, are also possible. In the future we will integrate additional code patterns. We are optimistic that such a basic leveling function will be implemented by the manufacturers in upcoming total station firmware. The hardware is ready now.

4.4 P-IV: A new approach for geo-monitoring using modern total stations and RGB + D images

Author: Andreas Wagner

Publication: Measurement, 82 , DOI: 10.1016/j.measurement.2015.12.025, pp. 64-74, 2016

.

Abstract: The objective of this study is to present a new approach to geo-monitoring. The approach is based on a combination of different existing as well as established methods while resolving present disadvantages. Herein, RGB + D images are used for a fused data analysis of scan and image data acquired by a single instrument. The used Image Assisted Total Station (IATS) – a multi-sensor system – is presented in detail, with particular focus on the integrated camera system. This includes an improved matrix based notation for the pixel angle relation.

The main feature of the analysis is a combination of point cloud and image data, which complement each other very well for monitoring tasks. The data is acquired in subsequent measurement epochs wherein RGB + D images are generated. As a result, any pixel position can be expressed as a polar measurement and transformed into a 3D world coordinate. With the help of image matching algorithms corresponding points/regions of two epochs can be found and displacement vectors calculated.

The single processing steps are explained and the practical usage is demonstrated by an application example.

Keywords: Geo-monitoring, RGB + D, Image matching, Landslide, IATS

4.4.1 Introduction

Monitoring in the form of repetitive or continuous check and control of artificial or natural structures is one of the key tasks in engineering geodesy. It is a process of periodical gathering of information of the current states for all aspects of the observed object. If the main objective is measuring and tracking displacements or changes in shape as a result of internal or external forces, it is specified as deformation monitoring (Settles et al., 2008).

In the field of geo-monitoring, geodetic sensors and methods are often used. These form a link between the large-scale methods of remote sensing and the non-georeferenced point-based geotechnical measurements of local applications. Specifically, these are Global Navigation Satellite Systems (GNSS), Terrestrial Positioning Systems (TPS), Terrestrial Laser Scanners (TLS), (Stereo) Photogrammetry (SP) and Ground-Based Synthetic Aperture Radar (GB-SAR). As shown in Wagner et al. (2014a), these methods generally differ from each other in cost, spatial and temporal resolution, range, dependence from weather or light conditions,

energy and communication link requirement as well as in the necessity to access the possibly endangered surveillance area. However, this also implies that they can complement each other.

Whilst on the hardware side most of these different sensors[1] unite into a single (universal) instrument, as described in Wunderlich et al. (2014), the data analysis is still performed separately. To change this fact, in this article a new approach is presented which utilises the full potential of a modern total station and its various built-in sensors. The main aspect is the merged evaluation of laser-scan and image data from a total station platform, directly acquired in a common coordinate system. When comparing these measurement methods it becomes clear that they complement each other very well. Changes in line of sight may be clearly detected in sequential TLS data as distance variation. In image sequences such displacements appear as (object) scaling and are hard to detect – if only image features are analysed such movements may not even be discovered at all. On the other hand, image and template matching algorithms are very sensible for identifying displacements in transverse direction, where the evaluation of laser scanner data weakens (in particular with low-structured surfaces). A combined data evaluation will generate 3D object points and vectors directly, which can be further processed in a classical geodetic deformation analysis. Unstable control points as well as significant and non-significant object movement are therefore detected.

In the new approach, movements will be uncovered by generating 3D displacement vectors of subsequent epochs. The measurements are done by a single instrument in permanent or periodical operation mode, which creates images and point clouds of the surveillance area. Distance data is converted into a depth image, meaning the distances from the station are converted into grey or colour values of an image, where the pixel coordinates correspond to theodolite angular values. The result forms the D-channel of a RGB panorama image. By using template matching methods, such as a normalised cross-correlation (NCC) of image parts in these RGB + D images, real 3D displacements can be detected.

Numerous examples have demonstrated that terrestrial, airborne, or satellite image based methods are suitable for producing displacement fields of landslides. These studies used subsequent images of two IATS devices in stereo configuration (Wagner et al., 2014a; Reiterer et al., 2009) or subsequent images of one camera and one "static" digital surface model (DSM) – mostly derived from aerial laser scanning – to generate 3D information (Debella-Gilo and Kääb, 2011; Travelletti et al., 2012; Schwalbe, 2013). As a result, the most limiting factors of the final accuracy are small movements of the camera and the use of a mono-temporal DSM (Travelletti et al., 2012). Other approaches take subsequent laser scans and generate projections of the resulting point clouds. This enables a simple 2D comparison based on a sliding window correlation in a plane perpendicular to the viewing direction while still preserving the 3D displacement information (Aryal et al., 2012; Travelletti et al., 2014). The input data of the correlation functions in these methods are the intensities of the reflected laser beam or the gradient of the distance between object point and TLS station. As

[1] With the current exception of GB-SAR

usual, the transformation parameters of each point cloud have to be re-calculated if the scanner has (even slightly) moved. In the proposed approach these drawbacks do not arise, as only a single IATS with scanning function is used. The stability of the station coordinate and orientation is permanently checked and recalculated by an internal dual axis inclinometer and measurements to surrounding control points. Even the use of GNSS baselines for surveillance is possible. The correlation or matching (input) data is based on optical images as algorithms for these are well evaluated and suited (Debella-Gilo and Kääb, 2011). However, it is also expandable to TLS derived metrics as described above.

This paper is divided in two main parts: The first part (Section 4.4.2) gives an overview about the used instrument type and compares available devices. In particular, the camera system is described in detail in Section 4.4.3, as it is often misunderstood and is often only described in German literature. A matrix based notation for the pixel angle relation is also presented here. The second part (Section 4.4.4 and Section 4.4.5) presents the proposed method in detail and shows an application example. A conclusion (Section 4.4.6) completes the paper.

4.4.2 Modern total stations

Theodolites are instruments for measuring angles in the horizontal and vertical planes. Modern Total Stations, in contrast, are multi-sensor systems which provide highly accurate angle and distance measurements to prisms and less precisely to nearly any other surface. Further functions are tilt correction by 2-axis inclinometers, automatic target recognition and tracking, GNSS positioning, overview and telescope cameras, as well as a scanning function with up to 1000 points per second. Due to this, the methodology of surveying has drastically changed and is continually changing, in particular for monitoring tasks (Wunderlich, 2006). While the hybrid usage of GNSS and TPS is standard in many survey tasks, the fusion of scanning, TPS and digital photogrammetry remains an object of current research (Wunderlich et al., 2014).

However, as shown in Table 4.8, appropriate hardware for this task is already available. All major manufacturers of surveying instruments offer a total station which is equipped with at least one (overview) camera. In literature these kind of instruments are therefore also called Image Assisted Total Station (IATS). Instruments of the Leica Nova and Topcon Imaging Station series also provide an additional coaxial camera which benefit from the magnification of the telescope. This results in a lower ground sampling distance (higher spatial resolution) of the images compared to the overview camera, albeit at a smaller field of view. A simple scanning function is also usually implemented. The measuring rate varies greatly, between 15 and 1000 points per second. This substantial increase in recent years is primarily the result of improved motorisation. The last mentioned scan rate is comparable to that of a laser scanner of the first generation, such as the Cyrax 2500. Certain total stations even use the same electronic distance measurement (EDM) units as seen in a TLS. Nevertheless, the scan rates are still far behind those of current laser scanner systems with rates of about 1 MHz. Due to design, TLS will always be faster than scanning total stations. The main reason for this is the

Table 4.8 – Specification of modern Total Stations (source: respective manufacturer)

				
	Leica Nova	**Pentax Visio**	**Topcon IS-3**	**Trimble S9**
Camera	wide-angle + coaxial	wide-angle	wide-angle + coaxial	wide-angle
Resolution	2560 x 1920	2048 x 1536	1280 x 1024	2048 x 1536
Field of view	15.5° x 11.7° 1.4° x 1.1°	7.0° x 5.3°	28° x 22° 1° x 1°	16.5° x 12.3°
Zoom	8x digital 30x optical	3x digital	4x digital 30x optical	8x digital
Scan speed	$\leq$ 1000 pts/s	-	$\leq$ 20 pts/s	$\leq$ 15 pts/s
Scan range	$\leq$ 1000 m	-	$\leq$ 2000 m	$\leq$ 250 m
Release	2013	2009	2011	2015

higher rotating mass of the telescope compared to a small, lightweight beam deflection unit of a TLS.

It should be noted that, in Table 4.8, the EDM range is stated as being up to 2000 m (at a substantially reduced scan rate). This is many times higher than most available TLS systems and it ends the limitation of earlier geo-monitoring projects with total station and reflectorless EDM to natural targets, e.g. Thuro et al. (2010).

The greatest advantage of such a multi-sensor instrument is the common coordinate system of all built-in sensors, with an appropriate calibration provided. In particular, the captured images and scanned point clouds are immediately georeferenced and oriented with no need for additional control points or further orientation processes.

4.4.3 Camera systems

In literature, different system descriptions of IATS cameras can be found:

Huang and Chen (2000) extend the collinearity equations by an additional camera rotation and translation, but possible theodolite errors are neglected. Juretzko (2004) uses a central projection in form of an oblique gnomonic map projection. An optional empirical correction matrix improves the accuracy (no theodolite errors are considered). In Bürki et al. (2010) a central projection is also used but is expressed as an affine transformation without theodolite errors. Knoblach (2009) extends this approach to be used for different focus lens positions. Walser (2004) describes the camera with an affine chip model and takes instrument errors into account. This and the previously mentioned approach can only be used for telescopic cameras. The

special feature of the model is a fixed principal point for all focus lens positions, which enables a constant virtual cross-hair over the entire focal range. In Vogel (2006) the collinearity equations are extended by additional camera parameters: a photogrammetric collimation axis error and a photogrammetric vertical index error, instrument errors, camera rotations and an additional distance between the theodolite and camera projection centres. This model may be used for overview as well as for telescopic cameras. However, as shown in Wasmeier (2009a), not all parameters may be determined in a single calibration process if the camera centre is too close to the theodolite centre.

Summarizing these system descriptions it can be said that none of them can be used for all different types of total station cameras while satisfying the high accuracy demands at the same time. By introducing homogeneous coordinates, the relationship between a 3D (world) coordinate (or spatial direction) and its image projection can be expressed in a single, compact 3 × 4 projection matrix $\boldsymbol{P}$. In contrast to the collinearity equations this enables a vectorized computational calculation and improved performance.

Basic equations

Using the pinhole model for cameras a 3D world point[1] $\tilde{\boldsymbol{X}} = [X, Y, Z, 1]^T$ is projected into an image at position $\tilde{\boldsymbol{x}} = [\lambda x, \lambda y, \lambda]^T$ by the projection matrix $\boldsymbol{P}$:

$$\tilde{\boldsymbol{x}} = \boldsymbol{P}\tilde{\boldsymbol{X}} = \boldsymbol{K}\left[\boldsymbol{R}|\boldsymbol{T}\right]\tilde{\boldsymbol{X}} \qquad (4.5)$$

The calibration matrix $\boldsymbol{K}$ represents the intrinsic parameters of the camera:

$$\boldsymbol{K} = \begin{bmatrix} f & 0 & x_0 \\ & f & y_0 \\ & & 1 \end{bmatrix}$$

where f denotes the focal length and (x_0, y_0) the coordinates of the principal point. In a more general form, $\boldsymbol{K}$ is extended to cover non-square camera-pixels by appropriate scaled focal lengths (f_x, f_y) and a non-orthogonal image coordinate system by a skew parameter $s_\alpha = f_x \tan\alpha$ (Hartley and Zisserman, 2003):

$$\boldsymbol{K} = \begin{bmatrix} f_x & s_\alpha & x_0 \\ & f_y & y_0 \\ & & 1 \end{bmatrix}$$

The extrinsic parameters – represented by the rotation matrix $\boldsymbol{R}$ and the translation vector $\boldsymbol{T}$ – summarise a group of three different Euclidean transformations:

$$\boldsymbol{R} = \boldsymbol{R}_c\boldsymbol{R}_t\boldsymbol{R}_w$$
$$\boldsymbol{T} = \boldsymbol{R}_c\boldsymbol{R}_t\boldsymbol{T}_w + \boldsymbol{T}_c$$

1. Transformation from the world or object coordinate system into the theodolite coordinate system ($\boldsymbol{R}_w, \boldsymbol{T}_w$).
2. Transformation into the telescope coordinate system ($\boldsymbol{R}_t$).
3. Transformation into the camera coordinate system ($\boldsymbol{R}_c, \boldsymbol{T}_c$).

[1] Represented in homogeneous coordinate form (labelled with ˜)

The first mentioned transformation depends on the specific survey task and may be solved by standard surveying methods like a resection to control points. In most cases, $\boldsymbol{R}_w$ will only consist of one rotation around the z-axis which is known as station constant or orientation unknown. It may also be simply omitted (replaced with an identity matrix) if a local system is used.

The second transformation $\boldsymbol{R}_t$ is a pure rotation by the theodolite horizontal and vertical angle readings (hz, v). For a single measurement it can be integrated also into $\boldsymbol{R}_w$. To tap the full accuracy potential of the system it is essential to also consider the instrument errors. A common way is to directly adjust the horizontal and vertical angle values, e.g. as described in Kahmen (2005), which requires previous determined adjustment parameters. Nevertheless the camera chip is still affected by these errors, which will cause inaccuracies in the pixel-angle conversion. Therefore, these errors should be modelled as additional rotations (as these are functions of the current angular readings):

$$\boldsymbol{R}_t = \boldsymbol{R}_\kappa(hz)\boldsymbol{R}_\varphi(e_t)\boldsymbol{R}_\omega(v)\boldsymbol{R}_\omega(e_i)\boldsymbol{R}_\varphi(e_c)$$

with the transit axis error e_t, the vertical index error e_i and the collimation error e_c.

As these errors are eliminated by double-face observations, it is possible to determine corrections by means of a system calibration. The effect of a non-verticality of the instrument axis – which is not an instrument error – may be eliminated by the transformation into the world coordinate system, or if a tilt sensor is used, as two additional rotations around a longitudinal inclination angle (i_l) and a transverse inclination angle (i_t):

$$\boldsymbol{R}_{t'} = \boldsymbol{R}_\omega(i_t)\boldsymbol{R}_\varphi(i_l)\boldsymbol{R}_t \tag{4.6}$$

The transformation between the camera coordinate system and telescope coordinate system $\boldsymbol{R}_c, \boldsymbol{T}_c$ can be described by constant parameters. That means these values are independent of the angular readings and may be determined by camera calibration.

Backward transformation

The projection of a pixel coordinate back to a 3D world point is not possible, as no unique inverse of a projective transformation exits. It is only possible to determine a spatial ray through the camera centre. All points of this ray are then mapped to the given pixel position.

To reconstruct this ray two points can be determined: One point may be calculated by the pseudo-inverse $\boldsymbol{P}^+$ of the projection matrix (Hartley and Zisserman, 2003):

$$\tilde{\boldsymbol{X}}(\lambda) = \boldsymbol{P}^+\tilde{\boldsymbol{x}} = \boldsymbol{P}^T\left(\boldsymbol{P}\boldsymbol{P}^T\right)^{-1}\tilde{\boldsymbol{x}}$$

The second point is the camera centre $\tilde{\boldsymbol{C}}$:

$$\tilde{\boldsymbol{C}} = -\boldsymbol{R}^{-1}\tilde{\boldsymbol{T}}$$

For better understanding and increased readability this equation may be simplified if a non-homogeneous coordinate form

is used. This changes Equation 4.5 to:

$$\begin{aligned} \boldsymbol{x} &= \boldsymbol{K}(\boldsymbol{R}\boldsymbol{X} + \boldsymbol{T}) \\ &= \boldsymbol{K}\boldsymbol{R}(\boldsymbol{X} - \boldsymbol{C}) \end{aligned}$$

The final spatial ray – expressed by two points (whereby one is the camera centre $\boldsymbol{C}$) – may be expressed by the inverse function:

$$\boldsymbol{X}(\lambda) = \left[\boldsymbol{K}\boldsymbol{R}\right]^{-1} \lambda \boldsymbol{x} + \boldsymbol{C} \tag{4.7}$$

Overview camera

All of the total stations presented in Table 4.8 are equipped with wide-angle cameras, providing an overview of the scene for users. Using Equation 4.5 it is possible to project measured or a priori known points and lines into the camera image. This is currently used by manufacturers to overlay video streams with measurement and planning data, as well as sketches and notes on the instrument's display.

To display a virtual cross-hair – i.e. visualising the direction the total station is aiming to – is more complex. As the overview camera should have a greater field of view than the telescope, the projection centre of the camera must be different from the theodolite centre (axis intersection point). The point which coincides with the physical cross-hair of the instrument is therefore projected as a line into the camera image, see Figure 4.24. This fact can be compared to an epipolar line in a stereo configuration. For example, for a Leica Nova instrument and a collimated target in a distance of 2 m and 1000 m, this line has a length of 300 pixels. Only if the distance to the target point (and subsequently the 3D coordinate) is known, the appropriate pixel position can be calculated.

It should be noted that, due to the wide field of view of these camera types, a radial distortion correction is necessary to exploit the full accuracy potential.

Telescope camera

Considering the necessities of the telescope camera, it is useful if the projection centre coincides with the theodolite centre. Thus, a pixel position can be directly converted into a polar angle without knowing the object distance. If the points $\boldsymbol{S}$ and $\boldsymbol{C}$ in Figure 4.24 coincide, the collimation axis is projected to one single position at the camera chip for any point on the spatial ray $\boldsymbol{X}(\lambda)$. This means there exists a unique inverse function Equation 4.7 and the theodolite angles can be calculated by a vector $\boldsymbol{L}$:

$$\boldsymbol{L} = \boldsymbol{X}(\lambda) - \boldsymbol{C} \qquad \lambda \in \mathbb{R}^{+}$$

and its projection into the horizontal and vertical plane[1]:

$$\begin{aligned} hz &= \arctan\left(\frac{X_L}{Y_L}\right) \\ v &= \arctan\left(\frac{\sqrt{X_L^2 + Y_L^2}}{Z_L}\right) \end{aligned} \tag{4.8}$$

It should be noted that, due to the restricted field of view of the telescope camera, small ro-

[1] Measuring positive angles in clockwise direction and using only positive λ in Equation 4.7

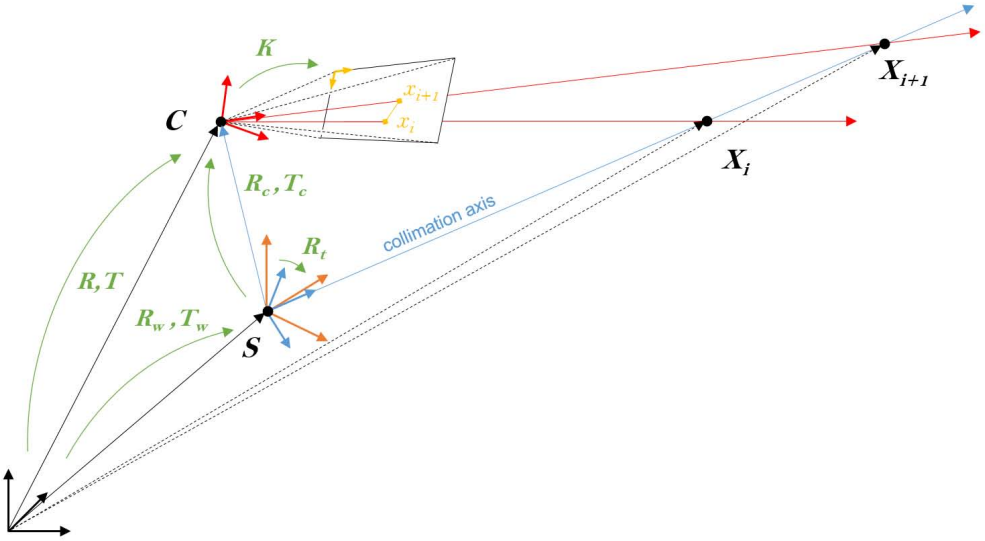

Figure 4.24 – Relation between total station centre S and (overview) camera centre C: The extrinsic parameters of the camera R, T are a combination of three single transformations. The collimation axis is projected as a line into the image if an eccentricity between S and C exists.

tations cannot be separated from small translations. This makes it difficult or even impossible to use a control field or calibration plate for a camera calibration procedure. A suitable solution is to use a virtual control field as described in Huang and Harley (1989), as well as a focusable collimator to simulate different distances.

In contrast to wide angle cameras, the field of view of telescope cameras is quite small (cf. Table 4.8) and in most cases a radial distortion correction may be neglected.

4.4.4 Geo-monitoring approach

By subtracting two 3D scans, displacements along the line of sight can be easily detected. For feature movements transverse to this (sighting) direction this is simply achieved using image sequences. Both methods therefore complement each other and should be used in combination to monitor natural and/or artificial objects. In the new approach image and scanning data is sequentially acquired and analysed as depict in Figure 4.25. The single processing and evaluation steps are:

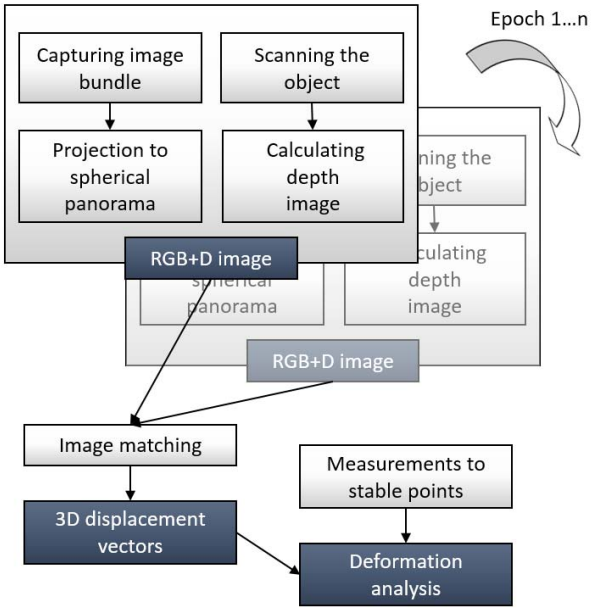

Figure 4.25 – Sequence diagram of data acquisition and analysis

1. Capturing an image bundle and projecting it into one single (spherical) panorama.
2. Scanning the object (by the distance facility of the total station) and calculating a depth image panorama.
3. Matching the two image panoramas of different epochs and calculating 2D displacement vectors.
4. Calculating the third dimension of the vector points from the depth images.
5. Performing a geodetic deformation analysis for statistically proven results.

All data is acquired by a single instrument, a modern total station as described in Section 4.4.2. The main advantage of using a single device is that the different data is captured instantly in the same coordinate frame, an appropriate system calibration provided. The stability of the station is continually checked and recalculated by an internal dual axis inclinometer. In modern instruments, small tilts are automatically corrected by adjusting the angular values. As previously mentioned, these corrections have also to be considered for the image orientations (cf. Equation 4.6). An inclination of the instrument always leads to an additional torsion, meaning a new orientation measurement is necessary. To solve this task, an IATS offers different methods:

- Standard survey methods, like (fully automated) aiming to signalised control points with co-operative prisms.
- Image analysis and recognition techniques to find and point to signalised passive targets, e.g. coded targets (Zhou et al., 2015). Or more generally by using natural, structured areas as templates to be (re-)located in subsequent epochs.
- Point-based methods, like relative co-registrations (e.g. ICP).

The necessary coordinate frame may be a local one, meaning the different epochs are only relatively compared. If a superior coordinate frame should used it can be (1) transferred by control points or (2) simultaneously determined by a GNSS antenna at the instrument. The last mentioned method presupposes another GNSS receiver at the orientation point. A consequence of all these different positioning and orientation possibilities are low requirements to an instrument station. A fixed installation, such as a measurement pillar or a temporary set-up on a tripod may be used. However, the last mentioned method decreases the measurement accuracy along with the stability of the station, even if corrections are considered.

In the following the single steps of the data acquisition and analysis are described in detail.

Panorama

To extend the small field of view of the telescope camera it is necessary to take several images of the monitoring area within an image bundle. A preselected region of interest (ROI), e.g. a rectangle defined by two coordinates or directions, is divided into single images based on a defined overlap between adjacent images. For each image the necessary acquisition angles are calculated and the scene is automatically captured.

For the subsequent analysis the images are stitched into one single panorama. As described above, the telescope camera can be described as stationary projective camera which is only rotating. Using Equation 4.5 with no translation, an image point $\tilde{\boldsymbol{x}}_i$ is projected into a another image at location $\tilde{\boldsymbol{x}}_j$:

$$\begin{aligned}\tilde{\boldsymbol{x}}_j &= \boldsymbol{K}_j \boldsymbol{R}_j \left[\boldsymbol{K}_i \boldsymbol{R}_i\right]^{-1} \tilde{\boldsymbol{x}}_i \\ &= \boldsymbol{K}_j \boldsymbol{R}_{ji} \boldsymbol{K}_i^{-1} \tilde{\boldsymbol{x}}_i\end{aligned} \tag{4.9}$$

which may be represented as a 3 × 3 homography matrix, often denoted by $\tilde{\boldsymbol{H}}$. With this relationship all images may be mapped into a common plane, e.g. the first image. While this is sufficient for small regions of interest, for wider areas it will distort the images the further away they are from the target image plane. If the projection angle exceeds 90° it cannot be displayed at all. To solve this problem the images are projected to a spherical surface instead of a plane by replacing $\boldsymbol{K}_j$ in Equation 4.9 with a Cartesian-spherical coordinate transformation. This enables a full 360° view and the theodolite angles to any pixel are directly given by its pixel position. A backward warping with bilinear interpolation is used to ensure that each point $\tilde{\boldsymbol{x}}_j$ maps exactly to one output pixel.

To compensate for possible exposure differences between the images these should be blended into each other, especially in the overlapping regions. For this a centre-weighting based on a distance map – also called feathering – is used. This means pixels are weighted based on their distance from the image border: pixels are weighted higher near the centre and lower near the edges. This more simple method, in comparison to Laplacian pyramid or gradient domain blending (Szeliski, 2010), is completely sufficient due to the high absolute angle measurement accuracy, e.g. 1″ ≙ ½ pixel for the instrument used in Section 4.4.5.

However, it has been found that the vignetting effect of telescope images is higher than for images of the overview camera, which must be considered when creating the panorama. This effect causes the brightness of an image to fall off towards the edge of the frame. The major vignetting impact may be the complex lens system of the telescope, which is also the reason for a weaker signal-to-noise-ratio (SNR) of theodolite camera systems compared to SNR of industrial imaging systems (Reiterer and Wagner, 2012). To reduce the vignetting effect an empirical correction model in form of a polynomial function is used. The result is shown in Figure 4.26.

Depth images

All available scanning total stations generate point clouds in the theodolite coordinate system. If the standard surveying set up and orientation procedures of the instruments are used, the data is directly generated in the world coordinate system and the results can be checked by a geodetic deformation analysis. Compared to conventional laser scans there is no need for (additional) control points, such as black and white targets or spheres. If stable regions are used for the co-registration of the point cloud data, these areas have to be selected manually and it may happen that movements remain uncovered, cf. Section 4.4.5. In summary, if point cloud data is acquired by a scanning total sta-

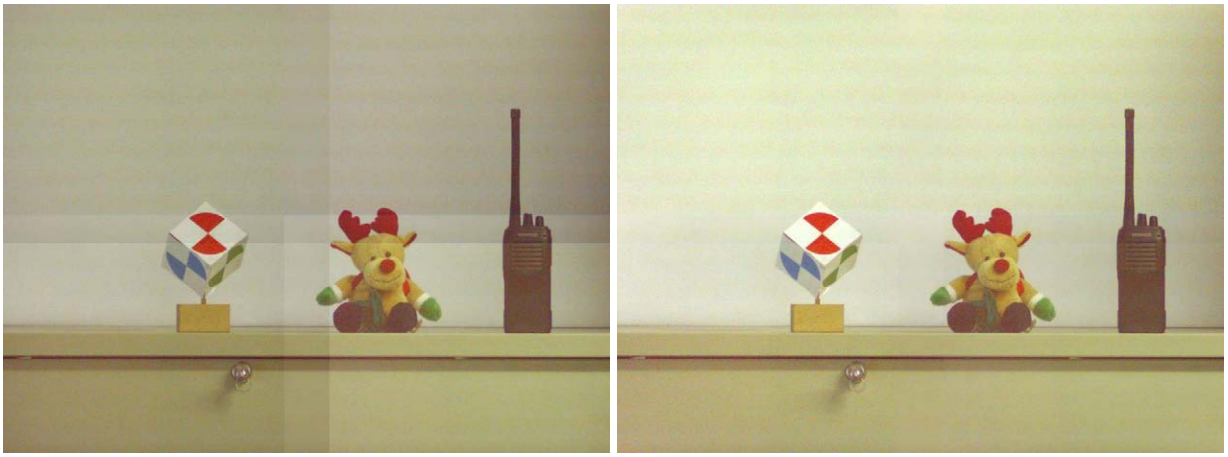

(a) (b)

Figure 4.26 – Stitched panorama (a) without and (b) with blending and vignetting correction (artificial laboratory scene)

tion, there exist more ways for registration and modelling.

For the further combined use with the image data, the points are (perspectively) projected into the previously generated panorama (if the panorama is projected onto a spherical surface, the depth image must also be spherical). The result is an irregular grid of 2D points and a distance from the camera projection centre to each of them. A depth image can be created by interpolating the points into a regular grid with the same grid dimensions of one pixel in the panorama. The data can then be displayed as an image by colouring the pixel values depending on the object distance, creating the depth channel of the RGB + D image. The result is an image with four channels: red, green, blue, and distance, as shown in Figure 4.27. The 3D world coordinate of each image pixel is therefore immediately available.

It should be noted that the accuracy of the depth information – and therefore the resulting 3D coordinate – is highly dependent on the ground sampling distance of the scan and the chosen interpolation method. That means the scan density has to be adapted to the angular resolution of a pixel. However, the image resolution of the telescope camera will always be higher than the distance resolution. One IATS telescope image pixel[1] corresponds to 0.61 mgon (1.98″), and therefore 0.09 mm at 10 m distance. Even currently available TLS give only a point to point resolution of ~0.6 mm at 10 m (at a many times larger spot size).

As a consequence, the lateral component of the resulting displacement vectors will be more accurate than the distance component. Nevertheless, the use of images in the proposed method brings significantly higher accuracies compared to intensity or distance-gradient images of pure TLS methods as mentioned in Section 4.4.1.

[1] For the instrument used in Section 4.4.5

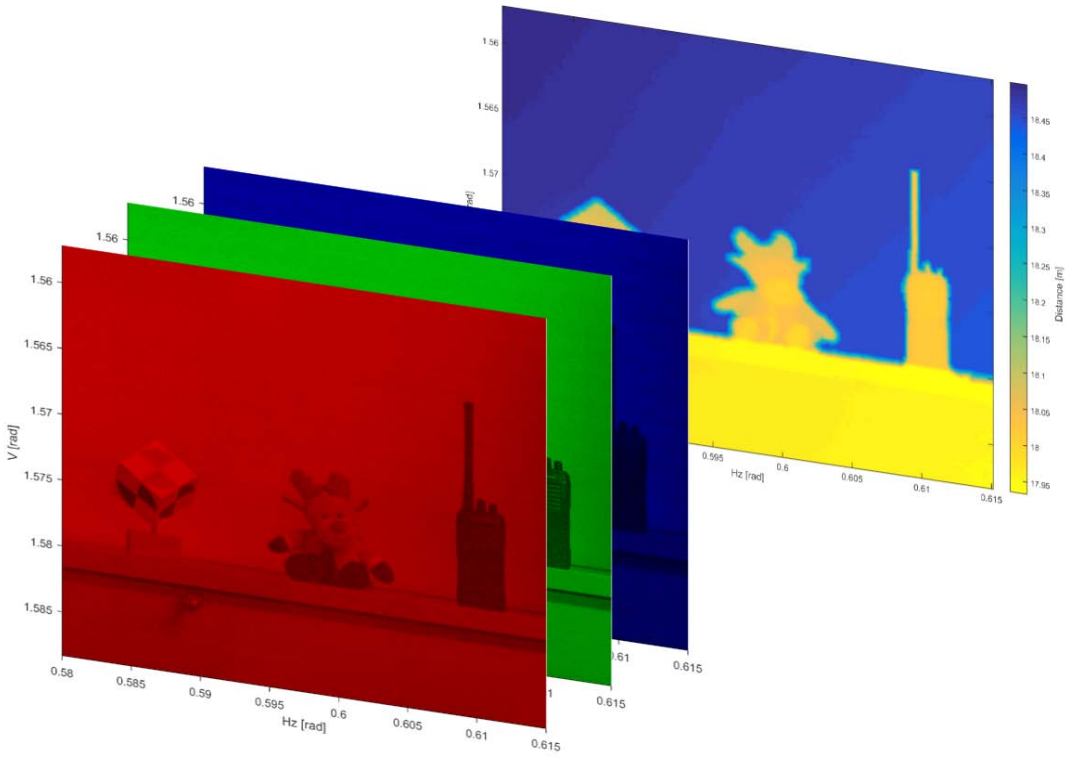

Figure 4.27 – The individual elements (channels) of a RGB + D image

Image matching

With the help of the above mentioned steps it is possible to generate 3D displacement vectors of two different measurement epochs by detecting corresponding points in the respective panoramas. In photogrammetry various approaches exist for image matching, which may be classified into three basic techniques: intensity-based, feature-based and relational (Gruen, 2012).

The intensity-based matching algorithms, e.g. Normalized Cross-Correlation (NCC) or Least Squares Matching (LSM), provide sub-pixel accuracy and are widely used. In feature-based matching algorithms, descriptions of key points are matched against each other. Most methods provide sub-pixel accuracy, including the most prominent methods; the SIFT and the SURF algorithm. In the last mentioned technique, geometric or other relations between features and structures are used.

In the field of computer vision, additional and more global algorithms, such as Semi-Global Matching (SGM) are used.

The appropriate method and its implementation depends strongly on the expected deformation between the measured epochs. The type of the displacement has to be considered, i.e. whether a rotation or pure translation is possible. Also, the displacement magnitude and the time interval between two epochs influences the processing strategy. Unfortunately, there is no optimal image matching function and for each application the most suited algorithm has to be specifically selected.

Geodetic deformation analysis

The identification of unstable reference points, as well as that of significant object movements, is a central task in monitoring applications and subject of geodetic deformation analysis, cf. Pelzer (1985). Only a statistically verified result of a measurement may be used for further processing or interpretation. This is valid in particular to reliable alarm systems for the prevention of human and material damage. Using a total station as a measuring device it is easy to take measurements of stable reference points, which should be located outside the deformation area on geologically stable ground. As the instrument is turnable to any direction and measurements to prisms are highly accurate (even at great distances) there are no limiting factors as with other systems. Based on these reference measurements the geodetic deformation analysis will separate stable points as well as significant point movements (in this case displacement vectors) and give statistically verified results. Possible station movements are also uncovered and are considered within the calculation.

It should be mentioned that the traditional task of deformation measurements has been a quasi static process (Pelzer, 1985). Nowadays it is a geodetic analysis of dynamic processes with real-time alarm systems and new methods for modelling measuring errors (Heunecke et al., 2013). Consequently, monitoring an object must be done by an interdisciplinary team of experts which understand the dynamics of the present processes.

4.4.5 Application example

The described method was tested at an alpine landslide area in Austria. The Hornbergl, near Reutte (Tirol), has been geodetically monitored since 1987 and shows point movements of tens of decimetres per year (Wunderlich, 2004). Currently, a hybrid TPS-GNSS net is measured every year by the TUM Chair of Geodesy. Additional convergence measurements, a permanent low-cost GNSS system and GB-SAR/DInSAR tests of various research institutes are being done or have been done (Wunderlich, 2012). An additional areal deformation monitoring of the peak rock face with TLS began in 2009. It turned out that deformations are difficult to detect if the scanned area is relatively flat and the displacement takes place perpendicular to the surface normals. Furthermore, if two point clouds are co-registered without control points, e.g. by an Iterative Closest Point (ICP) algorithm, stable regions have to be selected manually. The scanned area must therefore be big enough to enclose such geological stable regions which is not always possible. For the Hornbergl peak rock face (Figure 4.28) this is particularly difficult and pseudo stable regions must have been selected without knowledge if these have moved (Wiedemann, 2014).

All these issues could be solved by identifying corresponding points or patches in the point clouds by using RGB + D images and geodetic measuring methods, as proposed in the method described above.

The new approach was tested in one campaign, as shown in Figure 4.28. In the challenging alpine terrain the use of a single instrument brings additional advantages. Fewer devices and therefore less weight has to be

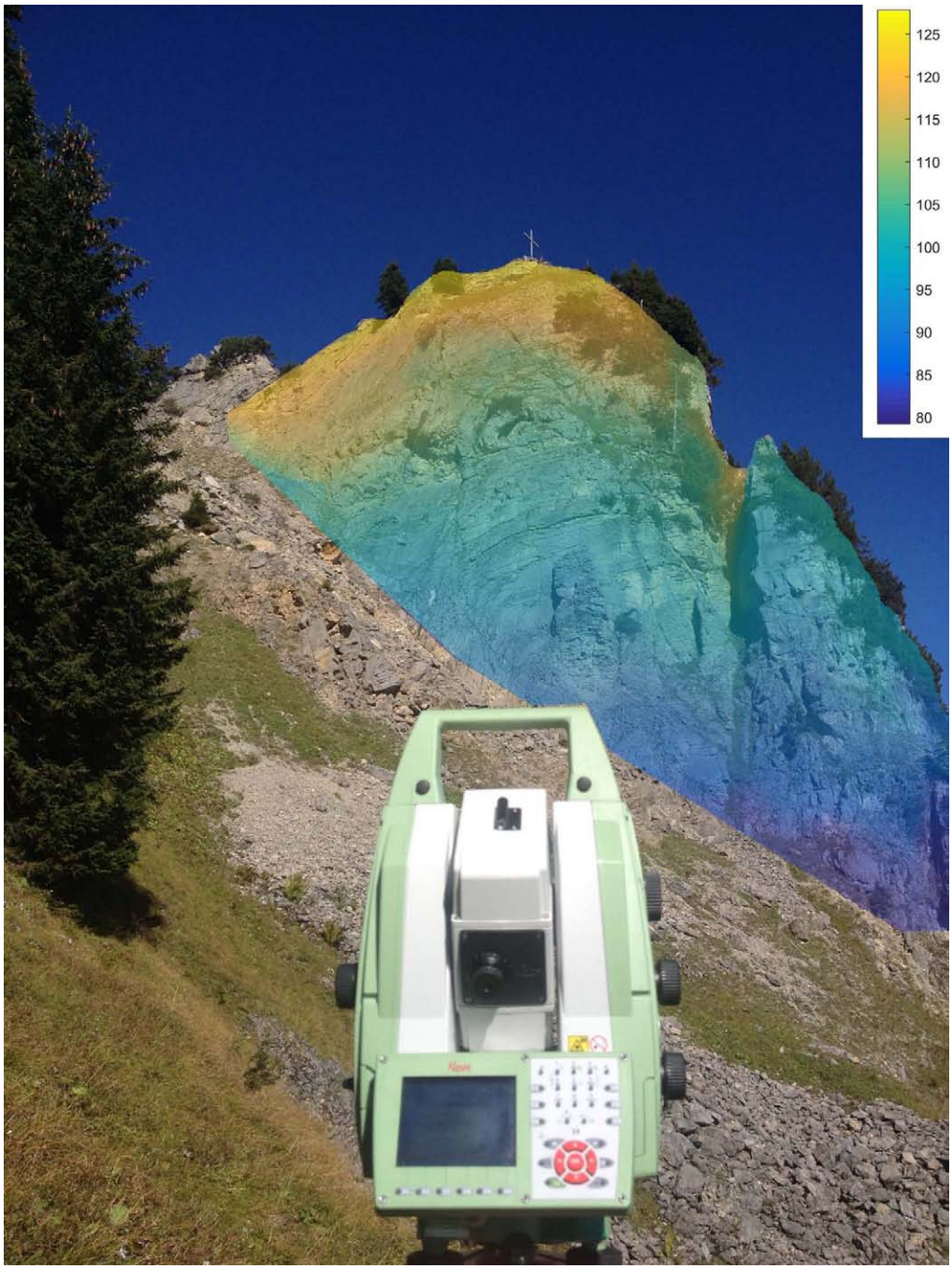

Figure 4.28 – IATS measurement campaign at the Hornbergl. Peak rock face overlayed by a derived depth image, i.e. colour coded distance from instrument station [m]

carried to the observation point. It is also easier to find or determine tie points for the use in multiple measurement epochs. In this campaign, control points of the existing hybrid TPS & GNSS monitoring net could be used. That means the total station was directly set up and orientated within this net. This simplifies the data evaluation and enhances their informative values, especially when compared to the previously realised pure TLS measurements.

The instrument used was a Leica MS50, a subversion of the Nova series, as described in Table 4.8. To exploit to the highest accuracy potential, the telescope camera images are used in all processing steps. These images are magnified 30 times by the telescope lenses, resulting in a pixel resolution of 0.61 mgon. The very high angle accuracy of 1″ (0.3 mgon) of the instrument enables a panorama stitching based solely on the measured image orientations.

For the data acquisition, a permanently marked net point was set up as station with a tripod. As already mentioned, this point is part of a hybrid survey net and its coordinate is calculated in a post processing net adjustment. Two additional net points, signalised with survey prisms, were used for the orientation determination. The rock face was subsequently scanned using the EDM of the total station and an image bundle recorded by capturing overlapping images. In a post processing task, a spherical panorama was created out of the single images, as previously described. Further, a depth image was calculated, as shown in Figure 4.28. Both results form a RGB + D image, in which each pixel position can be directly converted into a 3D coordinate.

The further analysis based on RGB + D images requires a second measurement epoch, including some displacements in between for demonstration purposes. To test the proposed processing chain, a gravel field in front of the rock (cf. Figure 4.28) has been used as an additional test data set. Figure 4.29 shows details of two measurement epochs. Both panoramas consist of nine stitched and blended single images taken by the telescope camera. The axis labels show angular values, as these are spherical panoramas. That means each pixel position corresponds to a spherical/theodolite direction. Together with the distance value of each pixel, coming from the D-channel, a complete spherical coordinate is formed, which can be easily transformed in a Cartesian one.

To simulate some displacement, one of the stones was moved manually. The time interval between both recordings was two hours while it was raining between, resulting in the differences in brightness of both panoramas. Despite these differences in both panoramas, the NCC algorithm found many corresponding regions, as shown in Figure 4.30. To speed up the process, the search was performed with the coarse-to-fine approach based on different pyramid levels.

The clear visible outliers were left deliberately in the image, but could be removed easily by comparing each vector with the orientation and length of neighbouring elements. The sub-pixel accurate start and end points of all vectors can now be determined as 3D coordinates by their pixel position (u, v), which correspond to the theodolite (bearing) angle and the pixel value of the D-channel. The result is a list of Cartesian coordinates of the start and end point (includ-

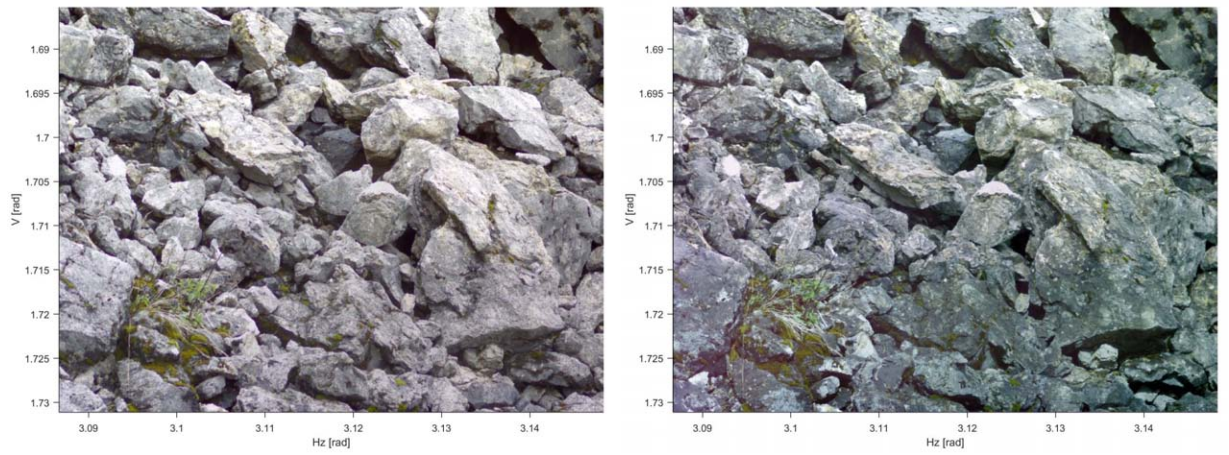

(a) (b)

Figure 4.29 – Details of gravel field – two measurement epochs. Both panoramas consist of 3 × 3 single images

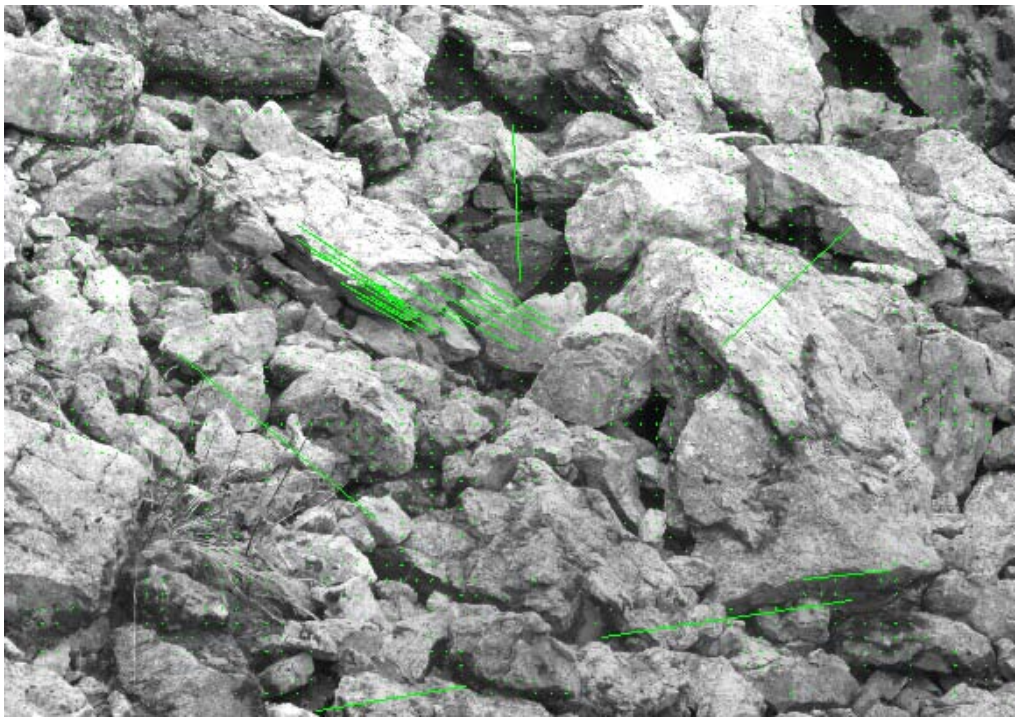

Figure 4.30 – Details of gravel field, with found correspondences calculated by normalised cross-correlation. Green dots depict no movement, green vectors represent displacement between both epochs

ing their accuracy information) of each vector. For visualisation purposes a 3D representation of the vector field, e.g. as a DWG or VRML file or an image overlay, as depicted in Figure 4.30, may be used. The results can be further used for interpretation by experts and decision makers.

4.4.6 Conclusion & outlook

The paper at hand presented a new approach of geo-monitoring using total stations and a fused analysis of image and distance data. Final product is a set of 3D displacement vectors including individual accuracy information. By using a combination of other analysis principles their advantages are adapted, e.g. the data evaluation is sensible for changes perpendicular to and in line of sight. Otherwise, the disadvantages of other comparable methods are avoided. Unlike monocular image sequences, for instance, in each epoch an up-to-date surface model is generated and used. Camera movements are considered by using a built-in inclinometer and survey, image, or point based orientation methods. Permanent and sequential monitoring is possible due to an easy re-installation of the device and within an superior coordinate frame. By using a stitched panorama it is possible to focus each single image separately. In particular at close range where the depth of field of a camera is limited this gives further advantages.

At the moment different image matching algorithms are being tested. It is planned to add the intensity information of the scan into the correlation function, that means to process RGBD + I images. Further, the norm of the 2D (image) gradient of the distance between the point cloud and the TPS station will be tested, as described in Travelletti et al. (2014).

During the next Hornbergl campaign the above mentioned rock face will be measured again according to the described method. With the help of the combined theodolite, image and scan data the exact 3D displacements will be made visible for the first time.

5 Discussion

The four methods presented in Section 4 show the various advantages of using IATS for monitoring applications. The order of the publications reflects the requirements on, resp. the development of the IATS hardware used. From one single prototype (P-I), to two devices in stereo configuration as described in P-II, follows the step to commercial instruments in P-III, and ultimately leads to the requirement for an additional scanning function (P-IV).

The methods are reviewed in the following Section 5.1. The individual strengths and weaknesses are described and compared by selected monitoring features in Section 5.2. Further, the benefits of these new approaches for the research community and upcoming practical usage are summarized (Section 5.3).

5.1 Review

The contemporary trend towards automatic and autonomous monitoring systems is a huge opportunity for surveyors. The metrology experts can offer various geodetic measurement systems and methods as well as analyzing strategies including results tested for significance. IATS can extend this list with a further data acquisition system and additional measurement methods as presented in this thesis.

IATS allow photogrammetric image measurement methods to detect signalized as well as non-signalized targets in combination with functions of the total station, such as precise angle and distance measurements. This amalgamation of sensors and measurement methods, each with their specified single advantages, can be unified and utilized in the single instrument IATS, already denoted as a (nearly) universal instrument (Wunderlich et al., 2014). As shown in Section 4, such an IATS monitoring system is able to determine its exterior orientation automatically, e.g. from signalized control points of the appropriate national coordinate system and can recheck this in regular intervals. The stability of the station can be tested in the same way and/or supported by inclination measurements. GNSS functionalities enable an easy reference to the geodetic datum in remote areas.

IATS offer a wide range of different measurement methods, suited to nearly any kind of application in structural monitoring and geo-monitoring. Continuous, high frequency measurements (P-I) can be realized, as well as mobile once-a-year data acquisitions (P-IV). The determined

results can vary in type from single 1D height differences (P-III) to a large number of 3D displacement vectors (P-II & P-IV). Some selected features are compared in more detail in the next section.

As shown in this thesis, the types of targets used are much more flexible compared to classical TS practice. Not only (expensive) co-operative prisms may be used, but also (low-cost) active targets as shown in P-I. Such target types are of particular importance when handling high frequency visual measurements. It must be guaranteed that each single image is exposed long enough, as the image analysis could otherwise become difficult to impossible. Both co-operative and active targets enable automated measurements at night. A more cost-effective solution is the use of passive targets as presented in P-III. The extraction of edges allows the creation of any kind of artificial target sign, e.g. black and white (scanner) targets (Reiterer and Wagner, 2012), coded targets (Zhou et al., 2016a), or targets based on CAD drawings (Wagner and Wasmeier, 2014). Furthermore, any kind of repeating or traceable structure like circular rivets (Reiterer and Wagner, 2012; Wagner and Wasmeier, 2014) can be extracted from IATS images. No signalization at all, but rather natural structures, are used in P-II and P-IV to fulfill the measurement task. As long as enough texture exists, any kind of surface can be used without the need to have access to this area. This allows even the most hazardous regions, such as landslides, to be monitored safely.

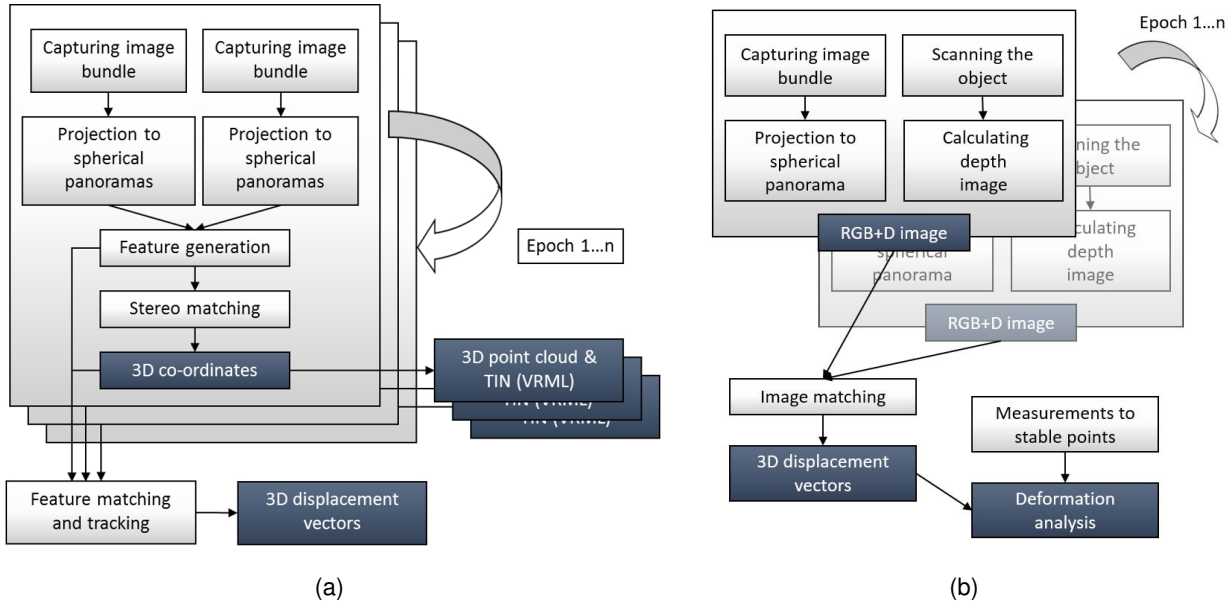

Figure 5.1 – Sequence diagram of data acquisition and analysis for the methods used in P-II (a) and used in P-IV (b).

IATS enable the determination of areal deformation like TLS systems, but with a different acquisition method. The distance measurements can either be done similarly with laser rangefinders (P-IV), or by intersection of direction vectors (P-II). Another important difference is the possibility to identify single interest points and to track these over time. Whilst on the TLS side rigorous

evaluation procedures are still under development and in most cases statistical tests for significance are missing (Wunderlich et al., 2016), IATS based systems deliver 3D displacement vectors (P-II & P-IV), Figure 5.1. These results can be used in classical geodetic deformation analyses, including statistical tests for significance. Compared to monitoring systems using (stationary) photogrammetric cameras, the rotatable telescope offers more flexibility. Larger areas (ROI) can be acquired using image bundles and the stability check can be done using surrounding targets/stable structures. For the latter, it is not necessary to be visible together with the deformation area.

To summarize, IATS enable flexible automation capability by detecting punctual, linear, and areal structural features, as well as mass points, closing the gap of existing solutions. Multiple targets can be measured with high precision in a single image, i.e. without moving the telescope. Every image is automatically geo-referenced and thus each direction derived from pixel coordinates. 3D points can be created with additional distance information (P-I, P-III and P-IV), or another direction measurement from another station (P-II). The relatively small field of view of IATS telescope cameras can be compensated by generating panoramic image mosaics (image bundles), cf. P-II and P-IV.

5.2 Comparison

Figure 5.2 depicts the performance of the individual monitoring tasks described in this thesis. The methods are compared based on five selected features: maximum measurement range, update rate, number of generated points, accuracy with respect to the destined measurement range, and dimensions of generated coordinates. It can be seen that there are high variations among the different monitoring approaches. A detailed look at each point is given in the following.

The metric **range** compares the maximum distance at which the actual method can be deployed. Here, the values differ strongly from each other: The stereo monitoring approach, as described in P-II, may be used at several kilometers distance. The maximum range to decode a (Leica) leveling staff (P-III) lies at 200 m. Above this distance it is not possible to separate two (of the smallest) bar code elements, as these are smaller than a single image pixel[1]. The RGB + D approach is limited by the maximal scanning distance of the instrument used. To achieve acceptable scanning rates, at the moment, the value is only slightly higher than for the leveling staffs. It can be expected, however, that this will increase in the near future. The method described in P-I can be listed below that of P-II at around 1 km. The limitations here are the size of the targets used and, for 3D measurements, the maximum EDM range.

Update rate indicates the time to complete a full measurement epoch. Obviously, the high-frequent LED tracking as described in P-I receives the highest value. The time to take an image of a leveling

[1] Valid for the instrument used in this publication.

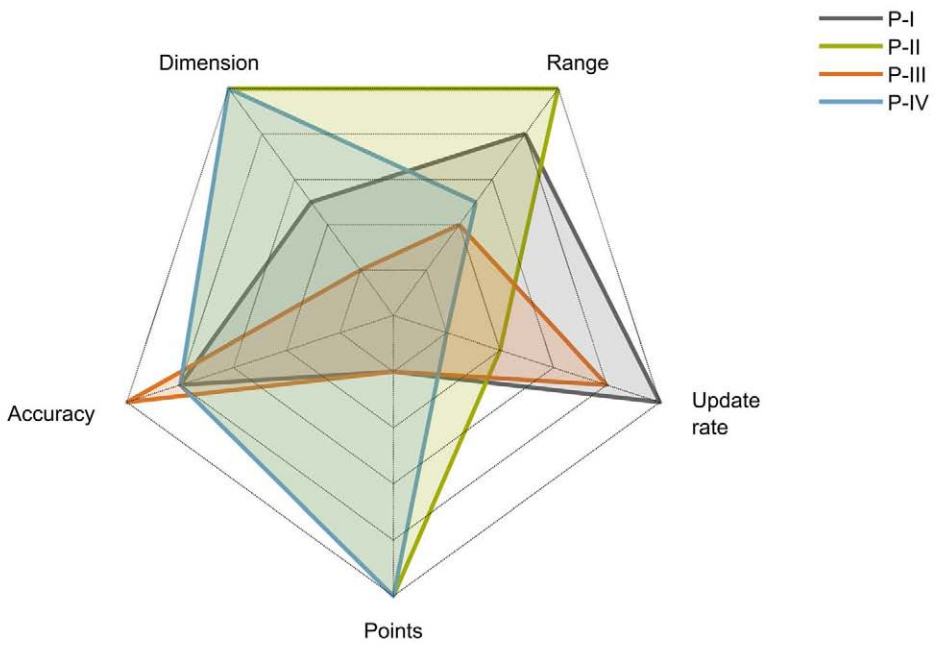

Figure 5.2 – Comparison of selected features of the described IATS monitoring methods: P-I (Bridge monitoring), P-II (Stereo IATS), P-III (Leveling staff) and P-IV (RGB + D)

staff and to decode the respective height reading (P-III) is also substantially faster than the geo-monitoring approaches as described in P-II and P-IV. Out of these, the RGB + D method is listed at the end, as the image bundle and the laser scan are done subsequently.

When comparing the number of **points**, which can be determined simultaneously, a clear difference in the structural and geo-monitoring approaches can be seen. The last mentioned methods (P-II & P-IV) resemble at the stage of image processing wherein corresponding points are searched for in image bundles. The dense information content of images is used to derive measurement elements, resulting in a comparable and high number of generated coordinates. If the displacement vectors of two subsequent measurement epochs are taken as result, their quantity is still far higher than the limited set of (active or passive) signalized points as acquired with the methods presented in P-I and P-III.

The **accuracy** of all described methods can be specified as high with respect to their intended measurement range, as well as in comparison to other systems. In case of P-I (bridge monitoring), not the frequency determination, but rather the directly measured vertical and horizontal displacements are used as an indicator. In doing so, the accuracy can be compared to the geo-monitoring approaches shown in P-IV and P-II. The latter is rated as highly accurate, particularly in relation to its long distance and small footprint. Height measurements done according to the method in P-III are classified with the highest possible value. The reason for this is, that the targets are meticulously constructed to a high quality standard, and are even calibrated sometimes.

The last feature is formed via comparison of the **dimension** of the results among each other. Measurements done according to P-III result in 1D height differences and are listed with the lowest value. In the case of P-I, the vertical and horizontal displacements are used for evaluation again, therefore the outcomes are two dimensional values. The RGB + D method (P-IV) and the long-range measurements described in P-II deliver full 3D coordinates and displacement vectors with 3D start and end points.

By reviewing all features in total, it can be noted that both structural and both geo-monitoring approaches exhibit similar behavior. The reason for this is the similar data analysis. Specifically, the image processing algorithms resemble each other in the respective monitoring type. In the structural monitoring approaches, single structures in the images are sought and extracted. A single image and a single distance measurement is carried out, if any. All this leads to high update rates, but a low number of points and dimensions, as can be seen in Figure 5.2. Contrary to that, the aim of the geo-monitoring approaches is to generate as many points as possible by using the same or similar image processing algorithms. However, this is more time-consuming and leads to lower update rates. In addition, several images are acquired as an image bundle and in one case an extra laser scan is conducted.

To summarize Figure 5.2, it can be seen that for each of the listed features, there is an IATS monitoring approach presented in this thesis which achieves the highest value. However, none of the methods can fulfill all task requirements with the highest rank. That means the most appropriate method for each monitoring task has to be chosen individually.

5.3 Research contributions

Four different methods are presented in this thesis for geodetic monitoring using Image Assisted Total Stations. These methods are either newly developed or are already existing approaches that have been advanced to form usable products. Different use cases provided the verification of the usability of the respective method. Some of these developments have already been adopted and used by other researchers and practical users.

A similar concept of the one utilized in P-I is used by Ehrhart and Lienhart (2015b), who monitored vibrations of civil engineering structures to detect changes of the natural frequencies. Accelerations and object displacements are derived based on target displacements in the video images. In this work, different image analysis methods and targets are used: (1) a blob detection for passive artificial targets, (2) template matching of artificial structures, (3) feature matching of natural structures, and (4) optical flow. The first three methods were previously described and tested in similar form in Wagner and Wasmeier (2014).

The measurement process and the data evaluation (software) of the method described in P-II was developed in a research project. The main objective of this project was to provide the participating industrial partners with a new kind of measurement system for long-range terrestrial deformation

measurements (Wagner et al., 2013a). The conducted research helped the partners to exploit new sensor technology in the field of geo-monitoring and is now available for commercial use. A former drawback for practical setup – the use of IATS prototypes – is solved by Briechle (2014) by transferring the measurement concept to a commercial device.

P-III is the newest publication used in this thesis and the approach had the shortest time to be taken up by the research community. However, first companies showed strong interest for this kind of measuring method. Currently, the implementation gets extended to also read other bar code patterns and the software re-written to be used as an on-board application, directly at the instrument for an improved practical usage.

A similar approach of the combined analysis of point cloud and image data (P-IV) is presented by Omidalizarandi et al. (2016), however using different instruments. In this publicaton, a terrestrial laser scanner is extended by a high resolution camera and a highly accurate system calibration is conducted. As a result, TLS data can be re-projected to the rectified RGB image and image analysis methods can be combined with the distance information of the TLS data. There are previous methods in which laser scan and image data are combined, e.g. Schneider and Maas (2007) or Hoegner et al. (2013). Herein, the registration of the different data types are performed on data level, e.g. by a bundle adjustment. In the methods presented in Omidalizarandi et al. (2016) and in P-IV, the data is combined by a previous calibration and therefore independent of the conditions during the acquisition.

6 Outlook

The number of total stations with integrated cameras has been rising in the recent years and will continue to increase further. The development is currently limited to instruments of the premium segment, but will be extended to all TS in future. One of the reasons is the general trend of using visual information and interacting with machines in daily life. An example of this worth mentioning is the today's use of (touch-sensitive) full-display smartphones instead of devices with a 12 button keypad which could only be used for phone calls. This shift from tactile buttons and switches to more predominantly visual human-machine interfaces can also be applied to total stations. Nowadays, an instrument should provide functions such as: overlay of survey, planning (stake-out), or sketch data into the live video stream at the instrument's display. A point or direction should be chosen by a click on the display image, not by a laborious view through the telescope optics. The exact position must be measurable by an automated target recognition algorithm. IATS are offering exactly these new demands. The pressure on manufacturers will further increase to include image and touch functionalities even in the lower and middle price class of TS.

Another reason for the increased use of IATS in the future is the ongoing fundamental change of the overall survey principle. The introduction of (robotic) one-man stations reduced the size of survey teams from previously three or more persons to a single one in many cases. The single engineer is no longer located next to the instrument station, he is remotely controlling it from the survey point. Images transferred to the controller are an enourmous help to the operator realizing in which direction the telescope is pointing. The logical and consequential next step in this development is to omit the ocular and save technical effort as done in the newest IATS from Trimble, cf. Section 2.2. Complex beam splitter elements can be avoided, allowing more light to reach the camera chip, which in turn improves the effectiveness of image analyzing algorithms.

It can generally be expected that more automation in the survey workflow will be made possible by image analysis in future. In particular, the kind of target signalizing (if any) will be changed and the target selection will be transferred from the operator to the device. The increasing computational power built in IATS allows a more complex image processing and e.g. the implementation of automated (knowledge-based) decision systems on-board. As described in Wagner and Wasmeier (2014) the following image analysis algorithms are particularly suited for automated and autonomous operation:

- Blob detection, whereby objects are segmented from the background by threshold operators based on their grayscale ranges.

- Edge detection, which localizes discontinuities in images mostly by first- or second-order derivatives.
- Template matching, which tries to find and localize objects based on a training pattern, e.g. by correlation.
- Feature matching, where the neighborhood of pixel locations is numerically described by (statistical) information to be used for matching.

These algorithms enable IATS to automatically detect punctual, linear and areal structural features and to derive directions measurements. However, the reliability of all aforementioned algorithms has to be further improved in order to successfully establish them (1) technically under different measurement conditions and (2) in the surveyors community. The difficulty is to get sufficiently accurate results even under changing illumination conditions. Images taken at bright sunlight, for example, appear blurred and sharp object boundaries are getting lost. Atmospheric influences, in particular refraction effects, cause an apparent change in the target positions, fluctuating shape deformations and increased blurring (Thuro et al., 2010). Another open issue is to guarantee consistently accurate image analysis results. The achievable detection accuracy depends on: the object size, the image resolution, and the quality of the optical focus (Reiterer and Wagner, 2012). To be accepted by the users, the new automatic functions must work at any time correctly and reliable. Already a few malfunctions may lead to a lack of confidence in the application which could fall back to the manufacturer.

The future may provide a further fusion of data and measuring methods. The techniques of the individual geodetic disciplines (engineering geodesy, photogrammetry, satellite geodesy, etc.) will be used in combined approaches and their strengths united. A landslide, for example, could be monitored by DInSAR, refined by data of unmanned aerial vehicles (UAV), and supported by IATS data (e.g. in forested areas). The situation is similar to the IATS as stated at the beginning of this thesis: the hardware is already available, but a concept for a combined processing and analysis of the data – and thus the usage of the full potential – is missing so far.

A look in the more distant future will likely bring significant changes to the measurement tasks of engineering geodesy. It is conceivable that all building trades will be using their own easy handling devices to stake out points, lines, or other geometrical objects at a construction site in order to build walls at the correct location or to install geometrically complex structural elements. When taking into further consideration the trend towards Building Information Modeling (BIM) and the replacement of 2D drawings with digital 3D representations of construction data, it becomes necessary for the craftsmen to get digital support at the site. Current instruments, like the Leica 3D Disto, are the first step into this direction. In consequence the direct stake out of detail points could drop out the surveyors task, for example. However, this development could also bring new tasks. The above mentioned instruments need to be sufficient accurate stationed on-site, i.e. an appropriately reference frame must be available. It is likely that new kind of control points are needed, e.g.

for augmented reality glasses to visualize construction data as overlay to the real-world environment.

Another possible new task is the increased demand for automatic progress monitoring of construction sites, i.e. the regularly (or permanently) comparison of the as-built state to the as-planned state. As shown in Tuttas et al. (2016) image-based techniques are well suited for this task. As IATS will be on-site anyway for site surveying, stake out, or monitoring this could be an additional future task.

Whatever the future brings, IATS will certainly replace total stations and an increasing automation in survey tasks will take place. New automatic (image-based) measurement features will be available in commercial devices, first for geodetic monitoring applications, as there are often repetitive tasks to fulfill. The methods and use cases presented in this thesis hopefully serve as a basis to support the future development.

Bibliography

Apaydin, N., 2002. Seismic analysis of Fatih Sultan Mehmet suspension bridge. PhD thesis, Boğaziçi University, Istanbul, Turkey.

Aryal, A., Brooks, B. A., Reid, M. E., Bawden, G. W., Pawlak, G. R., 2012. Displacement fields from point cloud data: Application of particle imaging velocimetry to landslide geodesy. Journal of Geophysical Research: Earth Surface 117 (F1), p. n/a.

Bauer, A., Paar, G., Kaltenböck, A., 2005. Mass movement monitoring using terrestrial laser scanner for rock fall management. In: van Oosterom, P., Zlatanova, S., Fendel, E. M. (Eds.), Geoinformation for Disaster Management. Springer-Verlag, pp. 393–406.

Bay, H., Tuytelaars, T., van Gool, L., 2006. SURF: Speeded Up Robust Features. In: Leonardis, A., Bischof, H., Pinz, A. (Eds.), Computer Vision – ECCV 2006. Vol. 3951 of Lecture Notes in Computer Science. Springer, pp. 404–417.

Briechle, S., 2014. Evaluierung berührungsloser 3D-Messmethoden mit der MS50. Master's Thesis, Technical University of Munich, Munich, Germany.

Bürki, B., Guillaume, S., Sorber, P., Oesch, H.-P., 2010. DAEDALUS: A versatile usable digital clip-on measuring system for Total Stations. In: Mautz, R., Kunz, M., Ingensand, H. (Eds.), Proceedings of the 2010 International Conference on Indoor Positioning and Indoor Navigation (IPIN). IEEE, Piscataway, NJ, pp. 1–10.

Burns, J. B., Hanson, A. R., Riseman, E. M., 1986. Extracting Straight Lines. IEEE Transactions on Pattern Analysis and Machine Intelligence PAMI-8 (4), pp. 425–455.

Chapman, D. P., Deacon, A. T. D., Hamid, A., 1994. Hazmap: a remote digital measurement system for work in hazardous environments. The Photogrammetric Record 14 (83), pp. 747–758.

Chikatsu, H., Murai, S., 1994. Utilization of a Video Theodolite System for Dynamic Analysis of Human Motion. Journal of the Japan society of photogrammetry and remote sensing 33 (3), pp. 77–80.

Crosetto, M., Monserrat, O., Jungner, A., 2009. Ground-based synthetic aperture radar deformation monitoring. In: Gruen, A., Kahmen, H. (Eds.), Optical 3-D Measurement Techniques. Vienna, Austria, pp. 1–3.

de Seixas, A., 2001. 3D-Objektkonstruktion mittels Gitterlinien-Verfahren. PhD thesis, Vienna University of Technology, Vienna, Austria.

Debella-Gilo, M., Kääb, A., 2011. Sub-pixel precision image matching for measuring surface displacements on mass movements using normalized cross-correlation. Remote Sensing of Environment 115 (1), pp. 130–142.

DIN 18710-1, 2010. Ingenieurvermessung - Teil 1: Allgemeine Anforderungen.

Dumanoglu, A. A., Brownjohn, J. M., Severn, R. T., 1992. Seismic analysis of the Fatih Sultan Mehmet (second Bosporus) suspension bridge. Earthquake engineering & structural dynamics 21 (10), pp. 881–906.

Ehrhart, M., Lienhart, W., 2015a. Image-based dynamic deformation monitoring of civil engineering structures from long ranges. In: Lam, E. Y., Niel, K. S. (Eds.), Image Processing: Machine Vision Applications VIII. Vol. 9405 of SPIE Proceedings. pp. CD–ROM.

Ehrhart, M., Lienhart, W., 2015b. Monitoring of Civil Engineering Structures using a State-of-the-art Image Assisted Total Station. Journal of Applied Geodesy 9 (3), pp. 174–182.

Ehrhart, M., Lienhart, W., 2017. Accurate Measurements with Image-Assisted Total Stations and Their Prerequisites. Journal of Surveying Engineering 143 (2), pp. 04016024–1–12.

Fabiankowitsch, J., 1990. Automatische Richtungsmessung mit digitalen Differenzbildern. PhD thesis, Vienna University of Technology, Vienna, Austria.

Flach, P., 2000. Analysis of refraction influences in geodesy using image processing and turbulence models. PhD thesis, ETH Zurich, Zurich, Switzerland.

Friedrich, K., 1927. Ueber Punktgenauigkeit. Zeitschrift für Vermessungswesen (ZfV) 56 (2 & 3), pp. 33–41 & 65–79.

Geiss, M., 17.04.2013. Topcon Europe. personal communication.

Gigas, E., Ebeling, K., 1957. Elektrisches Auge. In: DGK Reihe B. Vol. 51. Verlag d. Inst. f. Angewandte Geodäsie, Frankfurt.

Gong, D., Huang, Y. D., Ball, S. L., 1999. A laser scanning videotheodolite for 3d visualisation and metrology. In: ISPRS Archives - Volume XXXII-5/W13.

Gonzalez, R. C., Woods, R. E., 1992. Digital image processing, 2nd Edition. Addison-Wesley, Reading, MA.

Gottwald, R., 1987. Kern E2-SE – Ein neues Instrument nicht nur für die Industrievermessung? avn - Allgemeine Vermessungs-Nachrichten 94 (4), pp. 147–154.

Grafarend, E., 1971. Mittlere Punktfehler und Vorwärtseinschneiden. Zeitschrift für Vermessungswesen (ZfV) 96 (2), pp. 41–54.

Grimm, D. E., Kleemaier, G., Zogg, H.-M., 2015. ATRplus. White Paper.

Gruen, A., 2012. Development and Status of Image Matching in Photogrammetry. The Photogrammetric Record 27 (137), pp. 36–57.

Guillaume, S., Bürki, B., Griffet, S., Durand, H. M., 2012. QDaedalus: Augmentation of Total Stations by CCD Sensor for Automated Contactless High-Precision Metrology. In: FIG Working Week 2012. FIG, Rome, pp. CD–ROM.

Guillaume, S., Clerc, J., Leyder, C., Ray, J., Kistler, M., 2016. Contribution of the Image-Assisted Theodolite System QDaedalus to Geodetic Static and Dynamic Deformation Monitoring. In: 3rd Joint International Symposium on Deformation Monitoring (JISDM). pp. CD–ROM.

Hartley, R., Zisserman, A., 2003. Multiple View Geometry in Computer Vision, 2nd Edition. Cambridge University Press.

Hauth, S., Schlüter, M., 2009. Technische Präzisionsmessungen und kinematisches Tracking mit motorisierten Digitalkameratheodoliten. In: Luhmann, T., Müller, C. (Eds.), Photogrammetrie - Laserscanning - Optische 3D-Messtechnik. Wichmann, pp. 317–322.

Hauth, S., Schlüter, M., Thiery, F., 2012. Modular Imaging Total Stations – Sensor Fusion for high precision alignment. In: Schwieger, V., Böttinger, S., Zheng, B. (Eds.), 3rd International Conference on Machine Control & Guidance. pp. 202–210.

Hauth, S., Schlüter, M., Thiery, F., 2013. Schneller und ausdauernder als das menschliche Auge: Modulare Okularkameras am Motortachymeter. avn - Allgemeine Vermessungs-Nachrichten 120 (6), pp. 210–216.

Heunecke, O., Glabsch, J., Schuhbäck, S., 2011. Landslide Monitoring Using Low Cost GNSS Equipment- Experiences from Two Alpine Testing Sites. Journal of Civil Engineering and Architecture 5 (8), pp. 661–669.

Heunecke, O., Kuhlmann, H., Welsch, W., Eichhorn, A., Neuner, H., 2013. Handbuch Ingenieurgeodäsie. Auswertung geodätischer Überwachungsmessungen, 2nd Edition. Wichmann, Heidelberg.

Hirt, C., Guillaume, S., Wisbar, A., Bürki, B., Sternberg, H., 2010. Monitoring of the refraction coefficient in the lower atmosphere using a controlled setup of simultaneous reciprocal vertical angle measurements. Journal of Geophysical Research: Atmospheres 115 (D21), pp. 2010D21102–1–14.

Hoegner, L., Weinmann, M., Jutzi, B., HINZ, S., Stilla, U., 2013. Co-registration of Time-of-Flight (TOF) camera generated 3d point clouds and thermal infrared images (IR). In: Seyfert, E. (Ed.), Tagungsband der 33. Wissenschaftlich-Technische Jahrestagung des DGPF. Vol. 22. pp. 481–488.

Hovenbitzer, M., Schlemmer, H., 1997. A line-scanning theodolite-based system for 3D applications in close range. In: Gruen, A., Kahmen, H. (Eds.), Optical 3-D Measurement Techniques (IV). Wichmann, Heidelberg, Germany, pp. 339–345.

Huang, Y. D., 1992. 3-D Measuring Systems Based on Theodolite-CCD Cameras. In: Lawrence W. Fritz, James R. Lucas (Ed.), ISPRS Archives – Volume XXIX Part B5. pp. 541–544.

Huang, Y. D., Chen, D., 2000. Orientation of Images Captured with Video-Theodolites. In: Chikatsu, H., van den Heuvel, F. (Eds.), ISPRS Archives – Volume XXXIII-B5. pp. 388–394.

Huang, Y. D., Harley, I., 1989. Calibration of close-range photogrammetric stations using a free network bundle adjustment. In: Gruen, A., Kahmen, H. (Eds.), Optical 3-D Measurement Techniques. Wichmann, Karlsruhe, Germany, pp. 49–56.

Huber, N. B., 2014. Design and implementation of a high resolution, geo-monitoring system based on robotic stereo measurements from imageassisted-total-stations. PhD thesis, Graz University of Technology, Graz, Austria.

Huep, W., 2010. Scannen mit der Trimble VX Spatial Station. zfv - Zeitschrift für Geodäsie, Geoinformation und Landmanagement 135 (5), pp. 330–336.

Ingensand, H., 1990. Das erste digitale Nivellier der Welt. avn - Allgemeine Vermessungs-Nachrichten 97 (6), pp. 201–210.

Ingensand, H., 1999. The Evolution of Digital Levelling Techniques - Limitations and New Solutions. In: Lilje, M. (Ed.), Geodesy and Surveying in the Future. pp. 59–68.

Jordan, W., Eggert, O., Kneissl, M., 1963. Handbuch der Vermessungskunde, 10th Edition. Vol. II. Metzlersche Verlagsbuchhandlung, Stuttgart.

Juretzko, M., 2004. Reflektorlose Video-Tachymetrie - ein integrales Verfahren zur Erfassung geometrischer und visueller Informationen. PhD thesis, Ruhr University Bochum, Bochum, Germany.

Kabashi, I., 2003. Gleichzeitig-gegenseitige Zenitwinkelmessung über größere Entfernungen mit automatischen Zielsystemen. PhD thesis, Vienna University of Technology, Vienna, Austria.

Kahmen, H., 1993. Robot techniques and their impact on surveying systems. In: Linkwitz, K., Eisele, V., Mönicke, H.-J. (Eds.), Applications of Geodesy to Engineering. International Association of Geodesy Symposia. Springer, Berlin and Heidelberg, pp. 100–113.

Kahmen, H., 2005. Angewandte Geodäsie: Vermessungskunde, 20th Edition. De Gruyter, Berlin.

Katowski, O., 1989. Deformationsmessung an Bauwerken mit dem automatischen Theodolitmess-System ATMS. In: Gruen, A., Kahmen, H. (Eds.), Optical 3-D Measurement Techniques. Wichmann, Karlsruhe, Germany, pp. 393–403.

Knoblach, S., 2009. Entwicklung, Kalibrierung und Erprobung eines kameraunterstützten Hängetachymeters. PhD thesis, TU Dresden, Dresden, Germany.

Kolesnik, M., Paar, G., Bauer, A., Ulm, M., 1998. Algorithmic solution for autonomous vision-based off-road navigation. In: Verly, J. G. (Ed.), Enhanced and Synthetic Vision. SPIE Proceedings. SPIE, pp. 230–247.

Koppe, C., 1889. Die Photogrammetrie oder Bildmesskunst. Verlag der Deutschen Photographen-Zeitung, Weimar.

Lato, M. J., Bevan, G., Fergusson, M., 2012. Gigapixel Imaging and Photogrammetry. Development of a New Long Range Remote Imaging Technique. Remote Sensing 4 (12), pp. 3006–3021.

Leica Geosystems, 2001. DistoTM OEM module 3.0 WH15/WH30. Technical Reference Manual V1.00.

Leica Geosystems, 2009. Leica TPS1200+ Series. Technical Data V0.9.

Leica Geosystems, 2012. Leica Viva TS11. Datasheet.

Leica Geosystems, 2015. Leica MS60/TS60. User Manual. Version 1.0.

Lichtenberger, C., 2015. Automatisches Ablesen digitaler Nivellierlatten mit der Okularkamera einer modernen Totalstation. Bachelor's Thesis, Technical University of Munich, Munich, Germany.

Lienhart, W., 2011. The impact of image assisted surveying and image based documentation on traditional surveying workflows. In: Proceedings of AfricaGEO 2011. pp. CD–ROM.

Machotka, R., Hašová, A., Kalvoda, P., Kuruc, M., Pokorný, J., Vondrák, J., 2008. Image Processing and Total Station Instruments. In: 4th International Conference on Engineering Surveying, INGEO 2008, Proceedings. pp. CD–ROM.

Mischke, A., 1998. Entwicklung eines Videotheodolite-Messsystems zur automatischen Richtungsmessung von nicht signalisierten Objektpunkten. PhD thesis, Vienna University of Technology, Vienna, Austria.

Möser, M., Müller, G., Schlemmer, H., Werner, H., 2000. Handbuch Ingenieurgeodäsie, Grundlagen, 3rd Edition. Wichmann, Heidelberg.

Möser, M., Müller, S., 2010. Geodätische Lichtraumvermessung. Neues Verfahren zur Engstellenaufnahme mit der Trimble VX Spatial Station. Der Eisenbahningenieur 61 (4), pp. 40–43.

Müller, S., 2009. Anwendungsbeispiele mit der Trimble VX Spatial Station. avn - Allgemeine Vermessungs-Nachrichten 116 (1), pp. 31–35.

Niemeier, W., 2008. Ausgleichungsrechnung: statistische Auswertemethoden, 2nd Edition. Walter de Gruyter, Berlin.

Omidalizarandi, M., Paffenholz, J.-A., Stenz, U., Neumann, I., 2016. Calibration of Terrestrial Laser Scanner and Digital Camera for Structural Monitoring Applications. In: 3rd Joint International Symposium on Deformation Monitoring (JISDM). pp. CD–ROM.

Ott, M., 1895. Photogrammetrischer Theodolit für Hochgebirgsaufnahmen: nach Angabe von Professor Dr. S. Finsterwalder in München neu konstruiert. zeitschrift für instrumentenkunde 15, pp. 370–373.

Pelzer, H., 1985. Geodätische Netze in Landes-und Ingenieurvermessung II. Vorträge des Kontaktstudiums Februar 1985 in Hannover. Wittwer, Stuttgart.

Pentax, 2013. Total Station R-400VDN Series Specifications.

Poisel, R., Preh, A., 2004. Rock slope initial failure mechanisms and their mechanical models. Felsbau 22 (2), pp. 40–45.

Reiterer, A., 2004. A Knowledge-based decision system for an on-line videotheodolite-based multisensor system. PhD thesis, Vienna University of Technology, Vienna, Austria.

Reiterer, A., 2012. Modeling Atmospheric Refraction Influences by Optical Turbulences Using an Image-Assisted Total Station. zfv - Zeitschrift für Geodäsie, Geoinformation und Landmanagement 137 (3), pp. 156–165.

Reiterer, A., Lehmann, M., Miljanovic, M., Ali, H., Paar, G., Egly, U., Eiter, T., Kahmen, H., 2009. A 3D optical deformation measurement system supported by knowledge-based and learning techniques. Journal of Applied Geodesy 3 (1), pp. 1–13.

Reiterer, A., Wagner, A., 2012. System Considerations of an Image Assisted Total Station – Evaluation and Assessment. avn - Allgemeine Vermessungs-Nachrichten 119 (3), pp. 83–94.

Rinner, K., 1977. Über die Genauigkeit von abgesteckten Punkten. In: Festschrift zur Emeritierung von o. Prof. Dr. techn. Fritz Löschner am 30. September 1977. Veröffentlichung des geodätischen Instituts Aachen. Aachen, pp. 343–354.

Rödelsperger, S., Läufer, G., Gerstenecker, C., Becker, M., 2010. Monitoring of displacements with ground-based microwave interferometry: IBIS-S and IBIS-L. Journal of Applied Geodesy 4 (1), pp. 41–54.

Roic, M., 1996. Erfassung von nicht signalisierten 3D-Strukturen mit Videotheodoliten. Ph.D. thesis, Vienna University of Technology, Vienna, Austria.

Sakimura, R., Maruyama, K., 2007. Development of a New Generation Imaging Total Station System. Journal of Surveying Engineering 133 (1), pp. 14–22.

Schäfer, T., Penka, E., Wunderlich, T., Zilch, K., 2006. Efficient Local Deformation Recognition on Highway Bridges. In: Proceeding of the XXIII International FIG Congress. Munich, Germany, pp. CD–ROM.

Scherer, M., 2002. Advantages of the Integration of Image Processing and Direct Coordinate Measurement for Architectural Surveying - Development of the System TOTAL -. In: XXII FIG International Congress: ACSM-ASPRS Annual Conference and Technology Exhibition 2002. American Society for Photogrammetry and Remote Sensing, Washington, DC, pp. CD–ROM.

Scherer, M., 2004. Intelligent Scanning with Robot-Tacheometer and Image Processing a Low Cost Alternative to 3D Laser Scanning? In: Proceedings of the FIG Working Week. pp. CD–ROM.

Schirmer, W., 1994. Universaltheodolit und CCD-Kamera: ein unpersönliches Messsystem für astronomisch-geodätische Beobachtungen. PhD thesis, Technical University of Munich, Munich, Germany.

Schlüter, M., Hauth, S., Heß, H., 2009. Selbstkalibrierung motorisierter Digitalkameratheodolite für technische Präzisionsmessungen. zfv - Zeitschrift für Geodäsie, Geoinformation und Landmanagement 139 (1), pp. 22–28.

Schnädelbach, K., 1966. Simultane Ortsbestimmung durch Photographie der Sternbahnen. PhD thesis, Technical University of Munich, Munich, Germany.

Schneider, D., Maas, H.-G., 2007. Integrated bundle adjustment of terrestrial laser scanner data and image data with variance component estimation. The Photogrammetric Journal of Finland 20, pp. 5–15.

Schwalbe, E., 2013. Entwicklung von Verfahren zur Bestimmung räumlich-zeitlich hochaufgelöster Bewegungsvektorfelder an Gletschern aus monoskopischen Bildsequenzen. PhD thesis, TU Dresden, Dresden, Germany.

Settles, E., Göttle, A., von Poschinger, A., 2008. Slope monitoring methods - a state of the art report. Work Package 6.

Sookman, S., 2006. Blob Analysis and Edge Detection In the Real World. EE: Evaluation Engineering 45 (8), pp. 46–49.

Szeliski, R., 2010. Computer vision: algorithms and applications. Springer Science & Business Media.

Thuro, K., Singer, J., Festl, J., Wunderlich, T., Wasmeier, P., Reith, C., Heunecke, O., Glabsch, J., Schuhbäck, S., 2010. New landslide monitoring techniques – developments and experiences of the alpEWAS project. Journal of Applied Geodesy 4 (2), pp. 69–90.

Topcon, 2004. GPT-7000i. Specifications.

Topcon, 2007. GPT-9000Ai. Specifications.

Topcon, 2012. IS-3 Imaging Station. Specifications.

Travelletti, J., Delacourt, C., Allemand, P., Malet, J.-P., Schmittbuhl, J., Toussaint, R., Bastard, M., 2012. Correlation of multi-temporal ground-based optical images for landslide monitoring. Application, potential and limitations. ISPRS Journal of Photogrammetry and Remote Sensing 70, pp. 39–55.

Travelletti, J., Malet, J.-P., Delacourt, C., 2014. Image-based correlation of Laser Scanning point cloud time series for landslide monitoring. International Journal of Applied Earth Observation and Geoinformation 32 (0), pp. 1–18.

Trimble, 2010. Trimble VX Spatial Station. Datasheet.

Trimble, 2013. Trimble S8. Datasheet.

Trimble, 2015. Trimble S9. Datasheet.

Trimble, 2016. Trimble SX10. Datasheet.

Tuttas, S., Braun, A., Borrmann, A., Stilla, U., 2016. Evaluation of acquisition strategies for image-based construction site monitoring. In: Halounova, L., Šafář, V., Remondino, F., Hodač, J., Pavelka, K., Shortis, M., Rinaudo, F., Scaioni, M., Boehm, J., Rieke-Zapp, D. (Eds.), ISPRS Archives – Volume XLI-B5. pp. 733–740.

Uffenkamp, V., 1995. Konzeption, experimentelle Realisierung und Kalibrierung einer opto-elektronischen Schwenk-Neige-Kamera langer Brennweite. PhD thesis, Technical University of Munich, Munich, Germany.

Ullrich, R., Knoblach, S., Möser, M., 2012. Verwendung einer Okularkamera zur Realisierung eines automatisierten geometrischen Alignements. avn - Allgemeine Vermessungs-Nachrichten 119 (3), pp. 95–103.

Varshosaz, M., Dowman, I., Chapman, D., 2000. Towards automatic reconstruction of visually realistic models of buildings. In: Chikatsu, H., van den Heuvel, F. (Eds.), ISPRS Archives – Volume XXXIII-B5. pp. 180–186.

Vogel, M., 2006. Vom Pixel zur Richtung. Die räumlichen Beziehungen zwischen Abbildungsstrahlen und Tachymeter-Richtungen. PhD thesis, TU Darmstadt, Darmstadt, Germany.

von Webern, H., 2007. Algorithmen zur Oberflächenerfassung mit Gitterlinien-Verfahren. PhD thesis, Vienna University of Technology, Vienna, Austria.

Wagner, A., 2016. A new approach for geo-monitoring using modern total stations and RGB+D images. Measurement 82, pp. 64–74.

Wagner, A., Huber, B., Wiedemann, W., Paar, G., 2014a. Long-Range Geo-Monitoring using Image Assisted Total Stations. Journal of Applied Geodesy 8 (3), pp. 223–234.

Wagner, A., Stylianidis, E., Smagas, K., Trdlicka, J., Paar, G., Huber, B., Reith, C., Reiterer, A., 2013a. Geo-Monitoring By High-Resolution Optical Sensors. In: Luhmann, T., Müller, C. (Eds.), Photogrammetrie - Laserscanning - Optische 3D-Messtechnik. Wichmann, pp. 166–177.

Wagner, A., Wasmeier, P., 2014. Flächen- und Feature-basiertes Monitoring mit Videotachymetern. In: Sternberg, H. (Ed.), Multi-Sensor-Systeme – Bewegte Zukunftsfelder. Vol. 75 of Schriftenreihe des DVW. Wißner, pp. 75–88.

Wagner, A., Wasmeier, P., Özgur, A., 2011. On-line monitoring of Fatih Sultan Mehmet Bridge by means of Geodesy and Photogrammetry. AvH Progress Report 2010/2011, unpublished.

Wagner, A., Wasmeier, P., Reith, C., Wunderlich, T., 2013b. Bridge Monitoring by Means of Video-Tacheometer - A Case Study. avn - Allgemeine Vermessungs-Nachrichten 120 (8-9), pp. 283–292.

Wagner, A., Wasmeier, P., Wunderlich, T., Ingensand, H., 2014b. Vom selbstzielenden Theodolit zur Image Assisted Total Station. avn - Allgemeine Vermessungs-Nachrichten 121 (5), pp. 171–180.

Wagner, A., Wiedemann, W., Wasmeier, P., Wunderlich, T., 2016a. Improved concepts of using natural targets for geo-monitoring. In: 3rd Joint International Symposium on Deformation Monitoring (JISDM). pp. CD–ROM.

Wagner, A., Wiedemann, W., Wasmeier, P., Wunderlich, T., 2016b. Monitoring Concepts Using Image Assisted Total Stations. In: Paar, R., Marendić, A., Zrinjski, M. (Eds.), Proceedings of the International Symposium on Engineering Geodesy - SIG 2016. Croatian Geodetic Society, pp. 137–148.

Walser, B., 2004. Development and Calibration of an Image Assisted Total Station. PhD thesis, ETH Zurich, Zurich, Switzerland.

Wasmeier, P., 2003. The Potential of Object Recognition Using a Servo-Tacheometer TCA2003. In: Gruen, A., Kahmen, H. (Eds.), Optical 3-D Measurement Techniques (VI). Zurich, Switzerland, pp. II/48–II/54.

Wasmeier, P., 2009a. Grundlagen der Deformationsbestimmung mit Messdaten bildgebender Tachymeter. PhD thesis, Technical University of Munich, Munich, Germany.

Wasmeier, P., 2009b. Videotachymetrie – Sensorfusion mit Potenzial. avn - Allgemeine Vermessungs-Nachrichten 116 (7), pp. 261–267.

Wasmeier, P., 2012. Kalibrierung eines prototypischen Okularkamerasystems. In: Workshop Videotachymetrie - Wege in eine intelligente Zukunft. Munich, Germany, pp. CD–ROM.

Wasmeier, P., Foppe, K., 2006. A new CCD-based Technique for the Calibration of Leveling Rods. In: Proceeding of the XXIII International FIG Congress. Munich, Germany, pp. CD–ROM.

Wasmeier, P., Reith, C., 2009. Ingenieurgeodätisches Monitoring an historischen Kirchenbauwerken. In: Linke, H. J. (Ed.), Tagungsband. pp. 178–192.

Wenzel, H., 2009. Health monitoring of bridges. John Wiley & Sons, Hoboken, N.J.

Wester-Ebbinghaus, W., 1988. High resolution digital object recording by video-theodolite. In: ISPRS Archives – Volume XXVII-B5. pp. 219–223.

Wiedemann, W., 2014. Monitoring mit terrestrischem Laserscanning (TLS). Case Study „Hornbergl“. Handout. In: Tutorials des 17. internationalen Ingenieurvermessungskurs 2014. Zurich.

Wunderlich, T., 2004. Considerations Concerning Geodetical Long-Term Monitoring Tasks. In: Dörthe Malzahn, T. P. (Ed.), Disasters and Society–From Hazard Assessment to Risk Reduction. Karlsruhe, Germany, pp. 35–42.

Wunderlich, T., 2005. Automatisches Zielen mit Tachymetern und Theodoliten. Geowissenschaftliche Mitteilungen des Instituts für Geodäsie und Geophysik an der Technischen Universität Wien 2005 (71), pp. 29–43.

Wunderlich, T., 2006. Potential of Advanced Tacheometry for Challenging Monitoring Missions. In: Proceedings of the 5th Turkish-German Joint Geodetic Days. Berlin.

Wunderlich, T., 2012. Das Hornbergl in Tirol: Ein bergsturzgefährdetes Gebiet wird zum geodätischen Freiluftlaboratorium. In: Geodätisches Kolloquium. Technische Universität Braunschweig.

Wunderlich, T., 2013. Die Zukunft der geodätischen Absteckung von Bauwerken. In: Bundesanstalt für Gewässerkunde (Ed.), Geodätische Arbeiten für Bundeswasserstraßen. pp. 83–88.

Wunderlich, T., Niemeier, W., Wujanz, D., Holst, C., Neitzel, F., Kuhlmann, H., 2016. Areal Deformation Analysis from TLS Point Clouds - the Challenge. avn - Allgemeine Vermessungs-Nachrichten 123 (11-12), pp. 340–351.

Wunderlich, T., Wasmeier, P., Reith, C., 2010. Potentials and Limits of Geodetic Systems for Landslide Monitoring. In: Hoppe, A. (Ed.), GeoDarmstadt2010. Vol. 68 of Schriftenreihe der Deutschen Gesellschaft für Geowissenschaften. Dt. Ges. für Geowiss, Hannover.

Wunderlich, T., Wasmeier, P., Wagner, A., 2014. Auf dem Weg zum geodätischen Universalinstrument – wie nahe am Ziel sind IATS und MS50? In: Terrestrisches Laserscanning 2014 (TLS 2014). Vol. 78 of Schriftenreihe des DVW. Wißner, pp. 177–192.

Zhang, Z., Zheng, S., Zhan, Z., 2004. Digital terrestrial photogrammetry with photo total station. In: Orhan, A. (Ed.), ISPRS Archives – Volume XXXV Part B5. ISPRS Archives. pp. 232–236.

Zhou, Y., Wagner, A., Wunderlich, T., Wasmeier, P., 2015. Close Range Angles Deformation Monitoring by Telescope Camera of Total Station MS50 using Automatic Detection of Coded Targets. In: Proceedings of the 2nd Int. Workshop on Civil Engineering and Architecture. Istanbul, Turkey, pp. 153–162.

Zhou, Y., Wagner, A., Wunderlich, T., Wasmeier, P., 2016a. Calibration Method for IATS and Application in Multi-Target Monitoring using Coded Targets. Journal of Applied Geodesy (ahead of print).

Zhou, Y., Wunderlich, T., Stix, P., Wagner, A., 2016b. Automatic Prism Constant Setting with Image Assisted Total Stations. Survey Review (submitted).

Zhu, Z.-k., Yuan, Y., Zhang, X.-h., 2011. Theodolite-camera videometrics system based on total station. In: Ikeda, M. (Ed.), Proceedings of SPIE Vol. 8194. SPIE Proceedings. SPIE, Bellingham, Wash., pp. 81942R–1–10.

List of abbreviations

ATR	Automatic Target Recognition
AvH	Alexander von Humboldt-Foundation
BIM	Building Information Modeling
CAD	Computer Aided Design
CCD	Charge-Coupled Device
CMOS	Complementary Metal-Oxide-Semiconductor
DInSAR	Differential Interferometry Synthetic Aperture Radar
DSM	Digital Surface Model
DWG	Drawing (widely used file format for CAD drawings)
DXF	Drawing Interchange File Format
EDM	Electronic Distance Measurement
ETH	Eidgenössische Technische Hochschule (Swiss Federal Institute of Technology)
FFT	Fast Fourier Transformation
FI	Forward Intersection
FOV	Field of View
GB-SAR	Ground-Based Synthetic Aperture Radar
GB	Gigabyte
GDH	General Directorate of Highways
GLONASS	Globalnaja Nawigazionnaja Sputnikowaja Sistema (Global Navigation System)
GNSS	Global Navigation Satellite System
GPS	Global Positioning System
HFVM	Hierarchical Feature Vector Matching
IATS	Image Assisted Total Station

ICP	Iterative Closest Point
IR	Infrared
ITU	Istanbul Technical University
LED	Light-Emitting Diode
LSM	Least Squares Matching
MB	Megabyte
MFR	Maximum Frame Rate
MP	Megapixel
NCC	Normalized Cross-Correlation
PC	Personal Computer
RAM	Random-Access Memory
RC	Radio Control
RGB + D	Red Green Blue + Distance
RGB	Red Green Blue
ROI	Region Of Interest
SGM	Semi-Global Matching
SIFT	Scale Invariant Feature Transform
SNR	Signal-to-Noise Ratio
SP	Stereo Photogrammetry
SURF	Speeded Up Robust Features
TIN	Triangulated Irregular Network
TLS	Terrestrial Laser Scanner
TMS	Theodolite Measurement System
TPS	Terrestrial Positioning System
TS	Total Station
TU	Technical University
TUM	Technische Universität München (Technical University Munich)
UAV	Unmanned Aerial Vehicle
USB	Universal Serial Bus

UTC Temps universel coordonné (Coordinated Universal Time)

VGA Video Graphics Array

VRML Virtual Reality Modeling Language

List of Figures

List of Tables

Acknowledgement

Firstly, I would like to express my sincere gratitude to my supervisor Prof. Dr. Thomas Wunderlich for making this work possible. Thanks for the support, attention to detail and having always an open door. A special thanks also goes to my mentor PD Dr. Alexander Reiterer from the Fraunhofer IPM for the inspiration and the continuous support. Further, I want to thank Prof. Dr. Werner Lienhart (TU Graz) for the kind acceptance as a co-reviewer of this thesis.

I would like to thank all my colleagues at the Chair of Geodesy. In particular, Dr. Peter Wasmeier and Wolfgang Wiedemann for many interesting and fruitful discussions, and Inge Nominacher for the nice talks, sweets and help with administrative work.

I am grateful to Ben Huber and Gerhard Paar from the JOANNEUM RESEARCH for the their great support and very productive cooperation.

Finally, I wish to thank my family and especially my wife Anne for the support and encouragement throughout my study.